Spring 2020

Analysis of Clastic Cave Sediment in a Fluviokarst System, Russell Cave, Northeast Alabama

Jonathan Camelo
Fort Hays State University, jmcamelo@mail.fhsu.edu

ANALYSIS OF CLASTIC CAVE SEDIMENT IN A FLUVIOKARST SYSTEM,

RUSSELL CAVE, NORTHEAST ALABAMA

A Thesis Presented to the Graduate Faculty

of the Fort Hays State University in

Partial Fulfillment of the Requirements for

the Degree of Master of Science

by
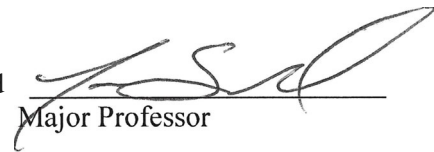
Jonathan M. Camelo

B.S. Geology, Louisiana State University

Date_ April 29, 2020 ....   Approved _____
                                                                                     Major Professor

                                                                      Approved_____
                                                                                      Graduate Dean

This thesis for

the Master of Science Degree

By

Jonathan M. Camelo

has been approved

Dr. Jonathan Sumrall, Committee Chair

Dr. Keith A. Bremer, Committee Member

Dr. Henry Agbogun, Committee Member

Chair, Department of Geosciences

i

ABSTRACT

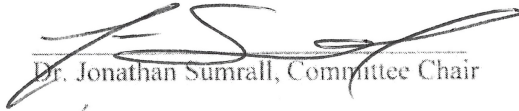Russell Cave is part of a fluviokarst system located along the edge of the Cumberland Plateau in northeast Alabama. The cave system acts as a surface-subsurface drainage system transporting, depositing, and accumulating large influxes of terrestrial-derived materials (sediments, organic material, and magnetic minerals) into the subsurface system forming sediment traps. Five core sites along various discontinuous sediment banks were collected and sampled in 2 cm intervals. Data collection involved Red-Green-Blue (RGB) color, loss on ignition (LOI), magnetic susceptibility (MS) grain-size analysis, end member mixing analysis (EMMA), and ^{14}C radiocarbon dating. The goals for this research were to identify the sedimentary facies in defined cave zones and understand how the flow history in these zones were preserved in the sediments. Results indicate: 1) various climatic changes are recorded in these sediments(the magnitude and nature of these changes is unable to be determined and/or quantified), 2) grain-size distribution is not dependent on the cave passage being the main passage, 3) the age of the organics within sediment cores is older than 2,000 years (as old as~25,000 years), and 4) sediment banks upstream are reworked and redeposited downstream. The significance of these results is that the age of organic material within sediment cores appear to correlate to near the last glacial maximum, the identification of reworking of material from upstream sediment banks, and identification of depositional mechanisms by end member analysis.

ACKNOWLEDGEMENTS

would love to express my appreciation to is Dr. Joe Collins. Without your help, support, and use of your equipment, EMMA modelling would not have been done. Thank you for your dedication to help make this thesis a success. Lastly, I would like to thank my committee members Dr. Henry Abogun and Dr. Keith Bremer. Thank you both for teaching me in the classroom, and with questions and issues that arose from my research.

I would love to give my deepest thanks to Chad Donovan for all the help and struggles we went through. You are the reason this research had so many laughs and I would like to personally thank you for coming up with the acronym SD. With the large list of people that has taken their time out to help with this project, I am not able to go into detail with the exactly what everyone has done, but I would like to also thank the following people: Dr. Grady Dixon, Patricia Duffey, Alex "Big Al" Lyles, Dr. Jeanne Sumrall, Dr. Richard Lisichenko, Dr. James Balthazor, and Dr. Clifton Clark. If I did not mention you, please know I am truly grateful for your help.

Finally, thank you to Dr. Jonathan Sumrall for inspiring me to love geology, dealing with all my issues, and also for being my advisor. Our first-time meeting was the summer of 2013 as my teacher for the LSU freshman geology field camp in Colorado Springs, CO, where back then I was clueless, having never even seen a mountain nor knew what geology was about. After the five-week field camp, we left each other to pursue our own goals in life, never thinking we will cross paths again. Though from that five-week field camp experience, you opened my eyes to pursue a bachelor's degree in geology, and I am really thankful for that. A few years later, after completing my senior LSU geology field camp, I was eager to get my masters. When applying for a master's degree, something in my mind thought to check out where you were in life, so I did, and

next thing you know I was accepting an acceptance letter from FHSU to be one of your graduate students. Things didn't start out smoothed as a new graduate student though. This was due to not knowing anything about karst geology, but that quickly changed by the end of the first semester with your teaching skills and extreme patience for me to get a true grasp of understanding karst geology. There is so much I can speak on about you and how you taught me so many valuable lessons in life both on a personal and professional level, but that would be like writing a book. So, I would like to end it by thanking you one last time, and with your commitment to have me finish a thesis in two years, some may say I would have been "lost in the sauce" if it wasn't for you.

TABLE OF CONTENTS

LIST OF TABLES

LIST OF FIGURES

LIST OF EQUATIONS

LIST OF APPENDICIES

CHAPTER I

INTRODUCTION

This chapter describes the objectives, goals, and hypotheses of this study. Data includes sediment cores that are collected from Russell Cave. This research seeks to improve the understanding of sediments in fluvial karst systems, especially in this region of the Southeastern United States.

The objective of this study is to analyze sediment deposits from Russell Cave in Jackson County, Alabama to determine the discontinuous flow history preserved throughout the cave system that reflects a direct tie to the surface. Jackson County, Alabama is deemed the county with the most documented caves per square mile, consisting of over 1500 caves (Godwin, 2008); however, no research on clastic cave sediment could be found for these caves. Cave sediment cores are the primary data source of this study for interpreting the nature of the deposits by giving insight on textural characteristics, depositional history, and environmental landscape disturbances.

The goals of this study were: 1) to identify the different lithological sediment facies in defined cave zones and 2) understand how the flow history in these zones was preserved in the sediments by building upon the classification system proposed by Bosch and White (2004). These goals were accomplished using grain-size distribution and end member analysis of cave sediment bank cores. Data collection from collected cores involved Red-Green-Blue (RGB) color, loss on ignition (LOI), magnetic susceptibility (MS), grain-size analysis, end member mixing analysis (EMMA), and ^{14}C radiocarbon dating. The hypotheses of this study were: 1) sediment profiles show a stable past climate outside the cave environment, 2) composition of sediment profile in main passages were

primarily composed of sand, and composition in side passages were primarily composed of clay, 3) the age of the sediments is younger than 2000 years, and 4) vertical profiles of sediment banks show bedding layers with no reworking after deposition. Climatic conditions will be determined using sediment color and magnetic susceptibility. The main passages (with an active stream present) should differ from side passages (lacking an active stream) with respect to sediment composition because of the role each type of passage plays in the hydrologic system of Russell Cave. The age of the organic material in the sediment is less than 2000 years due to anthropogenic influences in the region. Finally, sediment banks should represent stable, intact sequences that uniformly record the depositional history.

This research seeks to improve the limited understanding of sediments in fluvial karst systems, especially in this region of the Southeastern United States, by documenting the depositional signature of various sedimentary processes that have been preserved in sediment banks in Russell Cave. This research is important because it improves the poor understanding of surficial soils into an underlying karst system, trapping and storing of various anthropogenic pollutants, and preservation of geologic events (flooding, sedimentation, climate) within cave sediments. Additionally, it attempts to understand the complexity involved in sediment storage in caves.

CHAPTER II

DESCRIPTION OF STUDY AREA

This chapter describes the study location and the surrounding regional landscape of Russell Cave in a geographic and geologic context. The chapter is broken into two broader topics: geographic setting and geologic setting. The geographic setting section gives a summary of Russell Cave from a local scale (ex. cave length, Doran Cove, and Jackson County) to a regional scale (ex. TAG region, Cumberland Plateau, and Southeast, USA), climate influence, vegetation growth, and soil formations. The geologic setting section gives a summary of the tectonic history of the Cumberland Plateau and describes the stratigraphy in northeast Alabama.

2.1 Geographic Setting

The study location is within the karst region along the tri-state boundaries of Tennessee, Alabama, and Georgia, also known as the TAG region. The study area is Russell Cave, located in Jackson County, Alabama (Figure 1A). This region is known for its many karst features, especially caves (Dougherty, 1985). The TAG region has five major physiographic provinces based on specific bedrock and geomorphological characteristics: Central Basin, Highland Rim, Cumberland Plateau, and Ridge and Valley, Blue Ridge, and Piedmont (Figure 1B) (Sapp and Emplaincourt, 1975; Kambesis, 2014). The region is part of the Lower Tennessee River Basin that covers approximately 32,000 km^2 (~7,907,372 acres) of land (Figure 1C) (Kambesis, 2014). The regional base level of the Tennessee River controls the southern portions of these provinces: Cumberland Plateau, Central Basin, and Eastern Highland Rim (Kambesis, 2014).
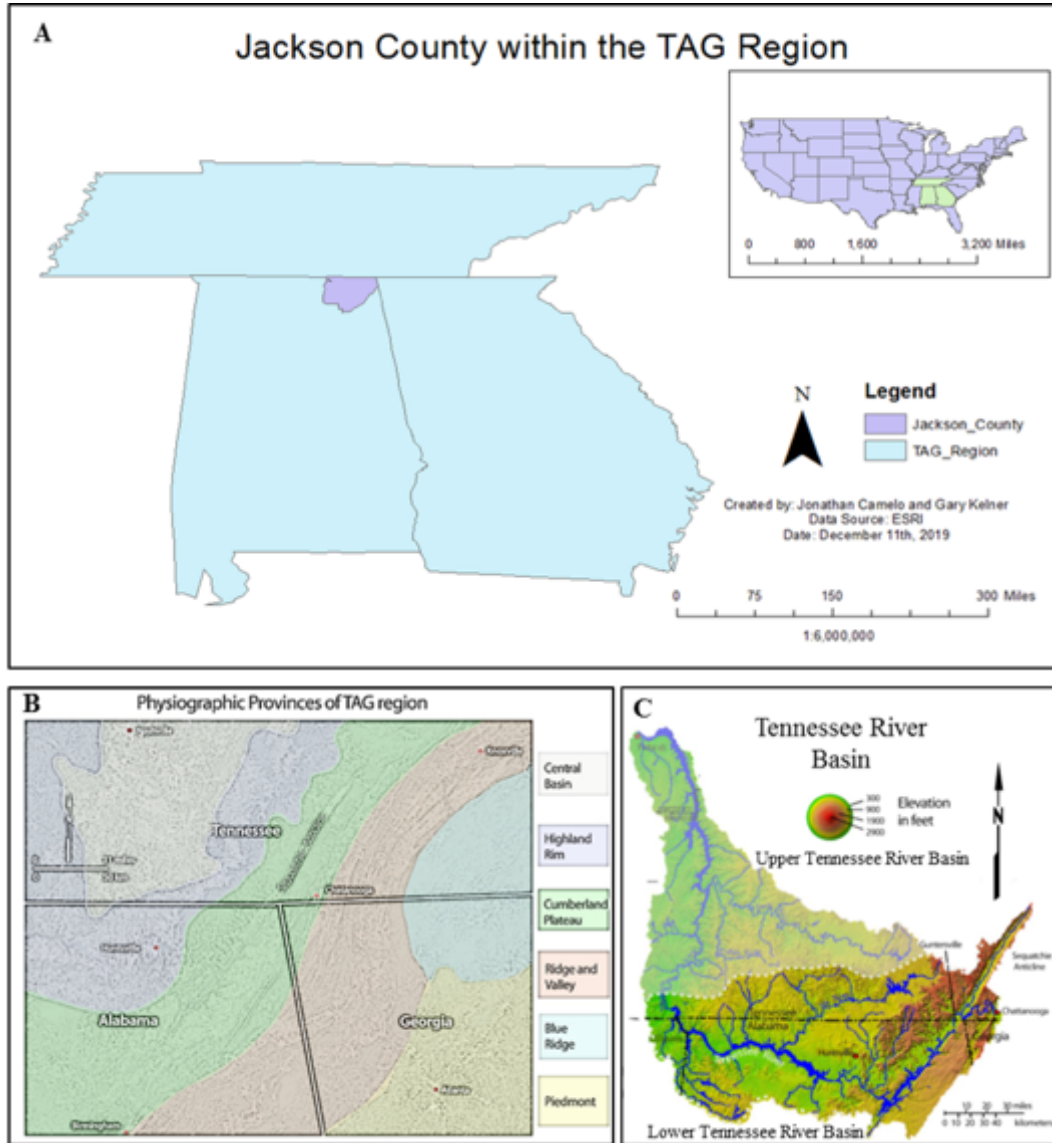
Figure 1. General geography of the TAG region. (1A) Location of Jackson County, Alabama; (1B) Extent of the Tennessee River Basin (dash line represents upper and lower basin). (1C) Physiographic Provinces of the TAG region. Adapted from Kambesis (2014).

Part of the Russell Cave system was declared a national monument in 1961 and consists of approximately 1.3 km^2 (~ 310 acres) of land (Thornberry-Ehrlich, 2014). The section of Russell Cave used in this study is privately owned and accessed by private land, downstream of the National Monument. The exposure of the national monument cave entrance occurred by sinkhole collapse approximately 9,000 to 11,000 years ago

near the end of the Last Ice Age (Hack, 1974). The entrance used to access this cave also represents a collapse entrance. These open karst features allowed habitation for Native Americans for thousands of years within the cave (Miller, 1957). There are ~12 km (~7.5 miles) of mapped passages within Russell Cave, making the cave the third most extensive mapped karst system in Alabama after Anvil Cave and Fern Cave, respectively (Figure 2) (Kambesis, 2014).
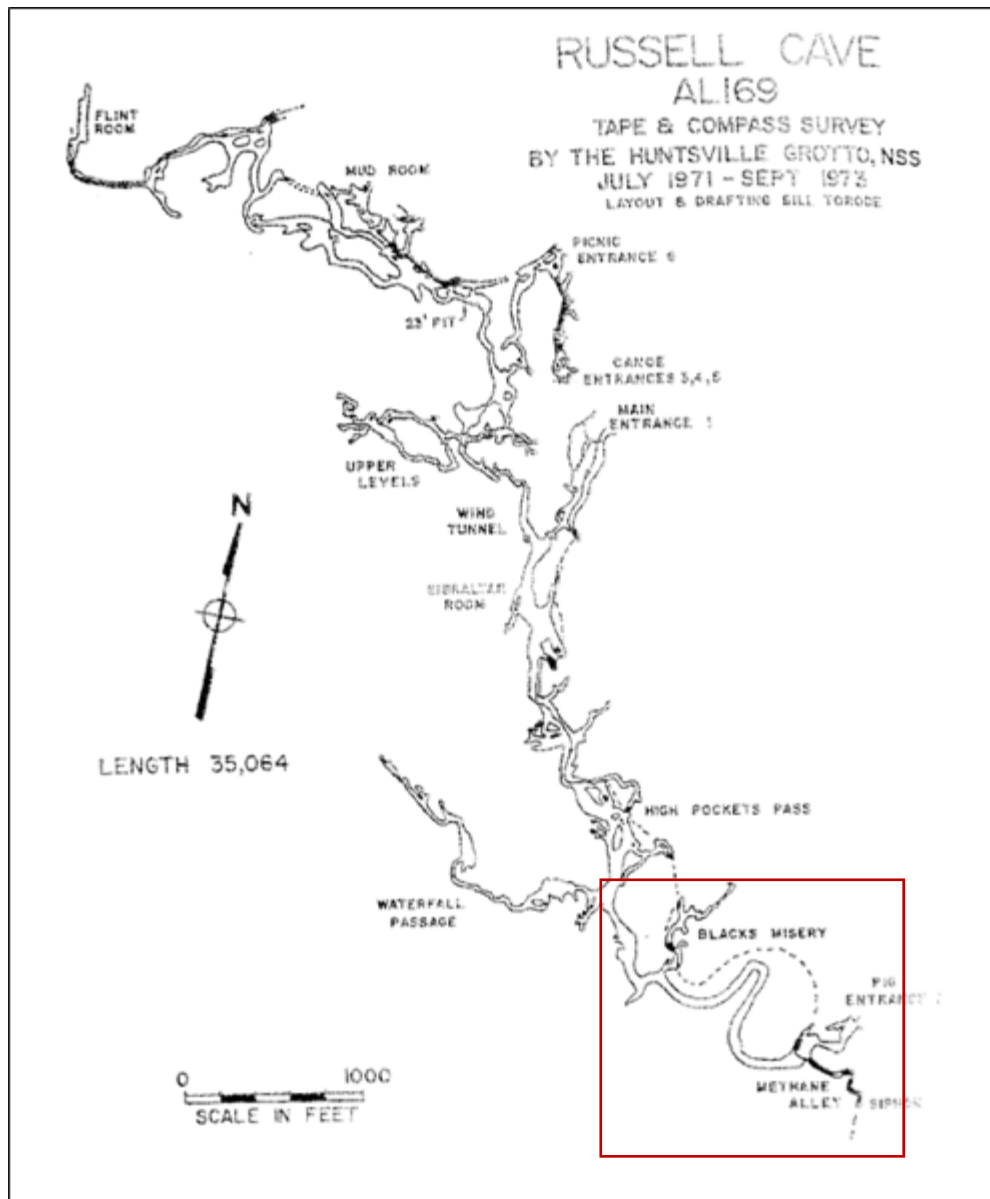
Figure 2. Map of Russell Cave. Red outline box shows the general area of this study.

The Cumberland Plateau extends from central Kentucky to northeast Alabama and is part of the Ohio River drainage basin (Figure 3) (Wilson and Stearns, 1958; Francis and Loftus, 1977). The Cumberland Plateau Escarpment represents an erosional remnant that occurs along the plateau boundaries that are defined by coves and valleys separated by narrow ridges or fingerlike spurs (Griffin, 1974). The elevation of the Cumberland Plateau ranges from 1,270 to 2,000 ft. (McNab and Avers, 1994). The highest relief occurs in the southeastern portion of the TAG region (Simpson and Florea, 2009). The formation of karst features (sinkholes, swallets, vertical shafts, and caves) occurs along the escarpments of the plateau in coves (Kambesis, 2014).
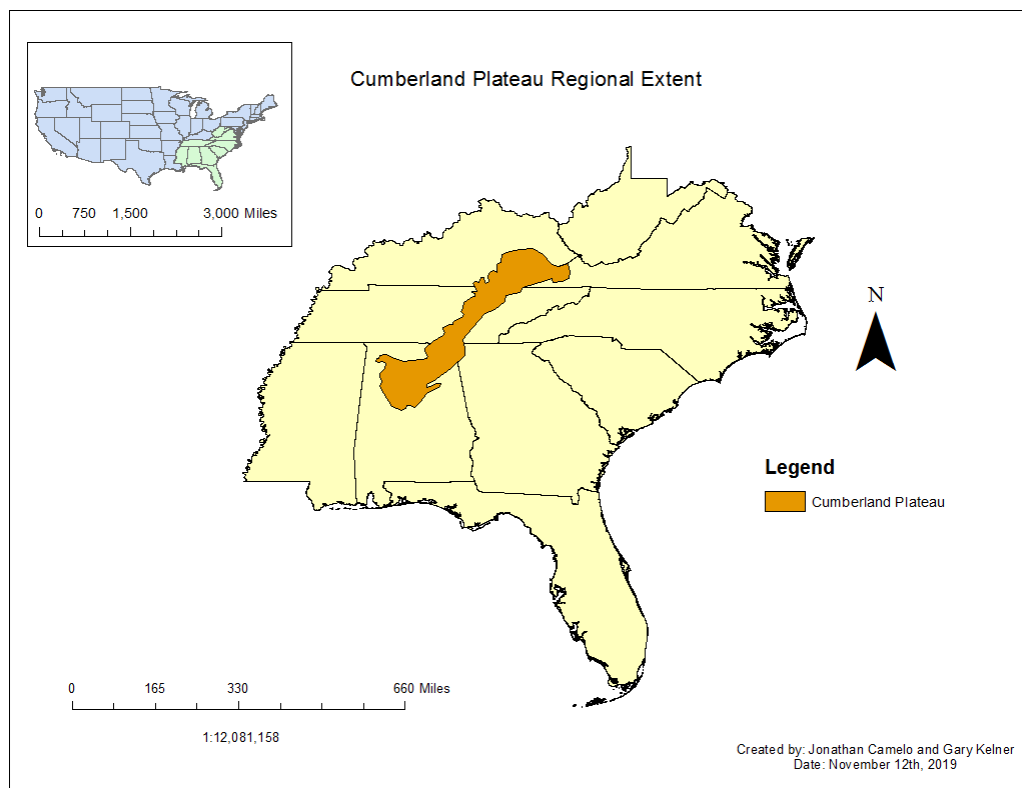
Figure 3. Cumberland Plateau regional extent in the southeast, United States.

Russell Cave is located within the cliffs of Doran Cove. Doran Cove is surrounded by three higher relief landscapes: 1) Orme Mountain to the north, 2) Montague Mountain to the west, and 3) Little Mountains to the east (Figure 4) (Hack, 1974). Russell Cave formed within the western side of Doran Cove in Montague Mountain (Torode, 1990).
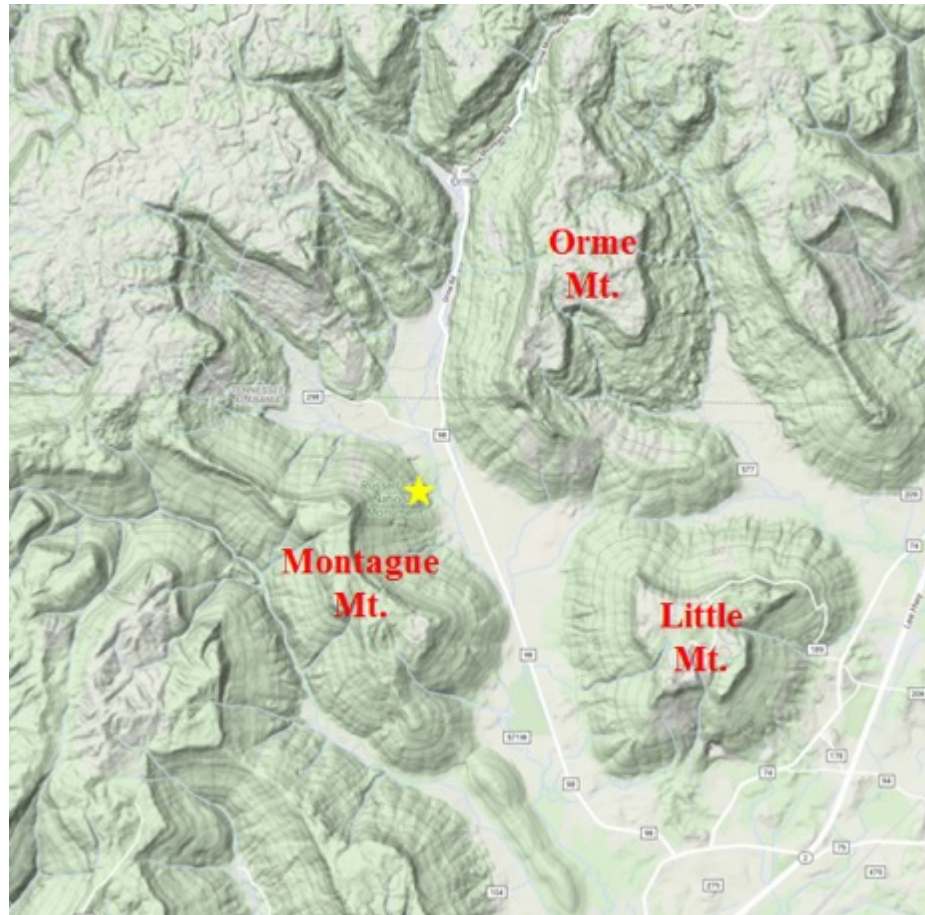
Figure 4. Major mountains surrounding Doran Cove. Yellow star represents the approximate location of Russell Cave.

2.1.1 Climate

The northeastern portion of Alabama is a temperate climate (*C*) classified using the Köppen climate classification scheme. The temperate climate is divided into different types based on seasonal precipitation and level of heat. The study area has a temperate

climate type that is classified as humid subtropical (*Cfa*). The climate in the area is influenced by the semi-permanent, Bermuda high-pressure system that migrates eastward and westward depending on the earth's tilt toward the Sun (Vega and Binkley, 1993). Northeastern Alabama receives an annual average of 150 cm (~ 60 inches) of rainfall (Thornberry-Ehrlich, 2014). This large volume of rainfall is favorable for sediment transport by turbulent flow. The Cumberland Plateau occasionally experiences snowfall during wintertime that averages under one inch and usually sticks to the surface for only a few days (Logan, 2019). There have been five documented historical flood events in Russell Cave: 1900, 1945, 1963, 1986 to 1987, and 2013 (Hack, 1974; Thornberry-Ehrlich, 2014).

2.1.2 Vegetation and Soil

Land use of the Cumberland Plateau over the past century and presently has consisted of small to medium-size family farms growing crops and cattle. The economic value of the areas is dominated by timber and coal mining that has led to logging and strip mine companies purchasing sections of land (Chester, 1995). Areas located throughout the Cumberland Plateau are under federal and state protection to preserve the ecosystem. The Cumberland Plateau is part of a mixed-mesophytic forest region (Küchler, 1965). The vegetation of northeast Alabama is an oak-hickory-pine forest type of the Southern Mixed Hardwood Forest (Brown and Smith, 2000). The ecoregion is a terrestrial habitat type known as temperate broadleaf and mixed forest biome (Martin et al., 1993). Before the settlement of Europeans, fire distribution from lightning strikes was the prime ecological force on the landscape, providing regeneration and growth regulation on vegetation (Delcourt and Delcourt, 1980).

Soil production on the Cumberland Plateau primarily occurs on the flanks of valleys and along the margins of the eroding uplands (Miller and Schaetzl, 2015). This surface landscape is known as hillslope and varies from steep to gentle gradients. Hillslopes are major zones where rocks and soils detach by weathering processes and then commonly transported downgradient by fluvial processes (Norton et al., 2003). Landforms (two-dimensional) of hillslopes are 1) summit, 2) shoulder, 3) backslope, 4) footslope, and 5) toeslope (Figure 5) (Ruhe and Waker, 1968).
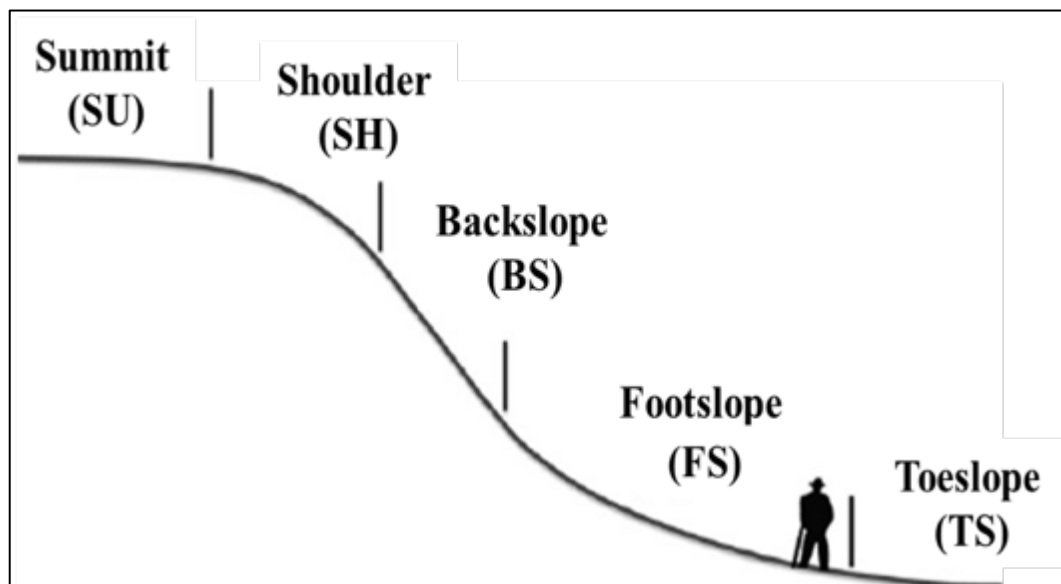
Figure 5. Major zones of the hillslope: summit (SU), shoulder (SH), backslope (BS), footslope (FS), and toeslope (TS). Modified from Miller and Randall (2015).

Over eighty percent of the area of interest in the Cumberland Plateau was composed of four soil types: 1). Rough stony land, Muskingum soil material (RsM), 2) Limestone rockland rough (Lr), 3) Muskingum (Gorgas) fine sandy loam, 10 to 20 percent slopes (Mfl), and 4) Quarry (Qa) (Figure 6) (Soil Survey Staff, 2019). RsM was the dominant soil type accounting for 50.0% of the total soils present and occurs on the backslope. Typical weathered soil profiles reach a depth of 16 inches and composed of stony, sandy loam derived from sandy residuum weathered from sandstone.

Underlying the RsM was Lr, accounting for 21.8% of the total soil type. Lr was located on the backslope and composed of stony silty clay soil derived from residuum weathered from limestone. Weathered soil profiles of Lr can reach a depth of 18 inches. Mfl accounted for 5.7% of the soil and located on the shoulder of the hillslope. The soil profile can be up to 18 inches of weathered soil composed of fine sandy, sandy loam derived from a loamy residuum weathered from sandstone. Qa accounted for 3.7% and located near the summit. Qa was formed from anthropogenic processes by the excavation of certain rocks for economic value. Remaining soil types were located in the following landforms: stream terraces, floodplains, and drainage ways. Floodplain and stream terrace soils can be located on the footslope. Drainage way soils may be located on the toeslope.
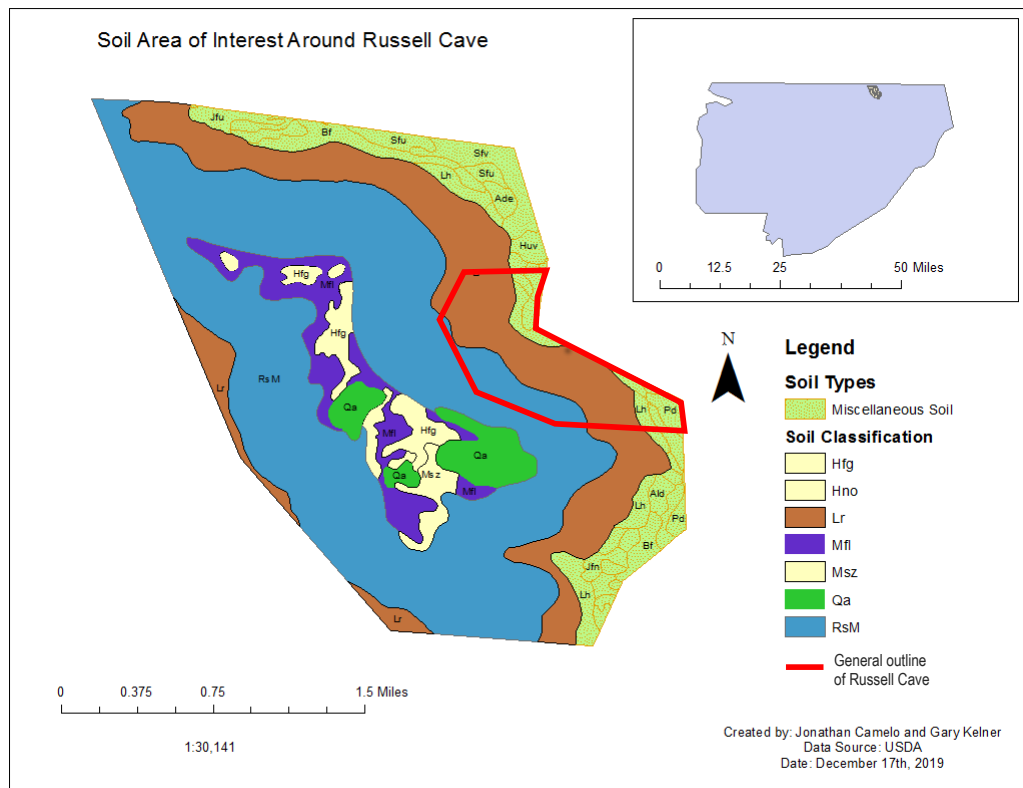
Figure 6. Soil Map of the Russell Cave area of interest. (Soil Survey Staff, 2019)

2.2 Geologic Setting

2.2.1 Tectonic History Cumberland Plateau

During the Early Paleozoic Era, 542 million years ago, the continent that would become North America was beginning to drift apart from the supercontinent Pannotia (Nardin et al., 2011), forming a longstanding marine basin (Pashin, 2005). The sedimentary rocks that would create the Cumberland Plateau were in a shallow sea on the continental shelf situated near the equator (Thornberry-Ehrlich, 2014). Accumulation of carbonate sediment was active throughout the Paleozoic until the Early Pennsylvanian Period. As the Pennsylvanian Period continued, the source material changed to terrestrial derived clastic sediment. The longstanding marine basin recorded many fluctuations of sea-level, depositing sediments from different depositional environments as a result of factors like tectonic activity and climate (Raymond et al., 1988).

Compressive tectonic activity formed low-lying basins separated by uplifted arches and domes (Briggs et al., 1980). Jackson County, Alabama, is situated on the southeastern edge of the Nashville Dome, which lies on the southern extent of the Cincinnati Arch (Stearns and Reesman, 1986; Thornberry-Ehrlich, 2014). The Nashville Dome causes the bedrock to have a gentle dip towards the southeast (Figure 7) (Hack, 1966).
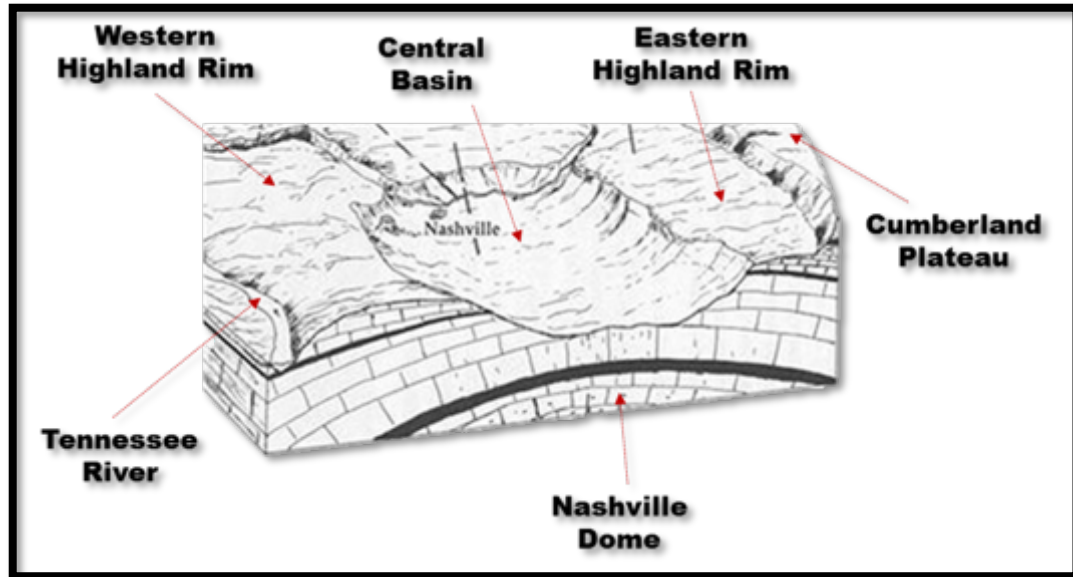
Figure 7. Cross-section of the Nashville Dome and surrounding physiographic provinces. Modified from Moore (1994).

The marine basin was part of a carbonate shelf that fluctuated between prodeltas, deltas, and marine shelf environments during the Mississippian Period (Briggs et al., 1980). Uplifting of the longstanding marine basin began in the Late Mississippian as a result of the Alleghany Orogeny, later forming the supercontinent Pangea (Thornberry-Ehrlich, 2014). A sea-level regression occurred during the Late Mississippian depositing sediments in a prodelta, barrier, back-barrier island system (Thomas, 1979). Uplift continued during the Pennsylvanian Period, changing the marine environment to a fluvial-deltaic landscape (Thomas, 1979; Raymond et al., 1988).

In the Mesozoic Era, sediment deposition into the basin ended, and the supercontinent Pangea began drifting. The breaking apart of the supercontinent resulted in minimal tectonic alteration on rock units of the Cumberland Plateau (Moore, 1994). The Cumberland Plateau began taking its recent shape as the erosion of the overlying non-carbonates occurred (Thornberry-Ehrlich, 2014). An in-depth chronology of geologic

12

events of this region can be found in the Russell Cave National Monument Geologic Resources and Inventory Report (Thornberry-Ehrlich, 2014).

2.2.2 Geology of the Cumberland Plateau in Northeast Alabama

The Cumberland Plateau is highly dissected in northeast Alabama compared to the rest of the plateau (Kambesis, 2014). The stratigraphy of Doran Cove consists of four formations: three Mississippian formations and one Pennsylvanian formation (Figure 8) (Hack, 1966; Thornberry-Ehrlich, 2014). The contact boundary between the strata can be difficult to distinguish because the two shale-dominated formations show very similar characteristics and are commonly mapped as one unit (Thomas, 1972). The Mississippian strata from oldest to youngest are Tuscumbia Limestone, Monteagle Limestone, Bangor Limestone, and the Pennington Formation (Thomas, 1972; Thornberry-Ehrlich, 2009). The nomenclature of the Pennsylvanian strata in Alabama groups all members into one formation, the Pottsville Formation (Hunter and Moser, 1990). Each formation is described in detail below.
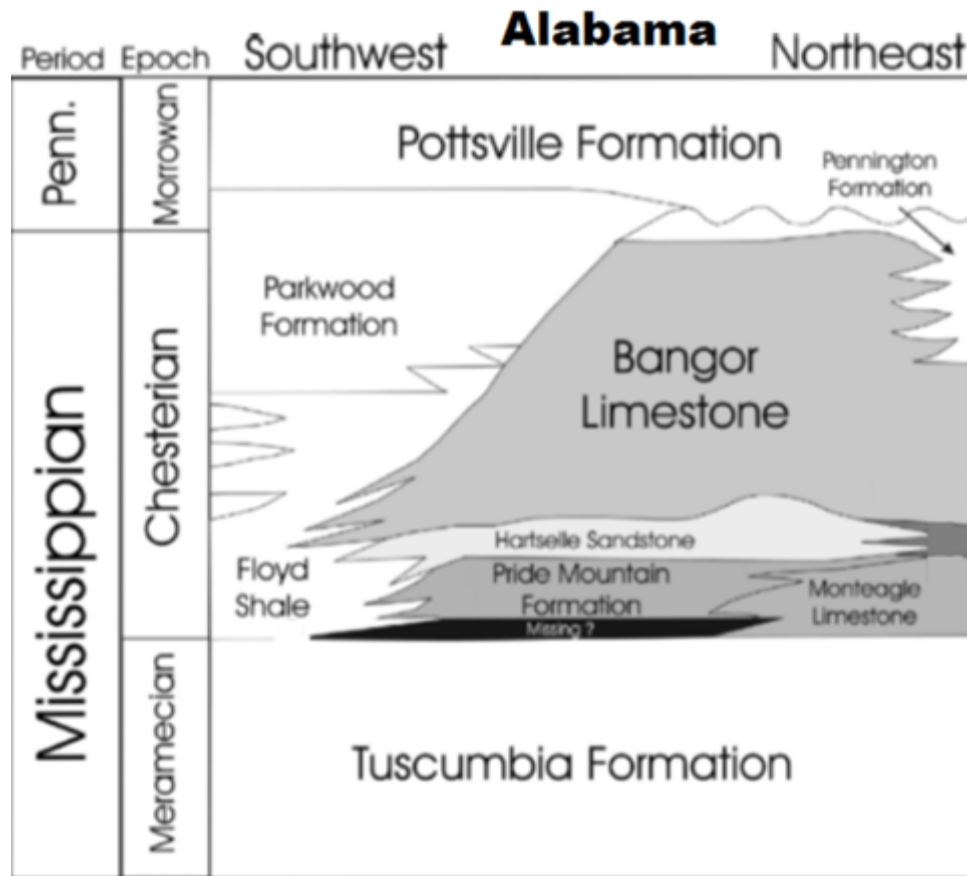
Figure 8. Stratigraphy of Northeast Alabama. Modified from Haywick et al. (2016) and adapted from Pashin (1994).

2.2.2.1 Mississippian Carbonate Complex

Tuscumbia Limestone

The Tuscumbia Limestone consists of light gray micrites and bioclastic limestone with a thin lens of crystalline dolostone and dolomitic limestone found in northeast Alabama (Smith, 1894; Ferguson and Stearns, 1967; Thomas, 1972). Oolites and white to dark-gray chert nodules are common throughout the formation (Szabo et al., 1988). Bed thickness ranges from 0 to 75 meters (0 - 245 ft) (Thomas, 1972). It is named after the town Tuscumbia in Colbert County, Alabama (Thomas, 1972).

14

Monteagle Limestone

The Monteagle Limestone consists of light grey oolitic and bioclastic limestone that formed in a high energy shallow marine environment (Stearns, 1963; Thomas, 1972). A distinctive eight-meter (~26 ft) bed of interbedded shales and limestone have been identified in the middle portion of the Monteagle Limestone in northeast Alabama (Thomas, 1972). The average thickness is approximately 61-meters (~ 200 ft) (Thomas, 1979; Bossong and Harris, 1987). A major marine fossil found in the Monteagle Limestone are crinoids (Burdick and Strimple, 1982). The name of the formation was proposed after the town of Monteagle, Tennessee (Vail, 1959). Russell Cave is located in the Monteagle Limestone (Thornberry-Ehrlich, 2014).

Bangor Limestone

The Bangor Limestone consists of medium to light gray, oolitic, and bioclastic limestone with interbeds of dolomite, and red to dark green shales (Thomas, 1972). The thickness of the formation ranges from 130 to 180 meters (420 - 590 ft.) with a maximum thickness in northeast Alabama (Thomas et al., 1980; Hunter and Moser, 1990). The type location of the Bangor Limestone is the town of Bangor in Blount County, Alabama (Smith, 1894). Butts (1926) reclassified the formation of limestone beds above the Hartselle Formation. The Bangor Limestone grades into the Monteagle Limestone in northeast Alabama due to the Hartselle Formation being absent or very thin (Thomas, 1967). The Hartselle Sandstone is a key formation to differentiate the Bangor-Monteagle contact (Thomas, 1972).

Pennington Formation

The Pennington Formation consists of grey limestone, fine-grained dolostone, argillaceous sandstone, greenish to red mudstones, and local seams of coals (Rodgers, 1953 and Milici, 1974). The thickness of the formation in northeast Alabama is approximately 122 meters (~400 ft) (Szabo et al., 1988). The base of the formation in Jackson County, Alabama has a distinctive fine grain gray dolostone beds approximately 18 meters (~60 ft) thick (Szabo et al., 1988). The Pennington Formation in Alabama is restricted to only the northeastern portion of the state (Thomas, 1967), and the type location ns Pennington Gap in Lee County, Virginia (Campbell, 1893).

2.2.2.2 Pennsylvanian Deltaic Complex

Pottsville Formation

The Pennsylvanian complex forms the caprock of the Cumberland Plateau. The ridge forming caprock has a thickness of 107 meters (~50 ft) in northeast Alabama and is termed the Pottsville Formation (PNp) (Hack, 1966). The Pottsville Formation is composed of conglomerates, sandstones, shales, and coal seams (Wanless, 1946). It overlies the Pennington Formation and is subdivided into the Upper and Lower Pottsville Formations in Alabama (Ferm and Ehrlich, 1967).

Interpretations of the depositional environment of the Pottsville Formation suggest two different depositional settings. The Lower Pottsville Formation was deposited as a prodelta/barrier/back-barrier, and the Upper Pottsville Formation as a delta plain. The Lower Pottsville Formation in the region is described as a well-sorted, light grey to pale, thick-bedded orthoquartzite sandstone with interbedded layers of dark shales, siltstones, and local seams of coal (Horsey, 1981; Hunter and Moser, 1990). Coal

is found in the lower Pottsville Formation in the region and is mined for use (Pashin, 2005).

CHAPTER III

LITERATURE REVIEW

This chapter describes karst formation, geologic processes and features of karst, hydraulic recharge influence, cave devolvement, sources of clastic sediment, and sedimentation of clastic sediment in karst systems. This section provides a framework for the study, while the previous section provided specific information related to Jackson County, Alabama.

3.1 Karst Processes

Karst is a type of landscape characterized by the dissolution of soluble rocks that form a distinct topography, both on the surface and within the subsurface (White, 1988). Karst landscapes in the United States are estimated to make up nearly 20% of the land area (Ford and Williams, 2007). Limestone and dolostone are the most common rock types that host karst. These carbonate rocks form karst features by dissolution (Palmer, 1991). Rock gypsum and other evaporite rocks are the most susceptible rock formations to form karst features by simple dissolution (Klimchouk, 1996); however, their limited surface exposure and high chemical instability lead to fewer preserved karst features found in evaporites. Carbonate rocks dissolve by acid dissolution of the rock. This chemical dissolution process begins when rainfall events introduce slightly acidic rainwater onto the carbonate landscape. The chemistry of limestone dissolution is discussed below.

3.1.1 Limestone Dissolution

Calcite ($CaCO_3$) is the dominant mineral that forms limestone. The process of limestone dissolution is a result of the reaction of carbonic acid with bedrock (Equation 1). Carbonic acid (H_2CO_3) forms naturally by the reaction of carbon dioxide and water in the atmosphere (Equation 2). Calcite dissolution liberates calcium ions (Ca^{+2}) and bicarbonate ions ($2HCO^{-3}$).

$$CaCO_3 + H_2CO_3 = Ca^{+2} + 2HCO^-_3 \hspace{4cm} \text{(Equation 1)}$$

$$H_2O + CO_{2(g)} = H_2CO_3 \hspace{5cm} \text{(Equation 2)}$$

Chemical dissolution of limestone forms sinkholes, sinking streams, caves, and springs. The rate of dissolution is primarily dependent on temperature and partial pressure of CO_2 (Palmer, 1991). CO_2 and other gases are more soluble in cold waters than warm waters (Figure 9). Temperature decreases will shift the reaction to produce carbonic acid resulting in the increased dissolution of calcite. Additionally, gases like CO_2 are more soluble with increased pressure and partial pressure. The soil has a higher partial pressure of CO_2 compared to the atmosphere, which results in soil water being more acidic due to higher CO_2 partial pressure. The rate of limestone denudation by carbonic acid is approximately 0.5 - 4 inches (~1 -10 cm) per 1000 years and is dependent on the amount of precipitation received (Smith and Atkinson, 1976).
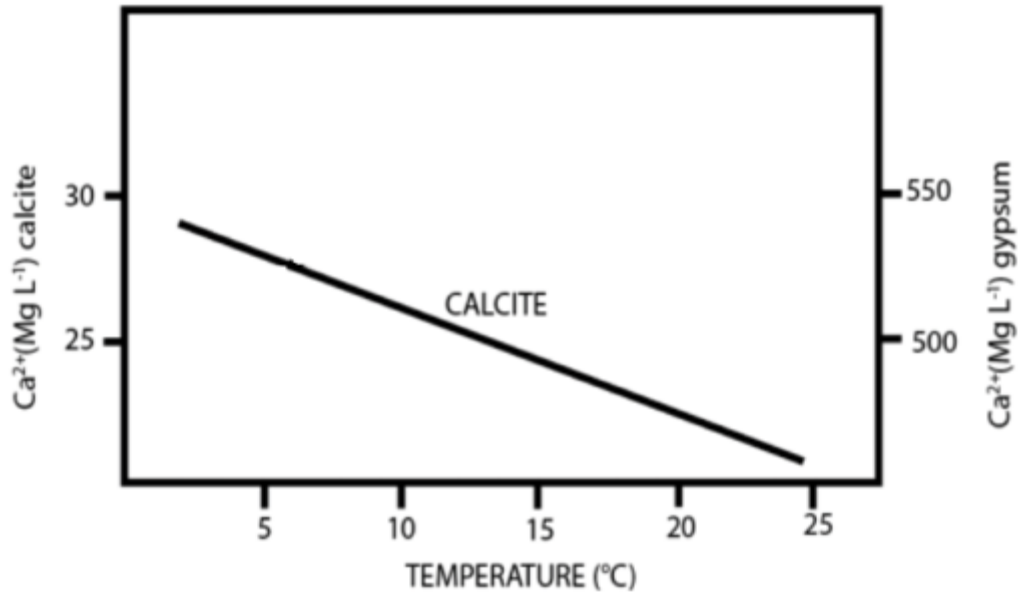
Figure 9. Productivity of calcite solubility based on temperature (°C). Adapted from White (1988).

3.1.2 Carbonate Caves

Carbonate caves are found in limestone, dolostone, and metamorphosed carbonate sedimentary rocks (ex. marble). These rocks are composed of the mineral(s) calcite, aragonite, and/or dolomite. Carbonate caves typically form in rocks that have high solubility and well-developed primary and secondary porosity (Ford and Williams, 1989). Carbonate caves are best developed in rocks that are pure, massive, dense, and coarsely fractured (Ford and Williams, 1989). Mechanical weaknesses (faulting or jointing) and/or heterogeneities (bedding planes) are typically the catalysts that lead to cave development (Palmer, 1991). Primary porosity is defined as the void space developed during a rock's deposition, and Secondary porosity is defined as the void space developed in a rock after lithification. Tectonic activity (faulting and jointing) and chemical dissolution are examples of processes that create secondary porosity.

3.2 Geomorphological Features of Karst

Within karst systems, there are two broad types of features: insurgence and resurgence features. Insurgence features direct surface water into the karst aquifer. Examples include sinking streams and sinkholes (dolines). The outer skin of karst development, which is sometimes considered a type of resurgence, is the epikarst zone. Caves are the product of subsurface dissolution and represent the chemical action by karst groundwater. Resurgence features result when karst groundwater returns to the surface. Springs are the most common type of resurgent karst feature.

3.2.1 Sinking Streams

Sinking streams (losing streams, sinks, or sieves) are a type of insurgence feature found when streams lie above the water table and lose water through openings in the underlying rock (Figure 10). Sink points that allow water to enter underlying rocks at localized positions called swallow holes (Monroe, 1970). Some sinking streams may not disappear into visible openings. Instead, they gradually seep through a sediment bed. Sinking streams may disappear into sinkholes, caves, other karst solution features, or fractures or faults (Palmer, 2001). The disappearance of surface streams is evidence of underground drainage systems (Galloway et al., 1998).
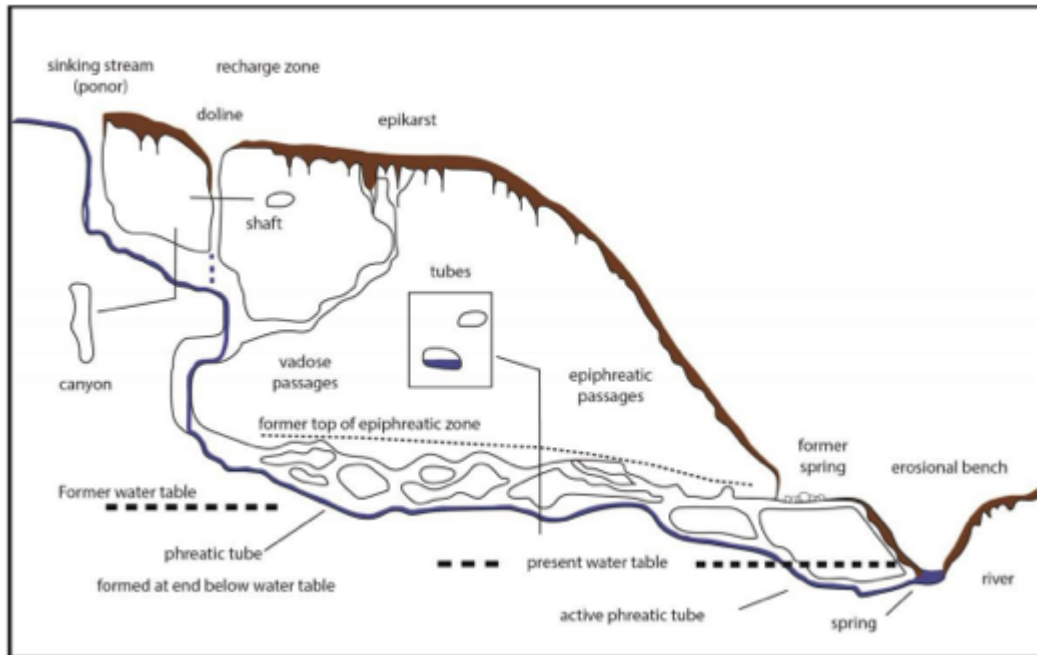
Figure 10. Cross-section of different zones and features in a karst system from Audra and Palmer (2011).

3.2.2 Sinkholes (dolines)

Sinkholes (dolines) are bowl-shaped depressions on the Earth's surface that have sloping walls to allow runoff water to converge to a centralized low point that drains underground (Figure 10). These depressions can range from a few meters to over 10 kilometers and in depth from a few centimeters to over 100-meters (White, 1988). Sinkholes may occur as an individual close depression or in clusters forming a pockmarked land surface (Ford and Williams, 2007). Three major types of sinkholes can occur in a karst landscape: solutional sinkholes, subsidence sinkholes, and collapse sinkholes (Tihansky, 1999). A solution sinkhole is relatively small depression that are exposed or covered by a thin layer of sediment. A subsidence sinkhole is formed by cover material gradually in filling a void area in the carbonate bedrock. A collapse sinkhole is

formed by water eroding cohesive material into the underlying carbonate rock, creating a void that migrates upwards by roof collapse until eventually breaching the surface.

3.2.3 Epikarst Zone

The epikarst zone is a network of solutionally enlarged openings formed by deeply etched fissures or pores on the surface of a soluble rock (Figure 10) (Palmer, 2007). A significant amount of water can be stored in soil-filled openings in the epikarst zone. Water and sediment stored leaks gradually into the underlying rock below through tectonic faults and joints (Klimchouk, 1995). Fissures in epikarst commonly pinch downward, causing water to travel short distances vertically. Water is then forced to drain laterally towards fissures that penetrate deeply into the underlying soluble rock (Williams, 1993; Bakalowicz, 2005).

3.2.4 Solution Caves

Solution caves form when chemically aggressive groundwater dissolves the bedrock and keeps undersaturated water in contact with the soluble walls (Figure 10) (Palmer, 1991). Cave development by solution is only possible in bedrock with a pre-existing network of openings that connect the recharge and discharge areas (Palmer, 2001). Beds, bedding planes, joints, fractures, and intergranular pores influence passage development in solutional caves (Palmer, 2001). Solutionally enlarged caves consist of an array of passages that form distinctive patterns (Figure 11). Solutional caves are separated into four types: 1) branchwork caves, 2) network caves, 3) anastomotic caves, and 4) spongework and ramiform caves (Palmer, 1991).
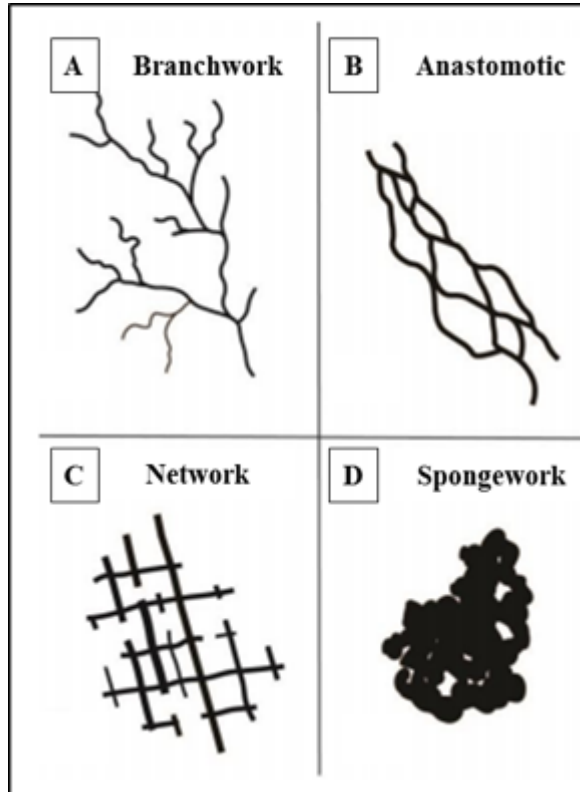
Figure 11. Plain view of common solutional cave patterns from Palmer (1991).

Branchwork caves consist of underground stream passages that join as tributaries that form a dendritic pattern equivalent to dendritic patterns of surface streams (Palmer, 1991; 2007). Insurgence features that recharge branchwork caves contribute to a single solution conduit, or occasionally more than one. The next three cave patterns are loosely grouped together as maze caves. Maze caves are close-loop passages that develop more or less simultaneously (Palmer, 2007). Network caves are angular grids of intersecting fissure passages that solutionally form by enlarging the major fissures (Palmer, 1991). Anastomotic caves are characterized by interconnected curvilinear tubes that form a braid pattern of closed loops (Palmer, 1991). Spongework and ramiform caves form random three-dimensional patterns. Spongework cave patterns consist of interconnected solution voids of various sizes, similar to pores in a sponge (Palmer, 1991). Spongework caves are commonly developed in reef rocks with high porosity. Ramiform caves have irregular

24

rooms with branches that extend outward from the central area of the cave (Palmer, 1991). The rising of sulfuric acid from oxidation of hydrogen sulfide commonly produces raniform cave patterns (Palmer, 2007). Spongework and ramiform caves have very similar patterns and often lumped together into as the spongwork pattern.

3.2.5 Springs

Springs are resurgence points found when groundwater flows out of the ground onto the surface (Figure 10). Caves, conduits, and fractures allow groundwater to emerge from springs onto the surface as distinct streams (Palmer, 2007). Karst spring commonly developed at the elevation of the water table. These springs are called base-level springs (Audra et al., 2004). Karst springs frequently develop in strata that are in contact between carbonate masses and impermeable layers (Palmer, 1991). Many springs are used as an entry point into caves, especially during low flow conditions.

3.3 Hydrologic Zones of Karst Terrain

3.3.1 Vadose Zone

The vadose zone (recharge zone) is the subsurface region that extends from the top of the land surface to the groundwater table (Figure 10) (Monroe, 1970). Groundwater recharge occurs in the vadose zone by sinking streams, sinkholes, and through the epikarst zone. Cave passages in the vadose zone form by free-flowing water under gravity that trend vertically along the steepest openings (Palmer, 1991). Canyons and vertical shafts are common passages found in the vadose zone (Figure 10) (Palmer, 1991). Gravitational flow in the vadose zone forces water to drain downslope into either the phreatic zone or out onto the surface. Free air is present in cave passages found in the

vadose zone, allowing for cave exploration without the use of a self-contained underwater breathing apparatus (SCUBA).

3.3.2 Phreatic Zone

The phreatic zone is the subsurface area below the groundwater table. Any open voids in the phreatic zone are water-filled (Figure 10). Phreatic cave passages are mostly tubular passages formed along horizontal routes of greatest hydraulic efficiency (least resistance) (Palmer, 1991). The weight of overlying groundwater causes the fluid pressure in the phreatic zone to be greater than atmospheric pressure (Maier and Pepper, 2009). The lowering in base-level relative to the local strata entrenches within the phreatic passage floor, forming a keyhole shape passage (Palmer, 1991). Abandoned phreatic passages are evidence of former groundwater levels before base-level lowering (Audra and Palmer, 2011).

3.3.3 Epiphreatic Zone

The epiphreatic zone is the subsurface area found below the vadose zone and above the phreatic zone. Voids in cave passages of the epiphreatic zone fluctuate from being air or water-filled (Palmer, 2001). The amount of groundwater recharge and base-level determines if voids are air or water-filled. Large scale flood events are often too large for the phreatic zone to absorb at once (because conduits do not have floodplains), causing water to back-up into the epiphreatic zone (Palmer, 1991). This diversion of water during flood events form complex overflow routes in the epiphreatic zone (Audra and Palmer, 2011).

3.4 Hydrologic Recharge in Karst Terrain

There are two types of recharge that contribute to the flow of water into a karst drainage network: autogenic recharge and allogenic recharge. The recharge type is determined by precipitation events, either falling on or draining to the surface of a karstic rock (Figure 12) (Gunn, 1983). Autogenic recharge is meteoric water falling directly onto a karst surface (Figure 12) (Monroe, 1970). Allogenic recharge is s meteoric water that falls onto a non-karst surface that drains into a karst system (Figure 12) (Monroe, 1970; Thrailkill et al., 1991). Allogenic recharge does not lose its aggressiveness when flowing on the land surface like autogenic recharge does, which dissolves carbonates at a much faster rate forming larger karst features when these waters encounter soluble rocks (White, 2002). This often results in distinct pits or points where infiltration into the karst aquifer occurs (Figure 12).
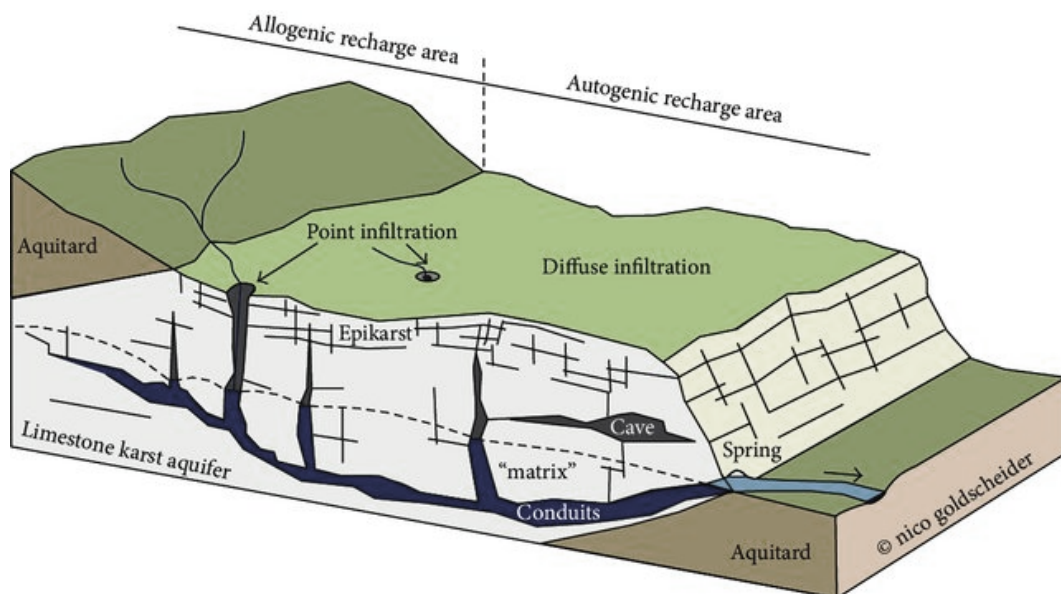
Figure 12. Types of recharge areas on a karst landscape. Modified from: Goldschneider and Drew (2007)

3.5 Hydrologic Classification of Solution Caves

Caves can be further classified by the origin of the acidic waters that lead to dissolution (Palmer, 1991). These acidic waters either originate at or near the surface or migrates from deep-seated origin (Palmer, 1991; Ford and Williams, 2007). Two broad classifications of solution caves are Epigenic and Hypogenic.

Epigenic caves are formed by the movement of aggressively CO_2-rich water from the surface or atmosphere that recharges the cave systems (Palmer, 2011). Caves formed by epigenic waters can be found worldwide, accounting for 80 - 85% of caves explored (Palmer, 2007). The major contributor of epigenic acid is carbonic acid from CO_2 derived from the atmosphere and soil. In soils, biogenic activity increases the input of dissolved carbon dioxide through the bacterial decomposition of organic material and, in some part, by root respiration (Dreybrodt, 1988). The oxidation of organic material allows water to become more acidic as it drains through the soil into the cave (Bray, 1972). Less important epigenic acids are organic acids, commonly from animal droppings (Shahack-Gross et al., 2004).

Hypogenic caves form when rising fluids result in the dissolution of a soluble rock (Palmer, 1991; Ford and Williams, 2007; Klimchouk, 2009). These caves have no primary entrances into the cave. Instead collapse produces entrances into the cave. Wall grooves, floor slots, ceiling channels, and cupolas are some features that suggest rising fluids develop hypogenic caves (Klimchouk, 2007; 2009). Cave patterns of hypogene origin are commonly network or spongework patterns (Klimchouk, 2007; 2009). The major acids are sulfuric acid (H_2SO_4) and carbonic acid (H_2CO_3) (Egemeier, 1973; Davis, 1980).

3.6 Karst of the Cumberland Plateau

The Cumberland Plateau is a form of karst landscape known as fluviokarst, a specific type of epigenic karst. Active fluviokarst systems have a defined drainage basin that is associated with a mixture of surface and subsurface hydrological processes on both fluvial and karst landforms within a catchment basin (Herman et al., 2012). Features of a fluviokarst landscape include karst windows, sinking and losing streams, springs, waterfalls, and caves (Kambesis, 2014). Regional base level and drainage pattern in the catchment basin links the development of all components in a fluviokarst system (Thrailkill et al., 1991). Fluviokarst drainage is based on the topography of the local surface landscape that channels water to interact and drain through both karst rock and non-karst rock (Thrailkill et al., 1991 and Jaillet et al., 2004). The abundance of multi-drop caves, open-air and deep shafts, and horizontal cave systems both large and small drain the deeply incised coves of the Cumberland Plateau (Kambesis, 2014).

3.7 Cave Development within the Cumberland Plateau

Caves located along the Cumberland Plateau share the same hydrogeological setting, developing similar passage characteristics that can be categorized as either a plateau margin or master conduit cave (Kambesis, 2014). A specific type of Master-conduit cave found in the Cumberland River Basin in middle Tennessee is called a Cumberland-style cave, which is outside this study area (Sasowsky and White, 1994). Plateau-margin and master-conduit caves occur in deeply incised coves of the southern Cumberland Plateau (Kambesis, 2014). Cave development is an important part of local and regional hydrology (Kambesis, 2014). The Tennessee River, located in the southern Cumberland Plateau, controls the regional base-level (Anthony and Granger, 2004).

3.7.1 Plateau-margin Caves

Plateau-margin caves are characterized by narrow, sinuous canyons that follow local dip and are mostly vertical passages (Figure 13) (Crawford, 1984). Plateau-margin caves are dominantly formed by sinking streams draining off the Cumberland Plateau caprock into a sink at the sandstone-limestone contact. These caves develop along the shortest route to the water table (Kambesis, 2014). The retreat of the Cumberland Escarpment exposes plateau-margin caves to the surface environment.
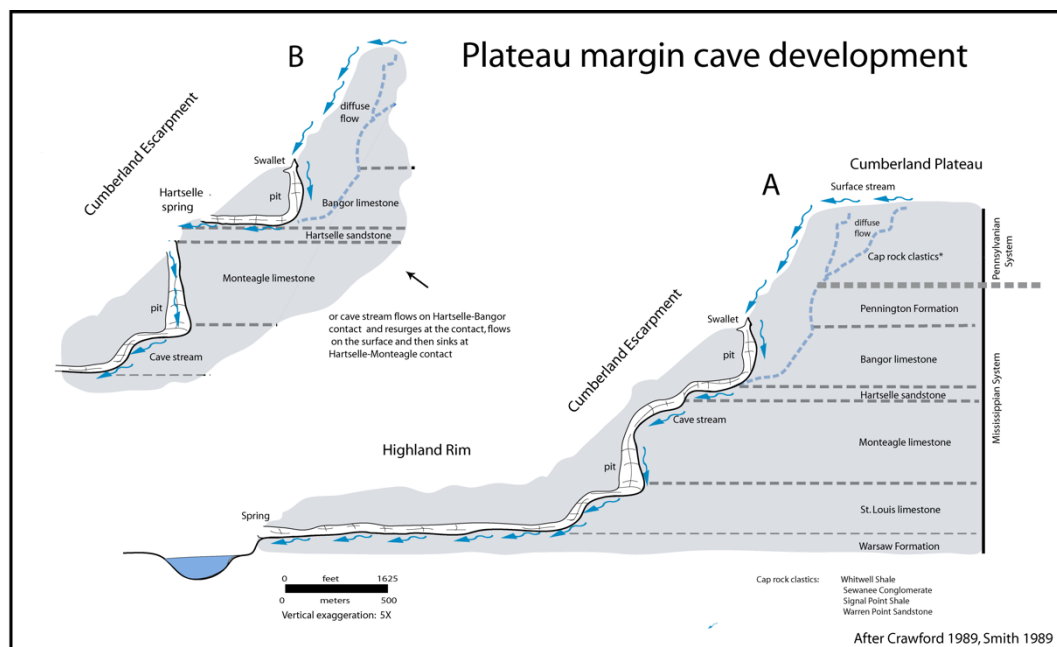
Figure 13. Diagram of a plateau margin cave development. Wall retreat of the Cumberland Escarpment and insoluble layers forcing water to move horizontally allow possible entrances into plateau margin caves.

3.7.2 Master-conduit Caves

Master-conduit caves are characterized by multi-level trunk passage development in valley walls (Figure 14). These caves form passages that parallel bedding plane contacts and regional dip direction (Sasowsky and White, 1994). Master-conduit caves are phreatic in origin, but now remain air-filled abandoned trunk passages, which are

30

predominantly horizontal and connected by narrow vadose canyons. Horizontal phreatic

passages are typically larger compared to vadose canyon passages of plateau-margin

caves (Kambesis, 2014).
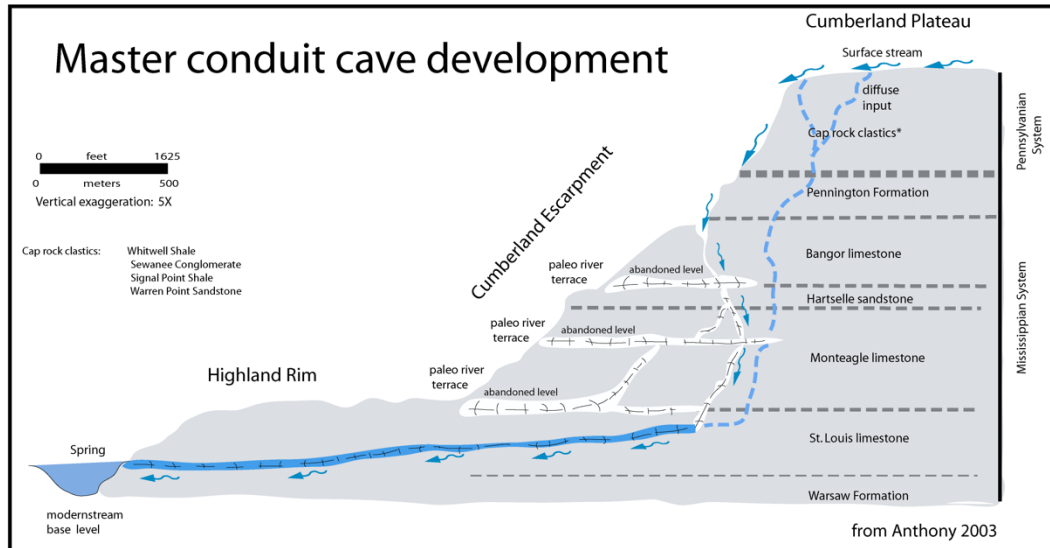
Figure 14. Diagram of a master conduit cave development.

3.8 Clastic Cave Sediments

Clastic sediments are solid particles formed by mechanical weathering of pre-

existing rocks that are eroded and transported by water, wind, or ice. Solid particles can

either be soluble or insoluble, ranging from boulders to clays. Soil is an unconsolidated

material composed of decaying organic matter from the surface and detritus from the

weathering of the bedrock. Sediments and soils in this research will be termed together as

cave sediment. Clastic sediments in caves are commonly transported by flowing water,

with the variables controlling deposition being source material, transport mechanisms,

and depositional environment (Leonard, 1997).

3.8.1 Grain-Size Classification of Clastic Sediments

The Udden-Wentworth scale is the classification scheme for determining the grain-size of sediments (Figure 15). The grain classes used in this scale are clay, silt, sand, and gravel (Figure 15). Grain classes are determined by the diameter of the particles (Figure 15).

Udden-Wentworth Scale			
Phi (Φ)	**Millimeters (mm)**	**Grain Size Name**	
-12.0	> 256.0	Boulder	Gravel
-8.0	256.0 - 64.0	Cobble	Gravel
-6.0	64.0 - 4.0	Pebble	Gravel
-2.0	4.0 - 2.0	Granule	Gravel
-1.0	2.0 - 1.0	Very Coarse Sand	Sand
0.0	1.0 - 0.50	Coarse sand	Sand
1.0	0.50 - 0.25	Medium sand	Sand
2.0	0.25 - 0.125	Fine sand	Sand
3.0	0.125 - 0.0625	Very fine sand	Sand
4.0	0.0625 - 0.031	Coarse silt	Silt
5.0	0.031 - 0.0156	Medium silt	Silt
6.0	0.0156 - 0.0078	Fine silt	Silt
7.0	0.0078 - 0.0039	Very fine silt	Silt
8.0 / 14.0	0.0039 - 0.00006	Clay	Mud

Figure 15. Udden-Wentworth grain-size classification scale.

3.8.2 Sources for sediment Input in Fluviokarst Systems

The sources for clastic sediment in fluviokarst systems are 1) allochthonous sediments injection by sinking streams, 2) soils and regolith flushed into sinkholes by storm runoff, 3) soil injection through fractures at the base of the epikarst, 4) sediment influx from overlying rocks through vertical shafts and open fractures, 5) weathering

residuum, and 6) sediments derived by base-level back-flushing (Figure 16) (White, 1999; Bosch and White, 2004).
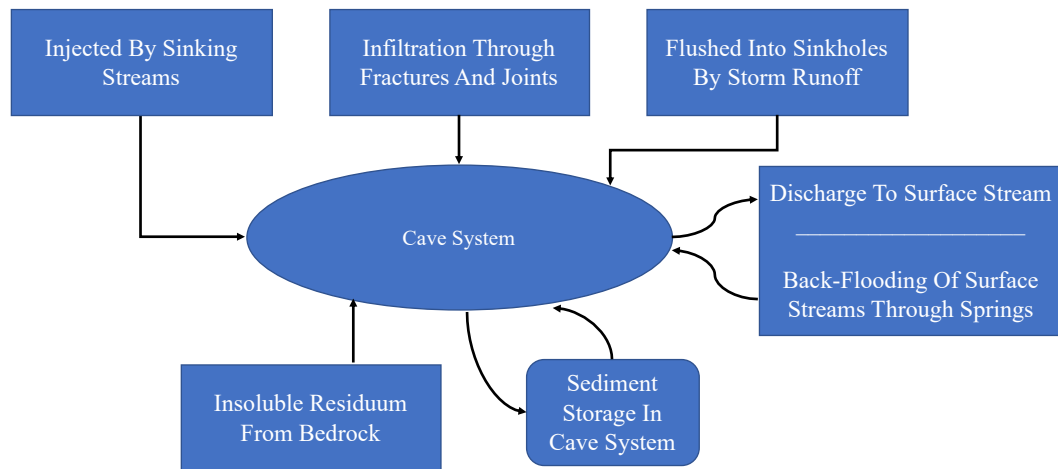
Figure 16. Fluviokarst system showing different insurgence points for sediments and soils to enter the underground drainage system. Adapted from: Bosch and White (2004).

Sediments that are eroded from the surface drainage basin that is transported by sinking streams into the subsurface drainage system. Allochthonous material injected by sinking streams is usually the major component of sediment supply into the fluviokarst system (White, 1999). Rising floodwaters in surface streams may reverse hydraulic flow causing water into springs (Gulley et al., 2011). Storm runoff on the karst surface can flush soils and regolith into sinkholes. Materials can be carried directly into the cave system through the open throat of the sinkhole, soil piping failures, and plug injections from sinkhole collapse (Herman et al., 2012). Soils can be injected into the cave system through narrow fractures at the base of the epikarst zone. Large fractures can develop to allow clastic material to be transported deep into the cave system, where the material becomes part of the sediment load. Siliciclastic formations overlying carbonate formations can input sediments ranging from clay to boulders (Herman et al., 2012). Sediment influx enters the underlying carbonate formation through vertical shafts and

open fractures that lie above the vadose zone (Bosch and White, 2004). Weathering of

carbonate bedrock forms autochthonous sediments that are mostly insoluble components

remaining from the carbonate rock that has been dissolved and carried away by

undersaturated groundwater. Other sources of autochthonous sediment are broken down

material weathered out from the cave walls and guano produced from large colonies of

bats. Sediment deposition by back flooding usually enters through springs of low gradient

master conduit caves that allow suspended sediment to be transported deep within the

conduit system (White, 1999; Herman et al., 2012).

Soils, organic matter, anthropogenic products, and any other material transported

from the surface into the karst system is considered allochthonous material (Drysdale et

al., 2001). The surface streams that enlarged and developed the cave system is the same

that carries in surface sediments (Palmer, 2007). Allochthonous sediments are material

from the surface landscape transported primarily by fluvial processes to the underlying

host carbonate bedrock (Bosch and White, 2004). Composition and textural

characteristics of allochthonous sediments are dependent on the catchment area that

provides the sediment source (Ford and Williams, 1989; White, 2007; Evans and

Soreghan, 2015).

Autochthonous sediments are weathered from the host carbonate bedrock

(Jackson, 1997). The primary source of autochthonous sediments in caves is the insoluble

components that remain after the limestone bedrock is dissolved. Components of

weathering detritus are clays, silicified fossils, iron oxides, and cherts. Other caves

specific autochthonous sediments are bat guano deposits and ceiling collapse blocks

(called breakdown; Figure 17F). Breakdown blocks may act as a natural dam or become a

trap for sediment deposition. The wide range of breakdown sizes and processes associated with collapse makes the classification of breakdown very complex (Jameson, 1991). Guano is defined as bat excrement deposited in the cave system. Cave systems with large bat colonies usually have large piles of guano that can be termed clastic sediment (Widga and Colburn, 2015).

Figure 17. Cave sediments found in Russell Cave passages. A) Dry stream bed with finer-grained sediments filling voids between gravels size grains. B) Streams bed composed of coarse-grained sediments compared to the finer-grained sediment of the sediment bank located along the cave wall. C) Crossbedding in a sediment bank formed by the deposition of organic material and sand-size grains. D) Fracture insurgence feature depositing a red finer-grained material. E) Outcrop of coarse-grained sediment (gravel size) overlying finer-grained sediments (silts and sands). F) Breakdown sediment from the cave roof. G) Bank failure due to undercutting by the channel to the sediment bank. H) Very fine-grained sediment appearing as pseudokarst when water mechanically carves away channels that appear dissolutional.

3.8.3 Sediment Transport

Sediment transport by fluvial processes is divided into two primary types of movement: bedload and suspended load (Figure 18). The mechanism of transport is

dependent on the following parameters: particle size, particle density, fluid viscosity, and fluid flow velocity.
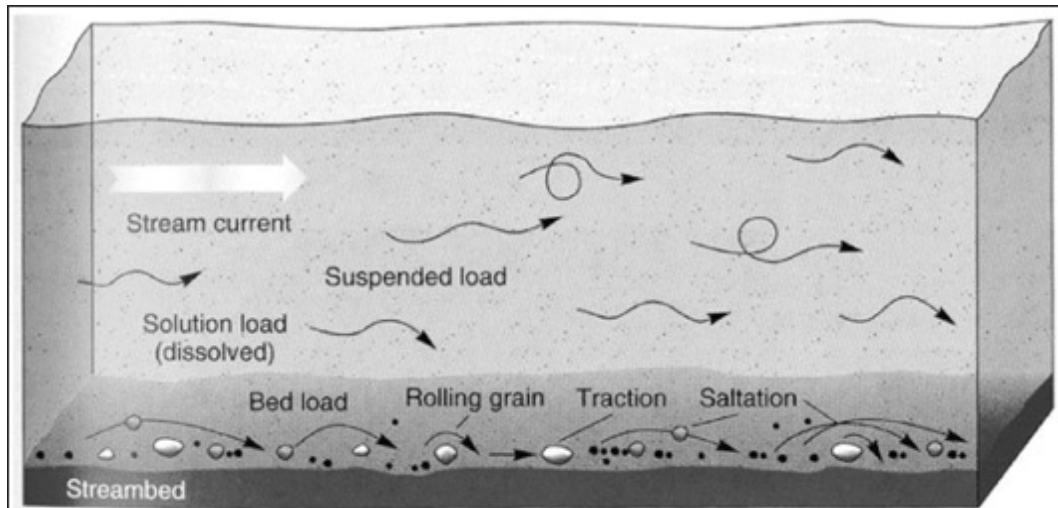
Figure 18. Diagram of sediment transport by fluvial processes: bedload and suspended load. Modified and adapted from Christopherson (2000).

Bedload transport is the result of sediment that is entrained in a flowing fluid, which transports the sediment along the bed surface layer. Sediment entrained in the bedload moves by constant contact (sliding, rolling) or saltation (jumping). Sediment sizes that move as bedload are commonly gravel and sands. The contact component of bedload is mostly coarse sands, and gravel that move in contact with streambed, and the bed itself supports movement (Loch and Donnollan, 1983). Sand particles are the main grain-size transported by saltation.

The suspended load consists of sediment carried in suspension within the water column, not in contact with the bed surface until deposition. For particles to stay in suspension, upward turbulence and buoyance effects must be equal to or be greater than the particles fall velocity. In general, the suspended load consists of finer-grained particles (silts and clays) compared to bedload (gravels and sands). The suspended load also includes an additional component, the wash load. The wash load is the very fine,

typically smaller than 0.0625 mm, that is swept through the cave system, leaving no depositional trace (Chang, 1988). Wind can also allow clay and silt-size sediments to be carried into a cave by suspension (Michie, 1997).

3.8.4 Depositional Environments Within Caves

Erosion, transportation, and deposition of sediments occur episodically throughout the cave systems during storm flow conditions (White, 2007). Caves streams and surface streams both have flow velocities that increase with discharge. In caves, however, the cave wall limits water from spreading out on a floodplain during high flood conditions. In floodwater conditions, there is a large difference in grain-size and distribution of sediment resulting from the variations in flow velocity (Palmer, 2001). Floodwater conditions are never the same from storm to storm. The input of water and sediment depends on the catchment area that recharges the cave system, which varies based on the magnitude of the storm event (Palmer, 1991). Figure 19 shows the necessary velocities of various sediment sizes to be eroded, transported, and deposited. These parameters are based on the widely accepted experiments by Hjulstrom (1935). The deposition of sediment mostly accumulates where water velocity is the slowest along the insides of bends, and in places where the channel or passages widen (Palmer, 2007). The deposition of sediments occurs when velocity drops below the threshold to move them. Sands are deposited at velocities around 10 cm/sec. The settling out of clays must have little to no turbulence and velocity near zero.
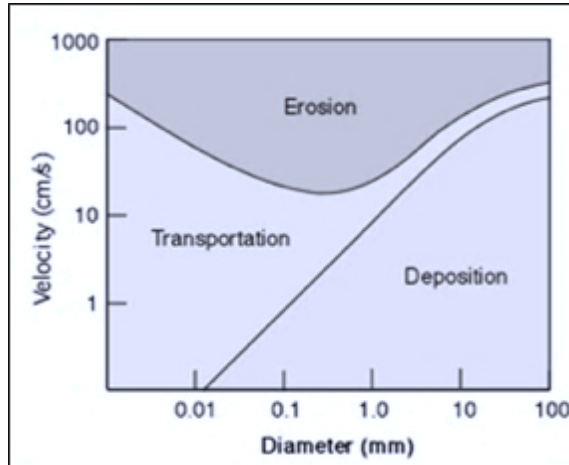
Figure 19. Flow velocity influence on various sediment grain-sizes (grain diameter).

3.9 Facies Classification of Clastic Cave Sediments

Cave sediment facies are classified by the particle size and the degree of sorting (Figure 20) (Bosch and White, 2004). The classification system of clastic sediment is separated into five facies classes: 1) Channel facies, 2) Thalweg facies, 3) Slackwater facies, 4) Diamicton facies, and 5) Backswamp facies.
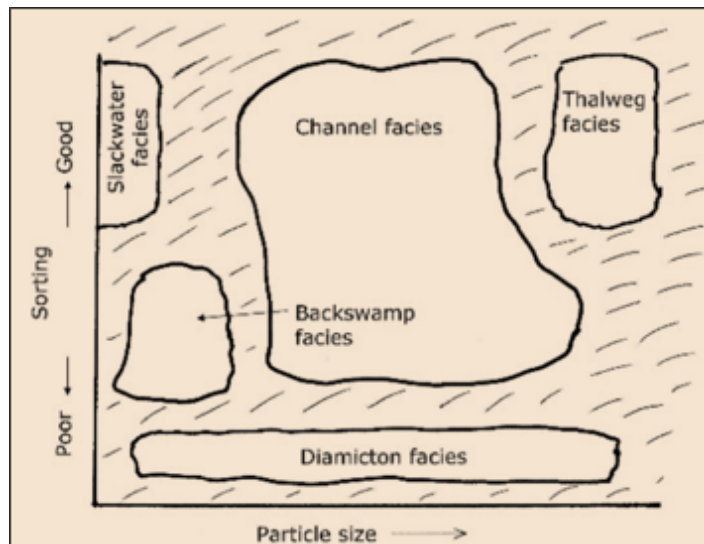
Figure 20. Facies of clastic cave sediment. Facies are classified based on sorting and particle size. Adapted from Bosh and White (2004).

Channel facies have the widest range of particle size and sorting that occur in most cave stream deposits (White, 2007). Different flow regimes allow channel facies to be composed of distinct beds of silts, sands, and gravels that are rarely continuous, and grain distribution varies from bed to bed (Bosch and White, 2004). Thalweg facies are secondary active stream channels that have cut through the Channel facies with bed material that consists of gravel, cobbles, and boulders (Bosch and White, 2004). This facies form when a new stream channel is cutting into the Channel facies retaining the coarser material while winnowing out the fine-grained particles of the bed (Pickle, 1985). Slackwater facies are thin layers of fine-grained clays and silts that are transported into the cave system as suspended load (Bosch and White, 2004). Deposition occurs by sediment settling out of suspension when floodwater fills cave passages, causing water to be ponded for periods of time. Slackwater facies can be during normal flow conditions and back flooding. In most cave deposits, the Slackwater facies is present as the top layer of the sequence (Bosch and White, 2004). Diamicton facies are unsorted and non-bedded sediment masses consisting of chaotic deposits with grain-size distribution from clay to boulders (Gillieson, 1986). The facies occur on high gradient cave passages and are interpreted as a debris flow. This entire sediment mass of the debris flow is entrained and transported by suspension. Backswamp facies are sediments that originate from weathering of residue from host bedrock and by soils that infiltrate by discrete fractures from the surface. Backswamp facies are associated with very fine particles that have little to no lateral transport movement. Commonly, these facies are locally derived in large maze caves, caused by slow rising water that acts as swamp hydrologically (Bosch and White, 2004).

Chapter IV

Methods

This chapter describes the methods and techniques used for analyzing clastic cave sediment in this research. The chapter starts by describing the fieldwork process of collecting clastic sediment in from Russell Cave (location sites, cave restraints, and photographic documentation). Sealed core barrels were transported to the laboratory for preparation of the sediment to be analyzed (core splitting, sample intervals, and photographic documentation). The chapter ends by explaining the five different techniques used to analyze certain aspects of the clastic sediment and the method used to accomplish these different techniques. The five analyses used in this study was loss on ignition, magnetic susceptibility, grain-size distribution, end member modeling analysis, and 14-carbon age dating.

4.1 Fieldwork

Coring was conducted in Russell Cave during normal flow conditions (23-25 July 2018) to examine the sediment banks within the cave. Five cores were collected in one-meter depth intervals in three-inch diameter PVC core barrels (Figure 21). The core locations varied throughout the entire cave due to the following: 1) the height of sediment banks relative to the ceiling, 2) heterogeneous sediment composition of sediment banks prevented manual coring (especially banks that contained gravel-sized grains), and 3) distribution of sediment banks within cave passages.
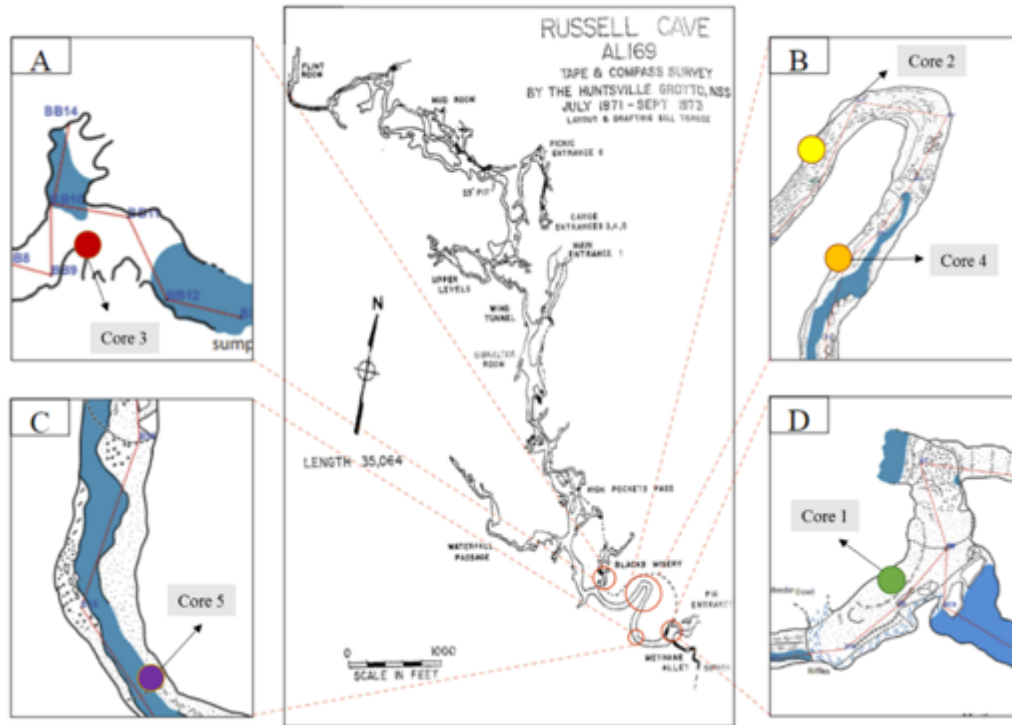
Figure 21. Locations where sediment profiles were collected using PVC core barrels. Cores are ordered based on the farthest location upstream. A) Core 3 location. B) Core 2 and Core 4 locations. C) Core 5 location. D) Core 1 location.

The PVC core barrels were manually driven into the sediment by hammering, forcing the barrel into the sediment bank (Figure 22A, B, C, D, and E). Depending on the viscosity of the sediment extracted, cores were either manually extracted (low water content) or dug out using a shovel (high water content) (Figure 22F and G). Manual digging prevented sediment loss of higher water content sediment cores (Figure 22F). Carefully, after extraction, the empty space in the core barrels was packed with foam to prevent movement of core sediment within the core barrels during transport, and then the core barrels were securely sealed (Figure 22H). The core barrel was marked in detail, referencing survey station markers, core name, and stratigraphic up direction (Figure 22 I).

Figure 22. The extraction process of collecting sediment cores. A) Equipment used for core extraction. B) Extraction location limited to cave roof. C) Manual hammering PVC core barrel into sediment using a small hammer. D) Manual hammering PVC core barrel into sediment using a sledgehammer. E) PVC core barrel located in sediment bank after manual hammering. F) Manual digging of PVC core to reduce sediment disturbance. G) Retrieval of PVC core from sediment bank. H) PVC cores packed and sealed to avoid disturbance during transport. I) The core is marked in detail, referencing survey station markers, core name, and stratigraphic up.

4.1.1 Cave Mapping and Photo-Documentation

Sections of the cave were surveyed to determine exactly where core excavation sites were located. Standard cave surveying techniques were used for all map data collection (Dasher, 1994). Extensive photo-documentation of each core location was

conducted using a Nikon D90 SLR camera. The photographs documented the: 1) cave morphology and profile, 2) excavations, and 3) sediment features and bedding.

4.2 CORE PREPARATION

Cores were split at Fort Hays State University with care not to disturb the sediment. The cores were photo-documented and wrapped in a plastic film to be stored. One half of the core was used to collect samples for data analysis, and the other half was stored as a repository for later analysis if needed. Photographs of cores are located in Appendix A. Due to the tops of Core 1 and Core 4 being disrupted by the coring process; these two cores were sampled at depths that did not correspond with the top of the core (Table 1). A total of 186 sediment samples were collected in two cm intervals (Table 1). Each core contained between 31 and 40 samples (Table 1).

Table 1. Starting depth and total samples of cores used in this research.

Core Name	Starting Depth (cm)	Ending Depth (cm)	Total Sample Intervals (2 cm)
Core 1	14	76	31
Core 2	0	70	35
Core 3	0	80	40
Core 4	12	90	39
Core 5	0	80	40

4.3 Red-Green-Blue (RGB) Color

Photographs of the five sediment cores were input into ImageJ, freeware software from the National Institute of Health (NIH), to measure the RGB color values to determine variations in color (Rasband, 2019). Photographs of the cores were raw,

unedited images, and did not focus on the absolute RGB intensity of the sediment color. The center profile of the five cores was selected as the area of interest to conduct RGB intensity measurements because of possible disturbances are like along the edges of the core profile. A plot showing the color variation along each core was produced within ImageJ.

4.4 Loss on Ignition (LOI) Analysis

Loss on ignition (LOI) was conducted using a conventional oven and muffle furnace set to 105°C and 550°C, respectively (Figure 23) (Heiri et al., 2001). Drying times were 48 hours (conventional oven) and four hours (muffle furnace) (Bengtsson and Enell, 1986). LOI samples for water content were collected in glass vials, and weighed in grams, and calculated as a percent of the total sample weight. The initial weights (IW) of each sediment sample were measured with a precision of $\pm$ 0.04 grams. The dry weight at 105°C (DW_{105}) for each sediment sample was measured after the drying duration in the conventional oven. LOI at 105°C (LOI_{105}) was determined by subtracting DW_{105} from IW (Equation 3).

Figure 23. LOI conducted using a conventional oven (Left) and muffle furnace (Right).

$$LOI_{105} = (IW - DW_{105}) / IW * 100\% \qquad \text{(Equation 3)}$$

LOI_{105} samples were transferred into ceramic crucibles and reweighed with a precision of ± 0.04 grams. Samples were placed in the muffle furnace to remove organic material. After cooling, the samples were weighed to determine the dry weight of the sediment at 550°C (DW_{550}). Loss on ignition (LOI_{550}) was determined from the following equation.

$$LOI_{550} = (LOI_{105} - DW_{550}) / LOI_{105} * 100\% \qquad \text{(Equation 4)}$$

4.5 Magnetic Susceptibility Analysis

Magnetic susceptibility was measured using the KLY 3S Kappabridge instrument under the supervision of Dr. Brooks Ellwood at Louisiana State University (LSU). The samples were collected continuously in vertical succession using specially designed 2.0 cm^3 plastic cubes (Figure 24). A total of 186 samples were collected. Each sample was measured three times to get the mean magnetic susceptibility value. Samples were induced into a very low inducing magnetic field to determine the concentration and composition of the magnetizable material in each sample (Ellwood et al., 1996).

Figure 24. Specially designed 2 cm^3 plastic cubes. (Photo by Brooks Ellwood)

4.6 Grain-Size Analysis

Grain-size analysis was conducted at Middle Tennessee State University under the supervision of Dr. Joe Collins. Pretreatment of the samples include: 1) the removal of organic content using hydrogen peroxide 30%, 2) decanting supernatant liquid, and 3) mixing of dispersing agent (sodium hexametaphosphate) (Heck, 2013). Grain-size distribution was measured using a Malvern Master-Sizer 2000 Laser Diffraction Particle-Size Analyzer equipped with a Hydro 2000G pump accessory following the procedures by Collins et al., (2017) (Figure 25). The obscuration range was primarily between 10-20%; however, some finer-grained samples had an obscuration range between 20-30%. Samples were diluted with deionized water to reduce obscuration values. The machine was monitored for precision and accuracy using standard coarse test dust (Powder Technology Inc.: ISO 12103-1, A4 Coarse Test Dust).
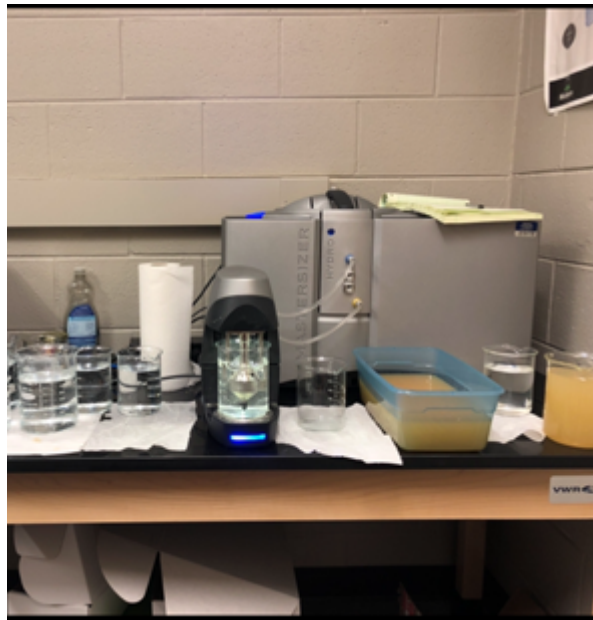
Figure 25 Malvern Master-Sizer 2000 Laser Diffraction Particle-Size Analyzer equipped with a Hydro 2000G pump accessory.

Individual and cumulative weight percentages were calculated for each sample by grain-size class. Grain-size classes were recorded in phi units. Phi units were calculated using Equation 5.

$-\log_2$ d (Grain-size diameter in mm) = phi units   (Equation 5)

Grain-size in phi units was plotted versus individual and cumulative weight percentages on the dependent axis. Individual weight percentages were plotted to create histograms. Cumulative weight percentages were plotted as a cumulative frequency curve. From the frequency curve, the following phi percentile values were interpolated: 5%, 16%, 25%, 50%, 75%, 84%, and 95% (Appendix B). Percentile values were used to calculate various graphical statistical parameters: mean, median, standard deviation (sorting), skewness, and kurtosis (Equations 6 – 10) (Folk and Ward, 1957).

$$\text{Mean} = \frac{\varphi16 + \varphi50 + \varphi84}{3}$$ (Equation 6)

$$\text{Median} = \varphi50$$ (Equation 7)

$$\text{Sorting} = \frac{\varphi16 + \varphi84}{4} + \frac{\varphi95 - \varphi5}{6.6}$$ (Equation 8)

$$\text{Skewness} = \frac{\varphi16 + \varphi84 - 2(\varphi50)}{2(\varphi84 - \varphi16)} + \frac{\varphi5 + \varphi95 - 2(\varphi50)}{2(\varphi95 - \varphi5)}$$ (Equation 9)

$$\text{Kurtosis} = \frac{\varphi95 - \varphi5}{2.44(\varphi75 - \varphi25)}$$ (Equation 10)

4.7 End Member Mixing Analysis (EMMA)

End member mixing analysis (EMMA) is an eigenspace decomposition technique that uses end members from the dataset based on the design of various scaling procedures. More details on the EMMA method are provided by Weltje (1997), Weltje

and Prins (2003, 2007). EMMA assumes that grain-size distributions are formed from distinct sediment populations and deposited by a limit number of geologic processes. Unmixed end member proportions will shift according to the proportional change that is contributing to the transport processes in a sample (Collins et al., 2018).

Grain-size classes containing zero values were ignored to avoid numerical instabilities, and all samples were normalized to a sum of 100% (Dietze et al., 2012). EMMA extracts end members from the eigenspace of a dataset. End member models compare the mean modeled coefficient of determination (R^2) across grain-size classes and samples. One issue that develops is keeping a balance between high R^2 and the number of end members in order to balance the EMMA model. Therefore, the maximum number of end members used in this study is six, with an R^2 coefficient of determination of 0.83.

EMMA for grain-size was calculated after Dietze et al. (2012) using the extension EMMAgeo from the R studio packages (Dietze and Dietze, 2019). The current package is an updated version of Dietze and Dietze (2013). Common practice to reduce bias interpretations is allowing an outside source to interpret a maximum number of end members. Dr. Joe Collins of Middle Tennessee State University provided the interpretations for maximum number of end members to balance the EMMA model.

EMMA modeling was applied to the grain-size distribution dataset to identify stratigraphic variations at a macroscopic level. EMMA generated a six-end member model (Figure 26) from the combined grain-size dataset explaining 83% of the cumulative variance across all 185 samples. This model was based on the explained variance curve of eigenvectors, the goodness-of-fit (mean total r^2), and the principle of

parsimony (Figure 27). The end member distribution was plotted for each sediment

sample to form a stratigraphic profile of the five cores (see figure 44).
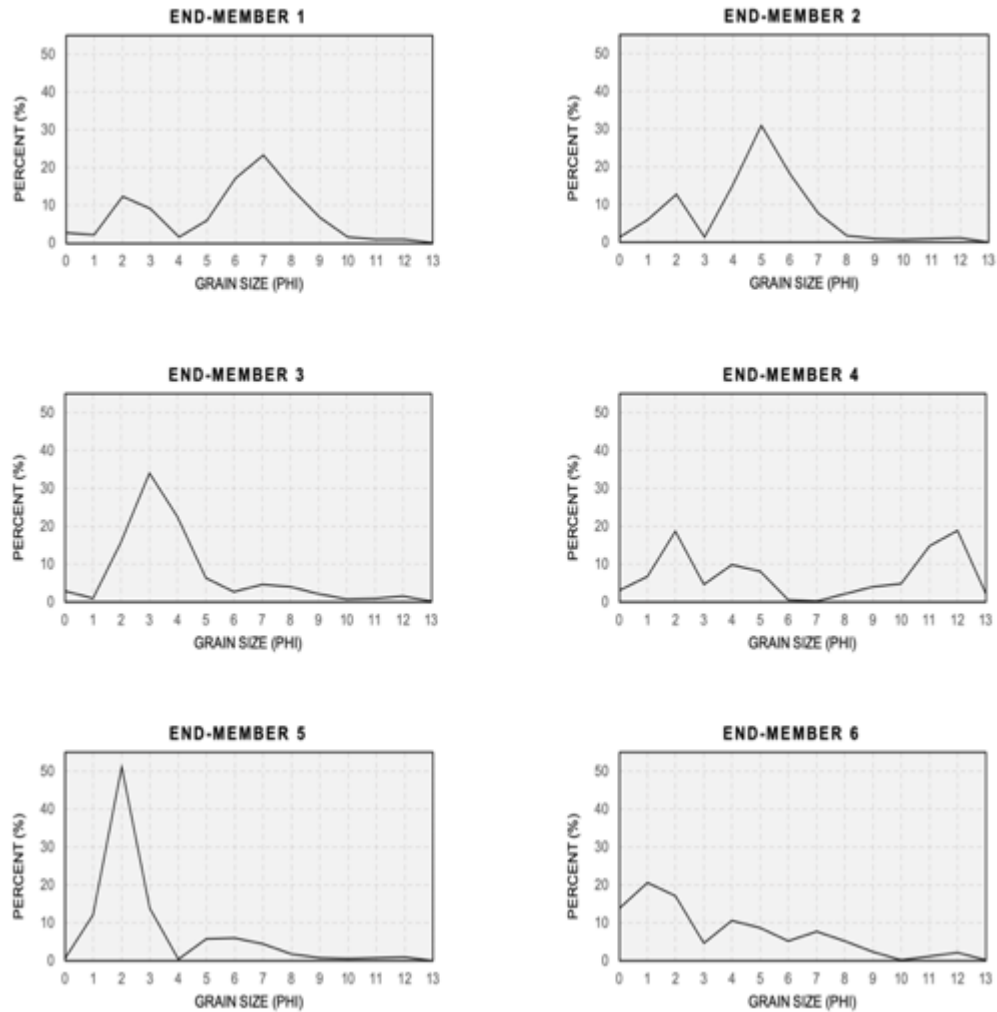
Figure 26. Six end members unmixed by EMMA.
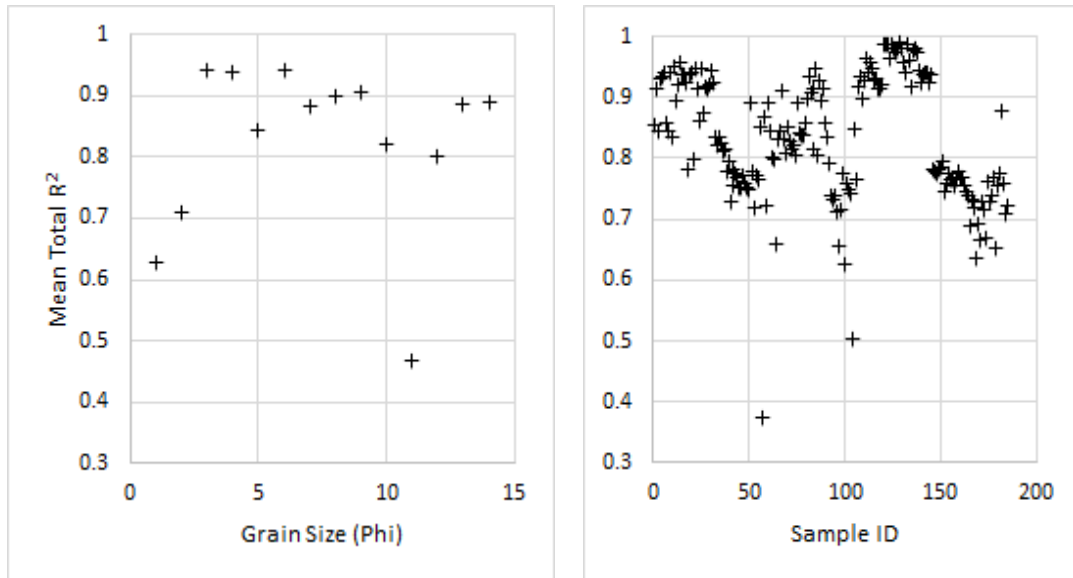
Figure 27. (Left) Mean total R^2 of the size end members versus variable (Grain-Size) and (Right) sample space (Sample ID).

4.8 Radiocarbon Dating

Accelerator mass spectrometry (AMS) - calibrated ^{14}C radiocarbon dates were performed in the Keck-Carbon Cycle AMS facility at the University of California, Irvine. Eight dates were obtained by measuring the total organic carbon fraction of the bulk sediment samples (Table 2). Samples were collected along the center of the core using a sterilized stainless-steel spatula to avoid any contact with the walls of the core to prevent contamination. The samples were extracted from the core and placed into a labeled sterilized glass vial.

Standard Operating Procedures at the Keck-Carbon Cycle AMS facility follow these guidelines:

"Radiocarbon concentrations are given as fractions of the Modern standard, Δ ^{14}C, and conventional radiocarbon age, following the conventions of Stuiver and Polach (Radiocarbon, v. 19, p.355, 1977). Sample preparation backgrounds have

been subtracted, based on measurements of ^{14}C-free coal. All results have been corrected for isotopic fractionation according to the conventions of Stuiver and Polach (1977), with d^{13}C values measured on prepared graphite using the AMS spectrometer. These can differ from d^{13}C of the original material and are not shown. These samples were treated with acid (1N HCl, 75°C) to remove carbonates prior to combustion."

Table 2. Core sample locations for ^{14}C radiocarbon dates.

Core Name	Sample Depth (cm)	Sample Material
Core 1	43 – 45	Organic Sediment
Core 1	67 – 69	Organic Sediment
Core 2	28 – 20	Organic Sediment
Core 2	61 – 63	Organic Sediment
Core 3	23 – 25	Organic Sediment
Core 3	46 – 48	Organic Sediment
Core 4	58 – 60	Organic Sediment
Core 5	26 – 28	Organic Sediment

CHAPTER V

RESULTS

This chapter describes the results of analyzing clastic cave sediments from Russell Cave in this research. Profiles of these results were produced for each core that was sectioned by the different techniques. The first section reports the results of the intensity of the sediment profile using RGB wavelength color. The second section reports the results of loss on ignition and magnetic susceptibility. The next three sections are developed using the grain-size distribution dataset acquired from grain-size analysis. The final section reports the results acquired from ^{14}C age dating.

5.1 Photo-Documentation and Color Description of Cores

Results of RGB color from each of the core showed gradual to sharp variations between the darker and lighter sediments (Figure 28). Lighter sediments (light browns, grays, oranges) caused RGB intensity values to be larger, while darker sediments (dark browns, grays, blacks) had lower RGB intensity values. Sharp contacts (peaks) were associated with significant changes in sediment color. Gradual contacts were associated with minor changes in sediment color. Mud cracks were present in Core 2, Core 3, and Core 5 (due to drying between zones of sediment grain-size change prior to photo-documentation), which caused significant drops in intensity values (Figure 28).
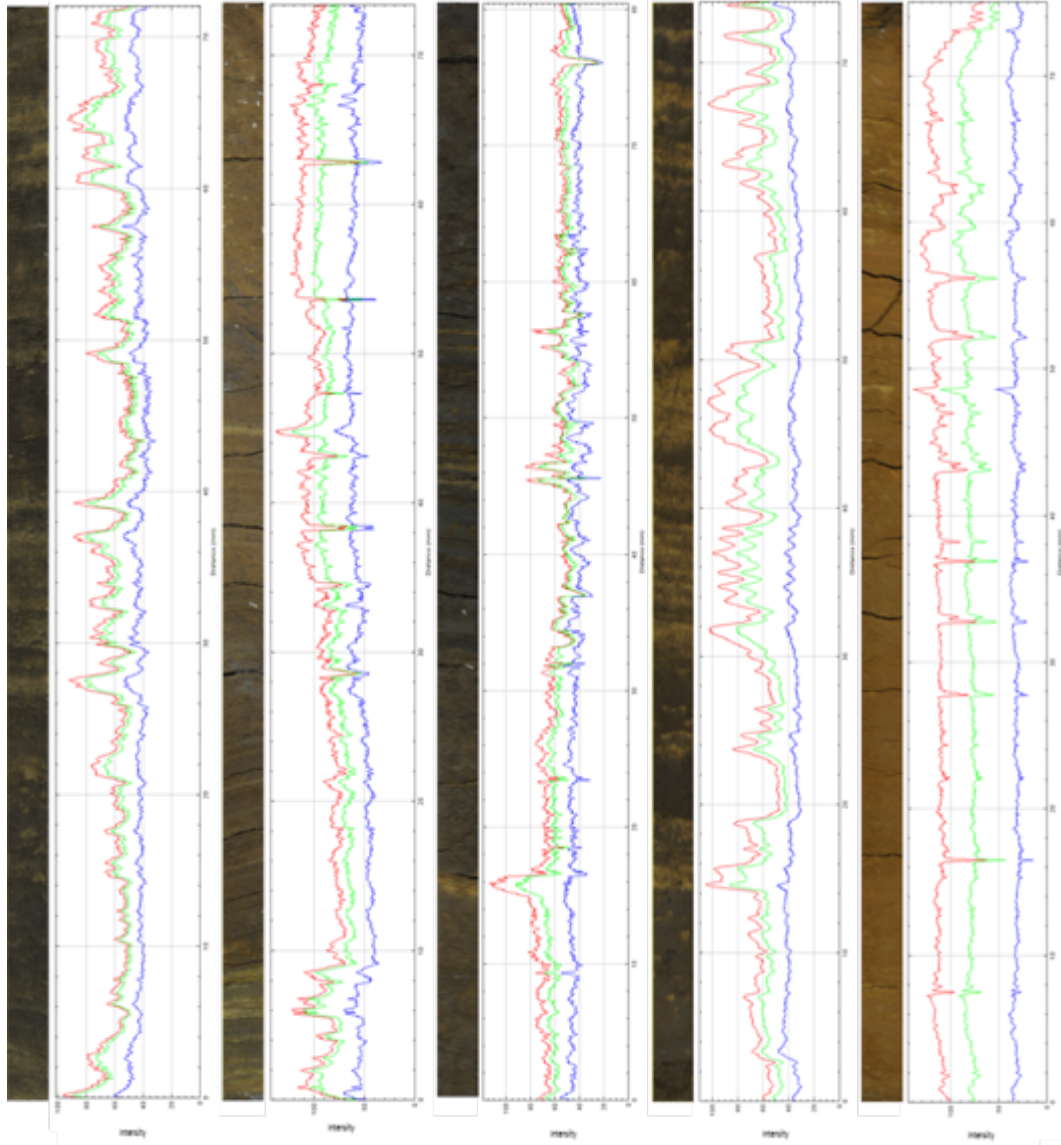
Figure 28. RGB color profiles with sediment core profiles

5.2 Loss on Ignition (LOI) and Magnetic Susceptibility

5.2.1 Core 1 LOI and Magnetic Susceptibility

Stratigraphic profiles of Core 1 were created for water content (LOI_{105}), organic matter (LOI_{550}), and magnetic susceptibility (Figure 29). The water content in Core 1 ranged from 7.67 – 21.71%, with an average of 15.12%. The lowest water content value was found at 44 – 46 cm, and the highest value was found at 64 – 66 cm. Organic matter ranged from 2.82 – 41.91%, with an average of 7.85%. The lowest organic matter value was found at 52 – 54 cm, and the highest value was found at 44 – 46 cm. g ranged from 2.96E-07 – 4.60E-07 m^3/kg, with an average of 3.79E-07 m^3/kg. The lowest magnetic susceptibility value was found at 44 – 46 cm, and the highest value was found at 58 – 60 cm. Organic matter value recorded and organic matter range in Core 1 was highest between all five of the cores. Organic matter and magnetic susceptibility averages values in Core 1 were the highest of all five cores. Tables showing raw data of water content, organic matter, and magnetic susceptibility in Core 1 can be found in Appendix C.
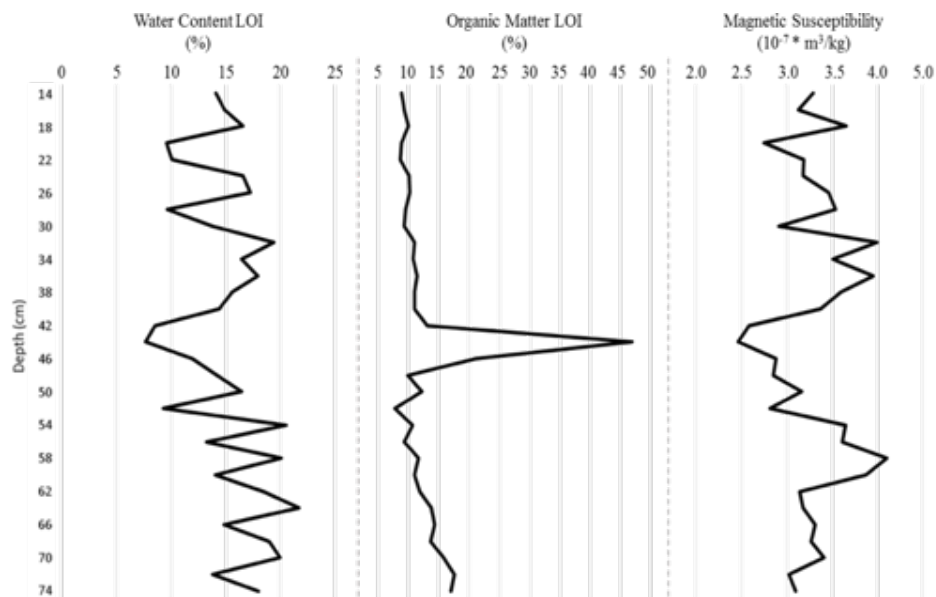
Figure 29. Core 1 stratigraphic profile showing water content, organic matter, and magnetic susceptibility.

Stratigraphic profiles of Core 2 were created for water content (LOI_{105}), organic

matter (LOI_{550}), and magnetic susceptibility (Figure 30). The water content in Core 2

ranged from 13.71 – 18.67%, with an average of 16.67%. The lowest water content value

was found at 68 – 70 cm, and the highest value found at 58 – 60 cm. Water content was

not measured at depth 60 - 62 cm due to errors during measurements. Organic matter

ranged from 1.63 – 2.69%, with an average of 2.22%. The lowest organic matter value

was found at 0 – 2 cm, and the highest value was found at 20 – 22 cm. Magnetic

susceptibility ranged from 0.536E-07 – 2.52E-07 m^3/kg, with an average of 1.93E-07

m^3/kg. The lowest magnetic susceptibility value was found at 66 – 68 cm, and the highest

magnetic susceptibility value was found at 56 – 58 cm. Water content and organic matter

ranges in Core 2 were the smallest compared to the other cores. Tables showing raw data

of water content, organic matter, and magnetic susceptibility in Core 2 can be found in

Appendix C.
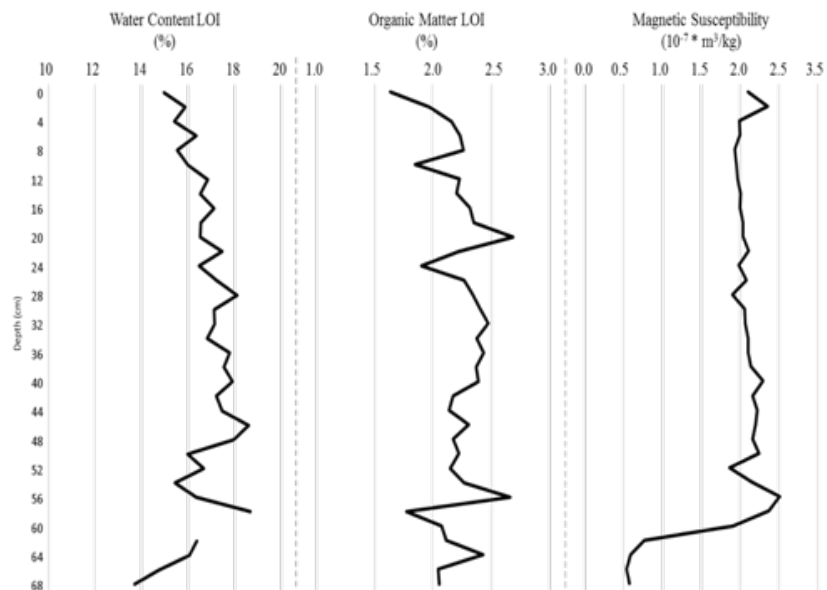
Figure 30. Core 2 stratigraphic profile showing water content, organic matter, and magnetic susceptibility.

Stratigraphic profiles of Core 3 were created for water content (LOI_{105}), organic

matter (LOI_{550}), and magnetic susceptibility (Figure 31). The water content in Core 3

ranged from 0.95 – 30.37%, with an average of 22.36%. The lowest water content value

was found at 68 – 70 cm, and the highest value was found at 38 – 40 cm. Organic matter

ranged from 2.78 – 13.87%, with an average of 7.33%. The lowest organic matter value

was found at 74 – 76 cm, and the highest value was found at 40 – 42 cm. Magnetic

susceptibility ranged from 1.34E-07 – 5.21E-07 m^3/kg, with an average of 3.73E-07

m^3/kg. The lowest magnetic susceptibility value was found at 30 – 32 cm, and the highest

value was found at 62 – 64. The lowest water content value between all five cores was in

Core 3. The highest organic matter value, magnetic susceptibility value, and average

water content of all cores were found in Core 3. Tables showing raw data of water

content, organic matter, and magnetic susceptibility in Core 3 can be found in Appendix

C.
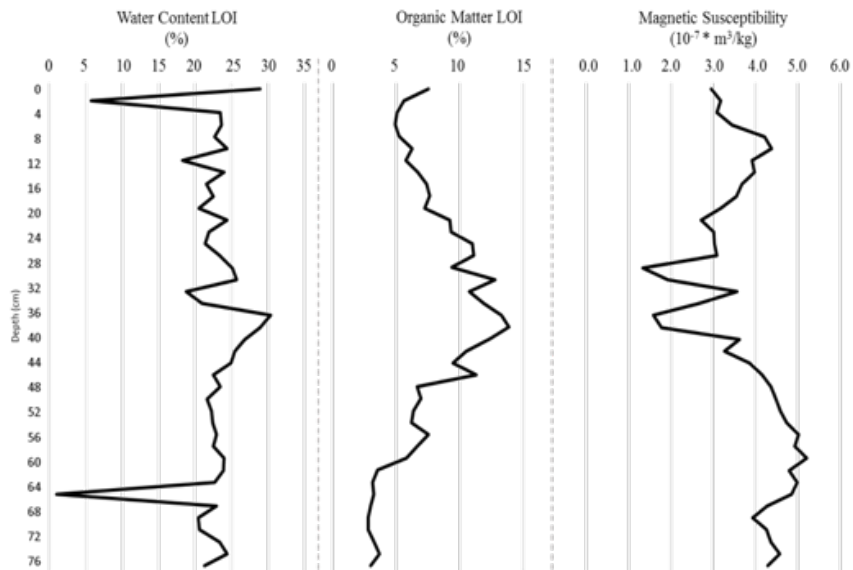
Figure 31. Core 3 stratigraphic profile showing water content, organic matter, and magnetic susceptibility.

5.2.4 Core 4 LOI and Magnetic Susceptibility

Stratigraphic profiles of Core 4 were created for water content (LOI_{105}), organic matter (LOI_{550}), and magnetic susceptibility (Figure 32). The water content in Core 4 ranged from 4.76 – 17.31%, with an average of 11.59%. The lowest water content value was found at 52 – 54 cm, and the highest value was found at 30 – 32 cm. Organic matter ranged from 0.95 – 4.45%, with an average of 2.05%. The lowest organic matter value was found at 50 – 52 cm, and the highest value was found at 12 – 14 cm. Magnetic susceptibility ranged from 1.41E-07 – 3.60E-07 m^3/kg, with an average of 2.46E-07 m^3/kg. The lowest magnetic susceptibility value was found at 40 – 42 cm, and the highest value was found at 16 – 18 cm. The lowest organic matter value recorded in five cores was in Core 4. Average values for water content and organic matter in Core 4 were also the lowest. Tables showing raw data of water content, organic matter, and magnetic susceptibility in Core 4 can be found in Appendix C.
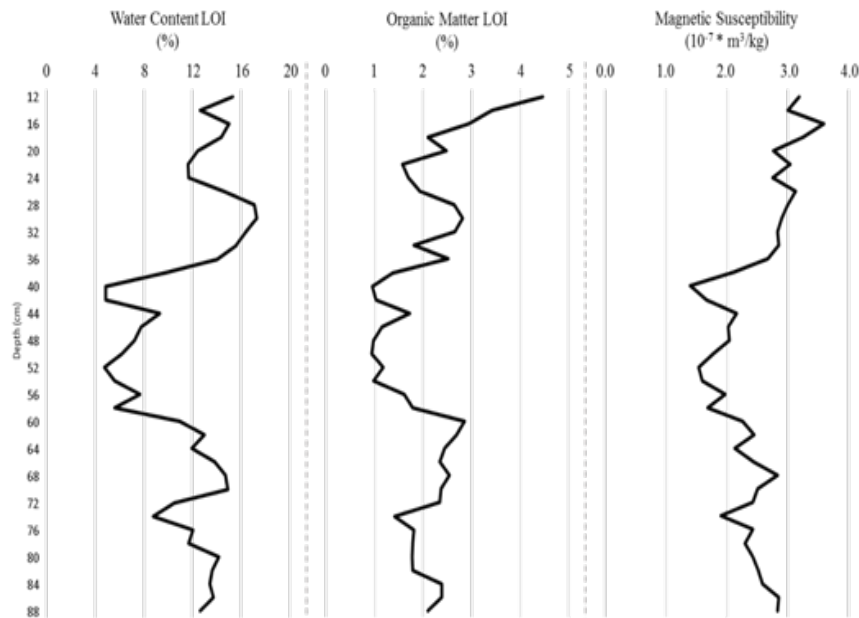
Figure 32. Core 4 stratigraphic profile showing water content, organic matter, and magnetic susceptibility.

5.2.5 Core 5 LOI and Magnetic Susceptibility

Stratigraphic profiles of Core 5 were created for water content (LOI_{105}), organic

matter (LOI_{550}), and magnetic susceptibility (Figure 33). The water content in Core 5

ranged from 14.25 – 21.25%, with an average of 18.35%. The lowest water content value

was found at 72 – 74 cm, and the highest value was found at 20 – 22 cm. Organic matter

ranged from 1.48 – 3.13%, with an average of 2.42%. The lowest organic matter value

was found at 12 – 14 cm, and the highest value was found at 20 – 22 cm. Magnetic

susceptibility ranged from 1.36E-07 – 2.68E-07 m^3/kg, with an average of 1.80E-07

m^3/kg. The lowest magnetic susceptibility value was found at 0 – 2 cm, and the highest

value was found at 72 – 74 cm. The average magnetic susceptibility value and magnetic

susceptibility range in Core 5 were the lowest of all five cores. Tables showing raw data

of water content, organic matter, and magnetic susceptibility in Core 5 can be found in

Appendix C.
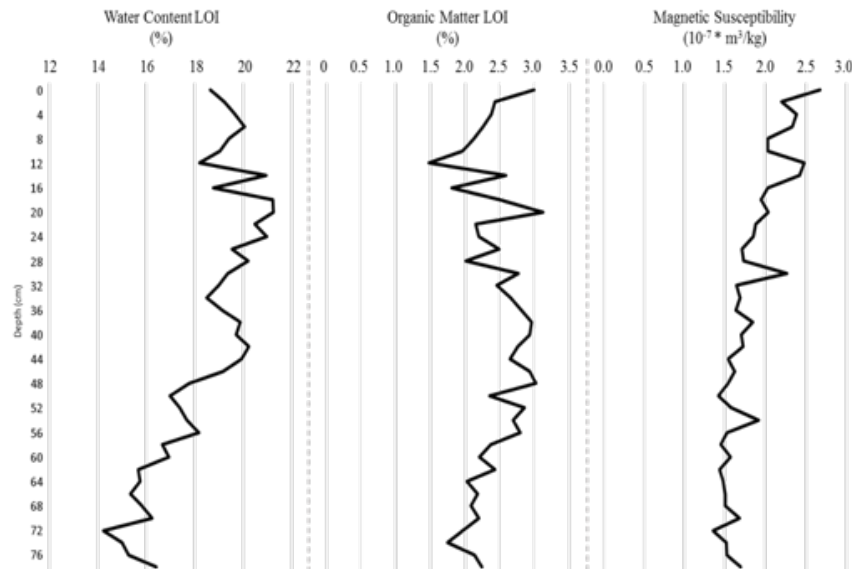
Figure 33. Core 5 stratigraphic profile showing water content, organic matter, and magnetic susceptibility.

5.3 Grain Size Distribution

5.3.1 Core 1 Distribution

      Grain-size distribution in Core 1 ranged from coarse sand to clays $(0 - > 8$ phi /

$1.0 - < 0.0039$ mm) (Figure 34). Based on the histogram, no single grain class had a

frequency distribution greater than 30% in Core 1 (Figure 34). Grain-size distribution

was mesokurtic to platykurtic. The skewness of Core 1 was coarse-skewed to very fine-

skewed. Core 1 was very poorly sorted, dominated by a sandy silt sediment texture.

Samples 8 and 10 had a clayey silt sediment texture, and samples 15, 16, 21, 30, and 31

had a silty sand sediment texture. Summary statistics were calculated for each sample

within Core 1 (Table 3). Sediment texture classification of Core 1 was plotted on a

Shepard diagram (Appendix D) to determine the sediment texture classification (ex.

sandy silt) (Table 3).

Figure 34. Grain-size distribution of Core 1 reported in phi units.

Table 3. Core 1 sample description using graphical statistics and sediment texture classification.

Sample Number	Sample Depth (cm)	Sample Description
1	14 – 16	Poorly sorted, near symmetrical, mesokurtic, sandy silt
2	16 – 18	Very poorly sorted, coarse-skewed, mesokurtic, sandy silt
3	18 – 20	Poorly sorted, near symmetrical, mesokurtic, sandy silt
4	20 – 22	Very poorly sorted, fine-skewed, platykurtic, sandy silt
5	22 – 24	Very poorly sorted, fine-skewed, platykurtic, sandy silt
6	24 – 26	Very poorly sorted, near symmetrical, platykurtic, sandy silt
7	26 – 28	Very poorly sorted, fine-skewed, platykurtic, sandy silt
8	28 – 30	Very poorly sorted, coarse-skewed, mesokurtic, clayey silt
9	30 – 32	Very poorly sorted, near symmetrical, platykurtic, sandy silt
10	32 – 34	Poorly sorted, coarse-skewed, leptokurtic, clayey silt
11	34 – 36	Poorly sorted, fine-skewed, mesokurtic, sandy silt
12	36 – 38	Very poorly sorted, near symmetrical, mesokurtic, sandy silt
13	38 – 40	Very poorly sorted, near symmetrical, platykurtic, sandy silt
14	40 – 42	Very poorly sorted, coarse-skewed, platykurtic, sandy silt
15	42 – 44	Very poorly sorted, very fine-skewed, platykurtic, silty sand
16	44 – 46	Very poorly sorted, fine-skewed, platykurtic, silty sand
17	46 – 48	Very poorly sorted, fine-skewed, platykurtic, sandy silt
18	48 – 50	Very poorly sorted, near symmetrical, platykurtic, sandy silt
19	50 – 52	Very poorly sorted, fine-skewed, platykurtic, sandy silt
20	52 – 54	Very poorly sorted, near symmetrical, platykurtic, sandy silt
21	54 – 56	Very poorly sorted, near symmetrical, platykurtic, silty sand
22	56 – 58	Very poorly sorted, fine-skewed, mesokurtic, sandy silt
23	58 – 60	Very poorly sorted, fine-skewed, mesokurtic, sandy silt
24	60 – 62	Very poorly sorted, fine-skewed, leptokurtic, sandy silt
25	62 – 64	Very poorly sorted, coarse-skewed, very platykurtic, sandy silt
26	64 – 66	Very poorly sorted, fine-skewed, mesokurtic, sandy silt
27	66 – 68	Very poorly sorted, near symmetrical, platykurtic, sandy silt
28	68 – 70	Very poorly sorted, fine-skewed, mesokurtic, sandy silt
29	70 – 72	Very poorly sorted, fine-skewed, platykurtic, sandy silt
30	72 – 74	Very poorly sorted, very fine-skewed, leptokurtic, silty sand
31	74 – 76	Very poorly sorted, very fine-skewed, mesokurtic, silty sand

Grain-size distribution in Core 2 ranged from medium sand to clays ($1 - > 8$ phi / $0.50 - < 0.0039$ mm) (Figure 35). Based on the histogram, no single grain class had a frequency distribution greater than 30% in Core 2 (Figure 35). Grain-size distribution was mesokurtic except samples 9 and 15, which were leptokurtic. The skewness of Core 2 was near symmetrical to very fine-skewed. Core 2 was very poorly sorted, dominated by a sandy silt sediment texture. Samples 9, 18, 22, 26, and 33 had a clayey silt sediment texture, and sample 32 had the only silt sediment texture in Core 2. Summary statistics were calculated for each sample within Core 2 (Table 4). Sediment texture classification of Core 2 was plotted on a Shepard diagram (Appendix D) to determine the sediment texture classification (ex. sandy silt) (Table 4).

Figure 35. Grain-size distribution of Core 2 reported in phi units.

61

Table 4. Core 2 sample description using graphical statistics and sediment texture classification.

Sample Number	Sample Depth (cm)	Sample Description
1	0 – 2	Very poorly sorted, fine-skewed, mesokurtic, sandy silt
2	2 – 4	Very poorly sorted, fine-skewed, mesokurtic, sandy silt
3	4 – 6	Very poorly sorted, fine-skewed, mesokurtic, sandy silt
4	6 – 8	Very poorly sorted, fine-skewed, mesokurtic, sandy silt
5	8 – 10	Very poorly sorted, fine-skewed, mesokurtic, sandy silt
6	10 – 12	Very poorly sorted, fine-skewed, mesokurtic, sandy silt
7	12 – 14	Very poorly sorted, fine-skewed, mesokurtic, sandy silt
8	14 – 16	Very poorly sorted, fine-skewed, mesokurtic, sandy silt
9	16 – 18	Very poorly sorted, fine-skewed, leptokurtic, clayey silt
10	18 – 20	Very poorly sorted, fine-skewed, mesokurtic, sandy silt
11	20 – 22	Very poorly sorted, fine-skewed, mesokurtic, sandy silt
12	22 – 24	Very poorly sorted, fine-skewed, mesokurtic, sandy silt
13	24 – 26	Poorly sorted, fine-skewed, mesokurtic, sandy silt
14	26 – 28	Very poorly sorted, fine-skewed, mesokurtic, sandy silt
15	28 – 30	Very poorly sorted, fine-skewed, leptokurtic, sandy silt
16	30 – 32	Very poorly sorted, fine-skewed, mesokurtic, sandy silt
17	32 – 34	Very poorly sorted, fine-skewed, mesokurtic, sandy silt
18	34 – 36	Very poorly sorted, fine-skewed, mesokurtic, clayey silt
19	36 – 38	Very poorly sorted, fine-skewed, mesokurtic, sandy silt
20	38 – 40	Very poorly sorted, very fine-skewed, mesokurtic, sandy silt
21	40 – 42	Very poorly sorted, fine-skewed, mesokurtic, sandy silt
22	42 – 44	Very poorly sorted, fine-skewed, mesokurtic, clayey silt
23	44 – 46	Very poorly sorted, fine-skewed, mesokurtic, sandy silt
24	46 – 48	Very poorly sorted, fine-skewed, mesokurtic, sandy silt
25	48 – 50	Very poorly sorted, fine-skewed, mesokurtic, sandy silt
26	50 – 52	Very poorly sorted, fine-skewed, mesokurtic, clayey silt
27	52 – 54	Very poorly sorted, very fine-skewed, mesokurtic, sandy silt
28	54 – 56	Very poorly sorted, very fine-skewed, mesokurtic, sandy silt
29	56 – 58	Very poorly sorted, very fine-skewed, mesokurtic, sandy silt
30	58 – 60	Very poorly sorted, very fine-skewed, mesokurtic, sandy silt
31	60 – 62	Poorly sorted, fine-skewed, mesokurtic, sandy silt
32	62 – 64	Poorly sorted, near symmetrical, mesokurtic, silt
33	64 – 66	Very poorly sorted, very fine-skewed, mesokurtic, clayey silt
34	66 – 68	Very poorly sorted, fine-skewed, mesokurtic, sandy silt
35	68 – 70	Very poorly sorted, near symmetrical, mesokurtic, sandy silt

Grain-size distribution in Core 3 ranged from coarse sand to clays (0 – > 8 phi / 1.0 – < 0.0039 mm) (Figure 36). Based on the histogram, one-grain class had a frequency distribution greater than 30% in Core 3. The frequency distribution of coarse silt from sample 33 was 30.9% in Core 3 (Figure 36). Grain-size distribution was mesokurtic to leptokurtic with the exception of samples 1, 10, 11, 14, and 16 that were platykurtic. The skewness of Core 3 was near symmetrical to fine-skewed. Core 3 was very poorly sorted, dominated by a sandy silt sediment texture. Samples 27 to 36 had a finer-grained sediment texture in Core 3 that was classified as silt to clayey silt. Summary statistics were calculated for each sample within Core 3 (Table 5). Sediment texture classification of Core 3 was plotted on a Shepard diagram (Appendix D) to determine the sediment texture classification (ex. sandy silt) (Table 5).

Figure 36. Grain-size distribution of Core 3 reported in phi units.

Table 5. Core 3 sample description using graphical statistics and sediment texture classification.

Sample Number	Sample Depth (cm)	Sample Description
1	0 – 2	Very poorly sorted, fine-skewed, platykurtic, sandy silt
2	2 – 4	Very poorly sorted, fine-skewed, mesokurtic, sandy silt
3	4 – 6	Very poorly sorted, near symmetrical, mesokurtic, sandy silt
4	6 – 8	Poorly sorted, fine-skewed, mesokurtic, sandy silt
5	8 – 10	Poorly sorted, fine-skewed, mesokurtic, sandy silt
6	10 – 12	Poorly sorted, near symmetrical, mesokurtic, sandy silt
7	12 – 14	Very poorly sorted, near symmetrical, mesokurtic, sandy silt
8	14 – 16	Poorly sorted, near symmetrical, mesokurtic, sandy silt
9	16 – 18	Very poorly sorted, fine-skewed, mesokurtic, sandy silt
10	18 – 20	Poorly sorted, near symmetrical, platykurtic, sandy silt
11	20 – 22	Very poorly sorted, near symmetrical, platykurtic, sandy silt
12	22 – 24	Poorly sorted, near symmetrical, mesokurtic, sandy silt
13	24 – 26	Very poorly sorted, fine-skewed, mesokurtic, sandy silt
14	26 – 28	Very poorly sorted, fine-skewed, platykurtic, sandy silt
15	28 – 30	Very poorly sorted, fine-skewed, mesokurtic, sandy silt
16	30 – 32	Very poorly sorted, near symmetrical, platykurtic, sandy silt
17	32 – 34	Very poorly sorted, near symmetrical, mesokurtic, sandy silt
18	34 – 36	Very poorly sorted, fine-skewed, mesokurtic, sandy silt
19	36 – 38	Very poorly sorted, fine-skewed, mesokurtic, sandy silt
20	38 – 40	Very poorly sorted, fine-skewed, leptokurtic, sandy silt
21	40 – 42	Very poorly sorted, near symmetrical, mesokurtic, sandy silt
22	42 – 44	Very poorly sorted, fine-skewed, mesokurtic, sandy silt
23	44 – 46	Very poorly sorted, near symmetrical, mesokurtic, sandy silt
24	46 – 48	Very poorly sorted, fine-skewed, leptokurtic, sandy silt
25	48 – 50	Very poorly sorted, fine-skewed, leptokurtic, sandy silt
26	50 – 52	Very poorly sorted, fine-skewed, mesokurtic, sandy silt
27	52 – 54	Poorly sorted, fine-skewed, mesokurtic, clayey silt
28	54 – 56	Very poorly sorted, fine-skewed, leptokurtic, clayey silt
29	56 – 58	Very poorly sorted, fine-skewed, leptokurtic, clayey silt
30	58 – 60	Very poorly sorted, fine-skewed, leptokurtic, clayey silt
31	60 – 62	Very poorly sorted, fine-skewed, leptokurtic, clayey silt
32	62 – 64	Poorly sorted, fine-skewed, leptokurtic, clayey silt
33	64 – 66	Poorly sorted, fine-skewed, mesokurtic, silt
34	66 – 68	Very poorly sorted, fine-skewed, leptokurtic, clayey silt
35	68 – 70	Poorly sorted, fine-skewed, mesokurtic, silt
36	70 – 72	Poorly sorted, fine-skewed, leptokurtic, silt
37	72 – 74	Very poorly sorted, fine-skewed, mesokurtic, sandy silt
38	74 – 76	Very poorly sorted, near symmetrical, mesokurtic, clayey silt
39	76 – 78	Very poorly sorted, fine-skewed, mesokurtic, sandy silt
40	78 – 80	Very poorly sorted, fine-skewed, mesokurtic, sandy silt

5.3.4 Core 4 Distribution

Grain-size distribution in Core 4 ranged from coarse sand to clays (0 – > 8 phi / 1.0 – < 0.0039 mm) (Figure 37). Based on the histogram, the fine sand grain class had 20 of its 39 samples with a frequency distribution greater than 30%. Grain-size distribution varied from mesokurtic, platykurtic, leptokurtic, and very leptokurtic in Core 4. The skewness of Core 4 was very fine-skewed except samples 24, 37, and 39, which were fine-skewed. Core 4 was very poorly sorted, dominated by a silty sand sediment texture. Very leptokurtic grain-size distributions were only associated with a sand sediment texture. Granules and pebbles with a max diameter of 15 mm were removed from sample 38 prior to grain-size analysis due to the inability of the Malvern Master-Sizer 2000 processing grains coarser than sand. Summary statistics were calculated for each sample within Core 4 (Table 6). Sediment texture classification of Core 4 was plotted on a Shepard diagram (Appendix D) to determine the sediment texture classification (ex. silty sand) (Table 6).
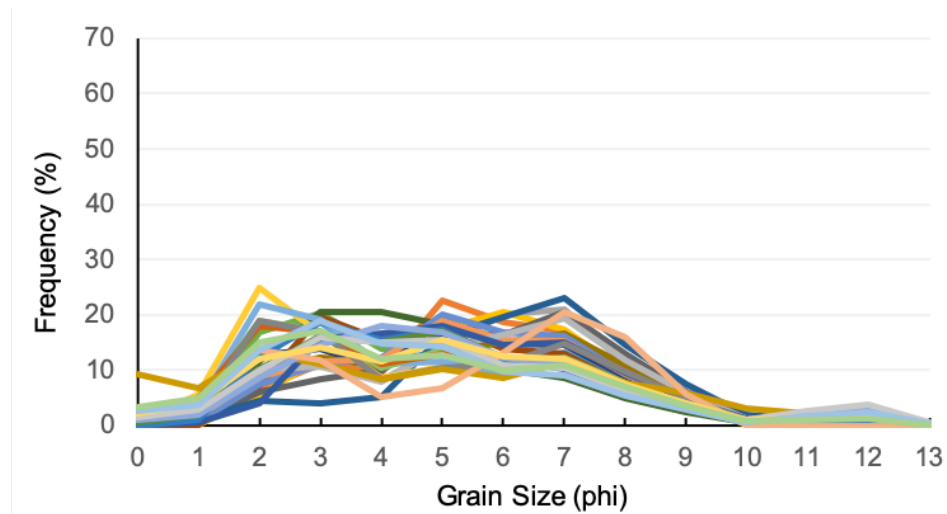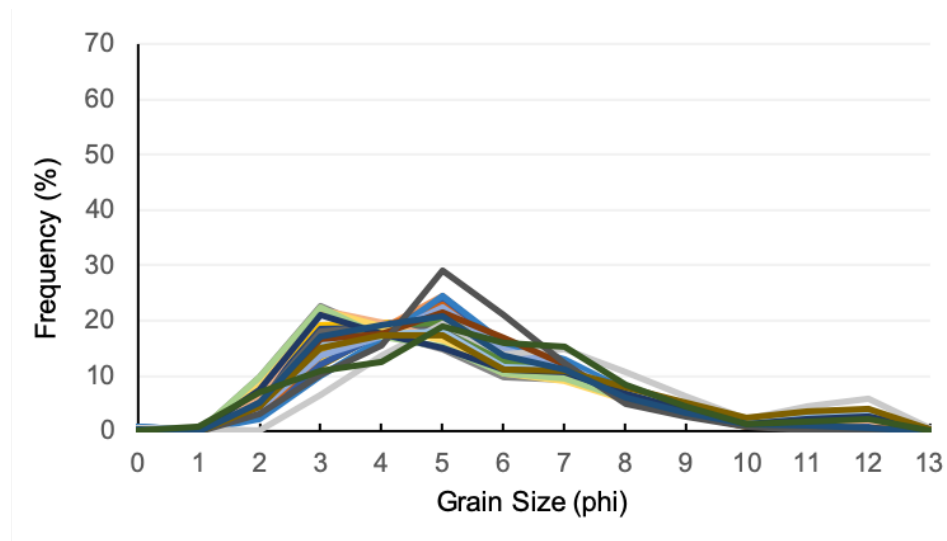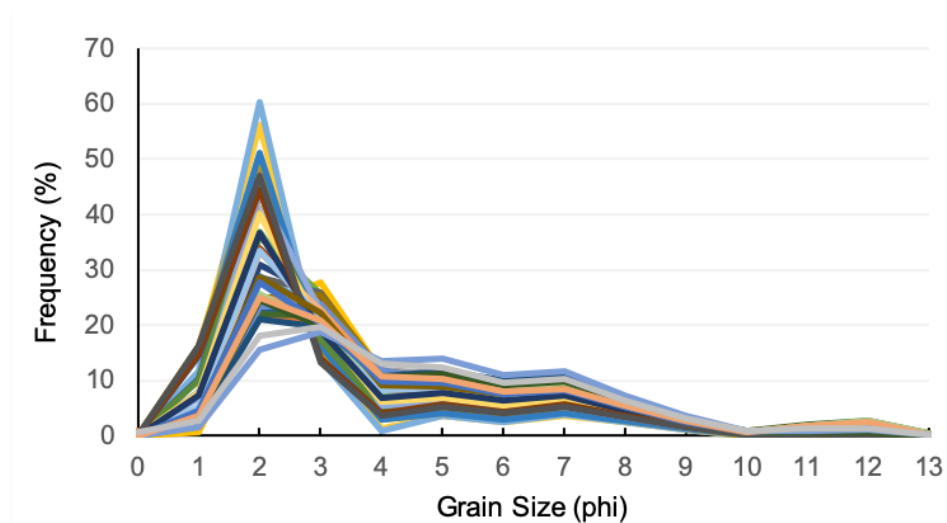

Figure 37. Grain-size distribution of Core 4 reported in phi units.

Table 6. Core 4 sample description using graphical statistics and sediment texture classification.

Sample Number	Sample Depth (cm)	Sample Description
1	12 – 14	Very poorly sorted, very fine-skewed, mesokurtic, silty sand
2	14 – 16	Very poorly sorted, very fine-skewed, platykurtic, silty sand
3	16 – 18	Very poorly sorted, very fine-skewed, mesokurtic, silty sand
4	18 – 20	Very poorly sorted, very fine-skewed, platykurtic, silty sand
5	20 – 22	Poorly sorted, very fine-skewed, leptokurtic, silty sand
6	22 – 24	Very poorly sorted, very fine-skewed, mesokurtic, silty sand
7	24 – 26	Very poorly sorted, very fine-skewed, mesokurtic, silty sand
8	26 – 28	Very poorly sorted, very fine-skewed, mesokurtic, silty sand
9	28 – 30	Very poorly sorted, very fine-skewed, platykurtic, silty sand
10	30 – 32	Very poorly sorted, very fine-skewed, platykurtic, silty sand
11	32 – 34	Very poorly sorted, very fine-skewed, mesokurtic, silty sand
12	34 – 36	Very poorly sorted, very fine-skewed, mesokurtic, silty sand
13	36 – 38	Very poorly sorted, very fine-skewed, mesokurtic, silty sand
14	38 – 40	Very poorly sorted, very fine-skewed, mesokurtic, silty sand
15	40 – 42	Poorly sorted, very fine-skewed, very leptokurtic, sand
16	42 – 44	Poorly sorted, very fine-skewed, very leptokurtic, sand
17	44 – 46	Very poorly sorted, very fine-skewed, mesokurtic, silty sand
18	46 – 48	Poorly sorted, very fine-skewed, very leptokurtic, sand
19	48 – 50	Poorly sorted, very fine-skewed, very leptokurtic, silty sand
20	50 – 52	Poorly sorted, very fine-skewed, very leptokurtic, sand
21	52 – 54	Poorly sorted, very fine-skewed, very leptokurtic, sand
22	54 – 56	Poorly sorted, very fine-skewed, very leptokurtic, sand
23	56 – 58	Very poorly sorted, very fine-skewed, leptokurtic, silty sand
24	58 – 60	Poorly sorted, very fine-skewed, leptokurtic, silty sand
25	60 – 62	Very poorly sorted, very fine-skewed, platykurtic, silty sand
26	62 – 64	Very poorly sorted, very fine-skewed, platykurtic, silty sand
27	64 – 66	Very poorly sorted, very fine-skewed, mesokurtic, silty sand
28	66 – 68	Very poorly sorted, very fine-skewed, platykurtic, silty sand
29	68 – 70	Very poorly sorted, very fine-skewed, mesokurtic, silty sand
30	70 – 72	Very poorly sorted, very fine-skewed, mesokurtic, silty sand
31	72 – 74	Very poorly sorted, very fine-skewed, leptokurtic, silty sand
32	74 – 76	Poorly sorted, very fine-skewed, very leptokurtic, sand
33	76 – 78	Very poorly sorted, very fine-skewed, platykurtic, silty sand
34	78 – 80	Very poorly sorted, fine-skewed, platykurtic, sandy silt
35	80 – 82	Very poorly sorted, very fine-skewed, platykurtic, silty sand
36	82 – 84	Very poorly sorted, very fine-skewed, platykurtic, silty sand
37	84 – 86	Very poorly sorted, fine-skewed, platykurtic, sandy silt
38	86 – 88	Very poorly sorted, very fine-skewed, platykurtic, silty sand
39	88 – 90	Very poorly sorted, fine-skewed, platykurtic, sandy silt

Grain-size distribution in Core 5 ranged from medium sand to clays ($1 -> 8$ phi /

$0.50 - < 0.0039$ mm) (Figure 38). Based on the histogram, one-grain class had a

frequency distribution greater than 30% in some samples. The frequency distribution of

medium silt from samples 4 to 7 was greater than 30% in Core 5. Grain-size distribution

was primarily mesokurtic. Platykurtic distribution was associated with four samples in

the lower portion of Core 5, and sample 24 had the only leptokurtic grain-size

distribution. The skewness of Core 5 was near-symmetrical to fine-skewed, except for

sample 27 that was very fine skewed. Core 5 was poorly sorted to very poorly sorted,

dominated by a silt sediment texture for the upper portion and by either clayey silt or

sandy silt sediment texture for the lower portion of the core. Summary statistics were

calculated for each sample within Core 5 (Table 7). Sediment texture classification of

Core 5 was plotted on a Shepard diagram (Appendix D) to determine the sediment texture
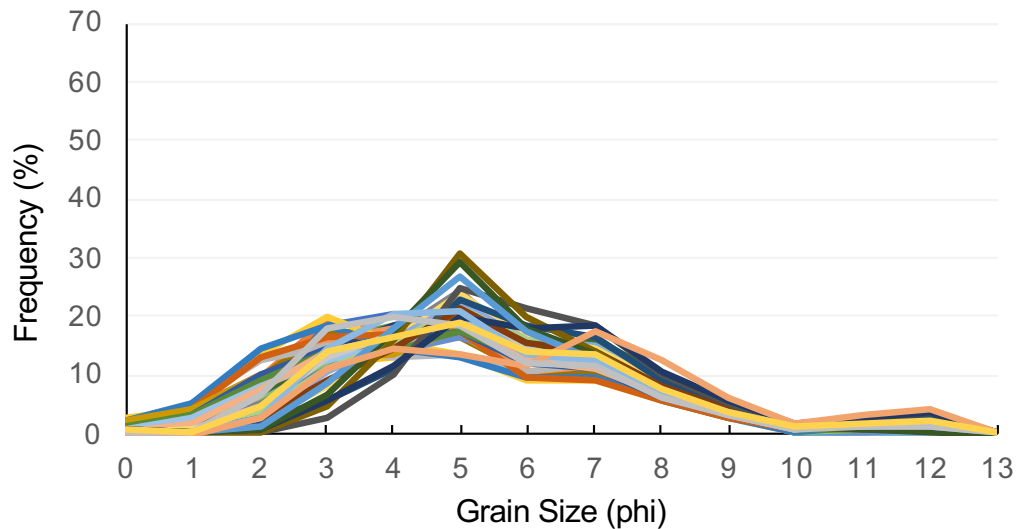
classification (ex. sandy silt) (Table 7).
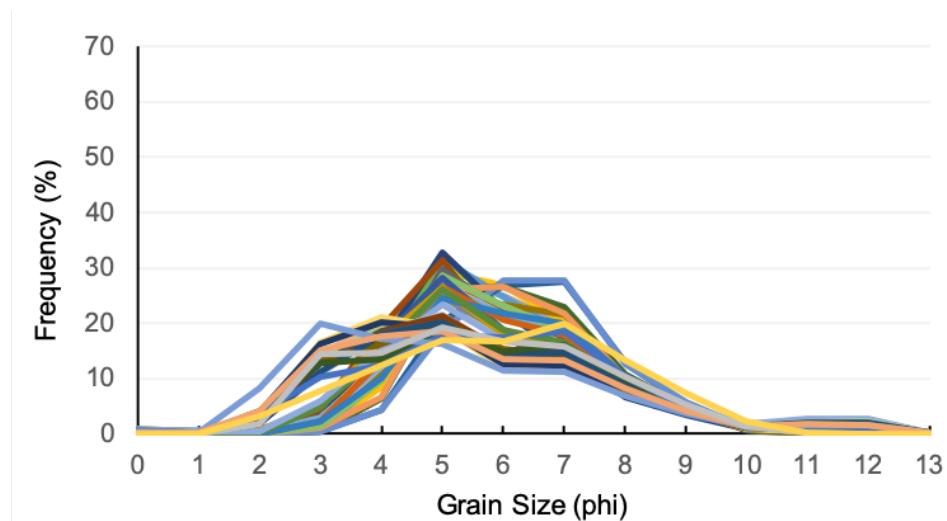
Figure 38. Grain-size distribution of Core 5 reported in phi units.

Table 7. Core 5 sample description using graphical statistics and sediment texture classification.

Sample Number	Sample Depth (cm)	Sample Description
1	0 – 2	Poorly sorted, fine-skewed, mesokurtic, silt
2	2 – 4	Poorly sorted, fine-skewed, mesokurtic, silt
3	4 – 6	Poorly sorted, fine-skewed, mesokurtic, silt
4	6 – 8	Poorly sorted, fine-skewed, mesokurtic, silt
5	8 – 10	Poorly sorted, fine-skewed, mesokurtic, silt
6	10 – 12	Poorly sorted, fine-skewed, mesokurtic, silt
7	12 – 14	Poorly sorted, fine-skewed, mesokurtic, silt
8	14 – 16	Poorly sorted, fine-skewed, mesokurtic, silt
9	16 – 18	Poorly sorted, near symmetrical, mesokurtic, silt
10	18 – 20	Poorly sorted, near symmetrical, mesokurtic, silt
11	20 – 22	Poorly sorted, fine-skewed, mesokurtic, silt
12	22 – 24	Poorly sorted, near symmetrical, mesokurtic, silt
13	24 – 26	Poorly sorted, fine-skewed, mesokurtic, silt
14	26 – 28	Poorly sorted, fine-skewed, mesokurtic, silt
15	28 – 30	Poorly sorted, fine-skewed, mesokurtic, silt
16	30 – 32	Poorly sorted, fine-skewed, mesokurtic, silt
17	32 – 34	Poorly sorted, fine-skewed, mesokurtic, silt
18	34 – 36	Poorly sorted, fine-skewed, mesokurtic, silt
19	36 – 38	Poorly sorted, fine-skewed, mesokurtic, silt
20	38 – 40	Poorly sorted, fine-skewed, mesokurtic, clayey silt
21	40 – 42	Poorly sorted, fine-skewed, mesokurtic, silt
22	42 – 44	Poorly sorted, fine-skewed, mesokurtic, silt
23	44 – 46	Poorly sorted, fine-skewed, mesokurtic, silt
24	46 – 48	Very poorly sorted, fine-skewed, leptokurtic, clayey silt
25	48 – 50	Very poorly sorted, fine-skewed, mesokurtic, sandy silt
26	50 – 52	Very poorly sorted, fine-skewed, mesokurtic, clayey silt
27	52 – 54	Very poorly sorted, very fine-skewed, mesokurtic, sandy silt
28	54 – 56	Very poorly sorted, fine-skewed, mesokurtic, clayey silt
29	56 – 58	Very poorly sorted, fine-skewed, mesokurtic, clayey silt
30	58 – 60	Very poorly sorted, fine-skewed, mesokurtic, sandy silt
31	60 – 62	Poorly sorted, fine-skewed, platykurtic, sandy silt
32	62 – 64	Very poorly sorted, fine-skewed, mesokurtic, clayey silt
33	64 – 66	Very poorly sorted, fine-skewed, mesokurtic sandy silt
34	66 – 68	Very poorly sorted, fine-skewed, mesokurtic, clayey silt
35	68 – 70	Very poorly sorted, near symmetrical, mesokurtic, clayey silt
36	70 – 72	Very poorly sorted, near symmetrical, mesokurtic, clayey silt
37	72 – 74	Very poorly sorted, fine-skewed, mesokurtic, sandy silt
38	74 – 76	Very poorly sorted, fine-skewed, platykurtic, sandy silt
39	76 – 78	Poorly sorted, near symmetrical, platykurtic, clayey silt
40	78 – 80	Poorly sorted, near symmetrical, platykurtic, clayey silt

5.4 Grain Size Composition

5.4.1 Core 1 Composition

The dominant grain-size class in Core 1 was silt, with an average of 15% clay, 53% silt, and 32% sand (Figure 39). Clay composition ranged from 8 – 26%. The lowest percentage of clay was at 34 – 36 cm, and the highest percentage at 32 – 34 cm. Silt composition ranged from 23 – 68%. The lowest percentage of silt was at 72 – 74 cm, and the highest percentage at 14 – 16 cm. Sand composition ranged from 10 – 68%. The lowest percentage of sand was at 32 – 34 cm, and the highest percentage at 72 – 74 cm. Silt and sand-size particles in Core 1 had the highest percentage in grain composition from the overall five cores. Clay, silt, and sand distribution percentages were normalized to 100% (Appendix E).
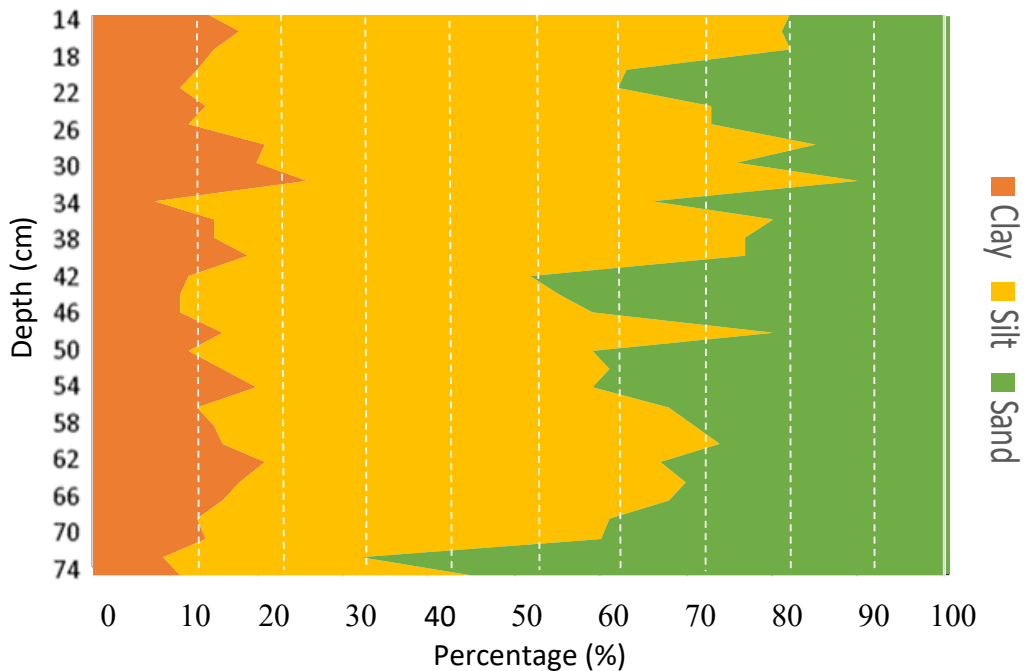
Figure 39. Core 1 stratigraphic profile of clay (left), silt (center), and sand (right) distribution.

5.4.2 Core 2 Composition

The dominant grain-size class in Core 2 was silt, with an average of 16% clay, 63% silt, and 21% sand (Figure 40). Clay composition ranged from 9 – 30%. The lowest percentage of clay was at 62 – 64 cm, and the highest percentage at 50 – 52 cm. Silt composition ranged from 52 – 78%. The lowest percentage of silt was at 38 – 40 cm, and the highest percentage at 62 – 64 cm. Sand composition ranged from 8 – 33%. The lowest percentage of sand was at 50 – 52 cm, and the highest percentage at 38 – 40 cm. Clay size particles in Core 2 made up the highest percentage in grain composition from the overall five cores. Silt and sand-size particles in Core 2 had the lowest distribution range in grain composition from the overall five cores. Clay composition was relatively stable from 0 – 50 cm, with a percentage of $15 \pm 2\%$. Clay, silt, and sand distribution percentages were normalized to 100% (Appendix E).
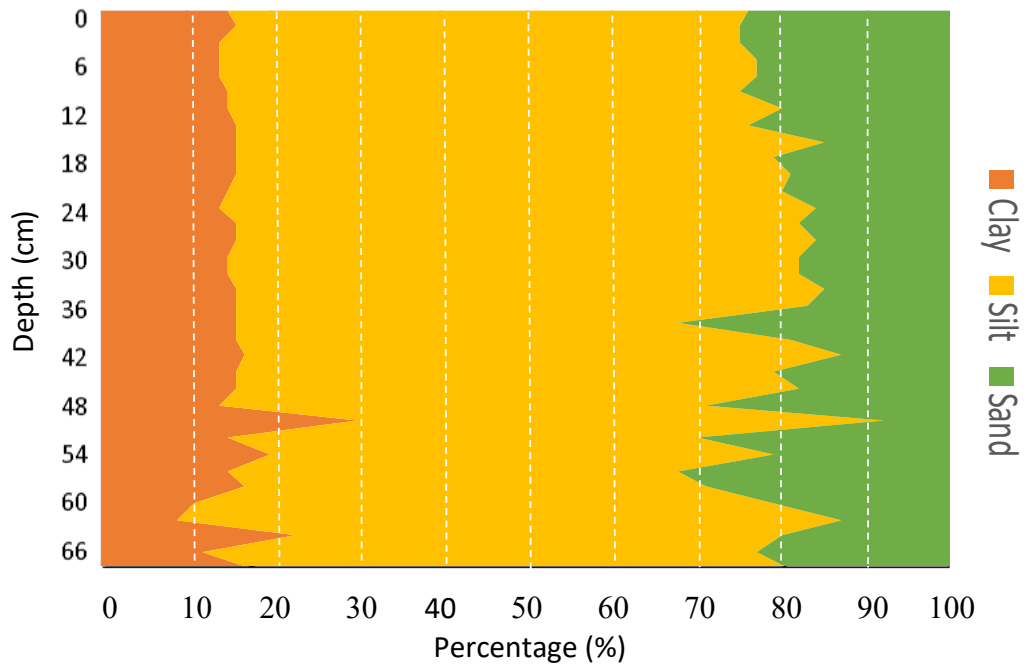
Figure 40. Core 2 stratigraphic profile of clay (left), silt (center), and sand (right) distribution.

5.4.3 Core 3 Composition

      The dominant grain-size class in Core 3 was silt, with an average of 16% clay,

63% silt, and 21% sand (Figure 41). Clay composition ranged from 11 – 29%. The lowest

percentage of clay was at 6 – 8 cm, and the highest percentage at 74 – 76 cm. Silt

composition ranged from 47 – 81%. The lowest percentage of silt was at 34 – 36 cm, and

the highest percentage at 64 – 66 cm. Sand composition ranged from 4 – 41%. The lowest

percentage of sand was at 62 – 64 cm, and the highest percentage at 28 – 30 cm. The

average percent of clay, silt, and sand in Core 3 was the same as the average percent of

clay, silt, and sand in Core 2. Silt and sand composition in Core 3 were larger than Core 2

silt and sand composition. The clay composition in Core 3 was smaller than the clay

composition in Core 2. Clay, silt, and sand distribution percentages were normalized to

100% (Appendix E).
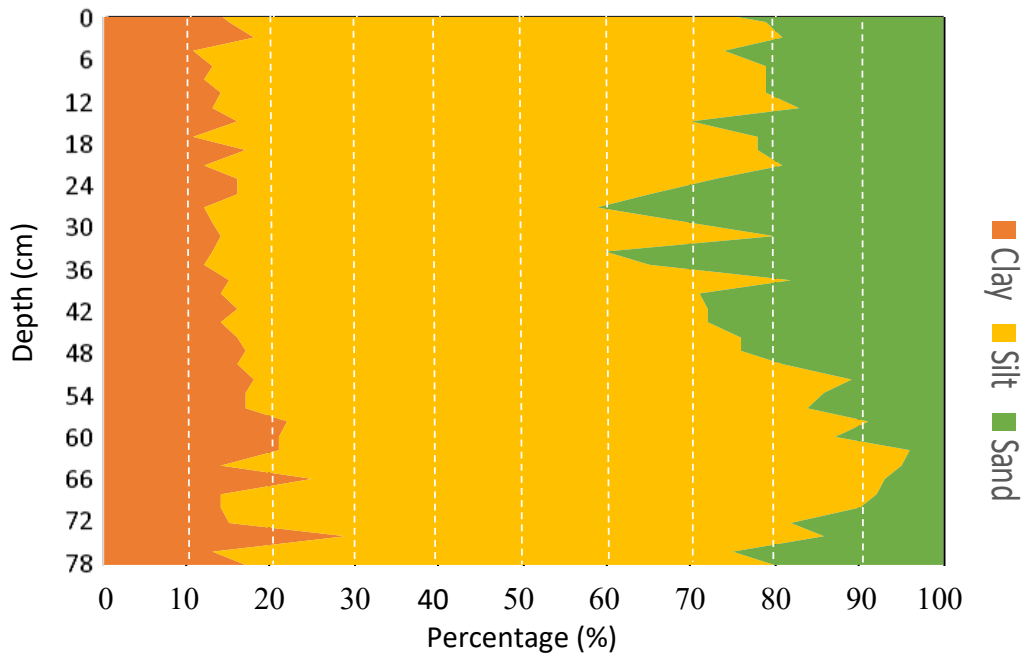
Figure 41. Core 3 stratigraphic profile of clay (left), silt (center), and sand (right) distribution.

5.4.4 Core 4 Composition

The dominant grain-size class in Core 4 was sand, with an average of 9% clay, 30% silt, and 61% sand (Figure 42). Clay composition ranged from 4 – 15%. The lowest percentage of clay was at 40 – 42 cm, and the highest percentage at 32 – 34 cm. Silt composition ranged from 11 – 50%. The lowest percentage of silt was at 42 – 44 cm, and the highest percentage at 84 – 86 cm. Sand composition ranged from 36 – 86%. The lowest percentage of sand was at 84 – 86 cm, and the highest percentage at 42 – 44 cm. The lowest average percent of clay composition and silt composition from the overall five cores was in Core 4. The highest average percent of sand composition from the overall five cores was in Core 4. Clay size particles in Core 4 had the lowest percentage of grain composition from the five cores. Clay, silt, and sand distribution percentages were normalized to 100% (Appendix E).
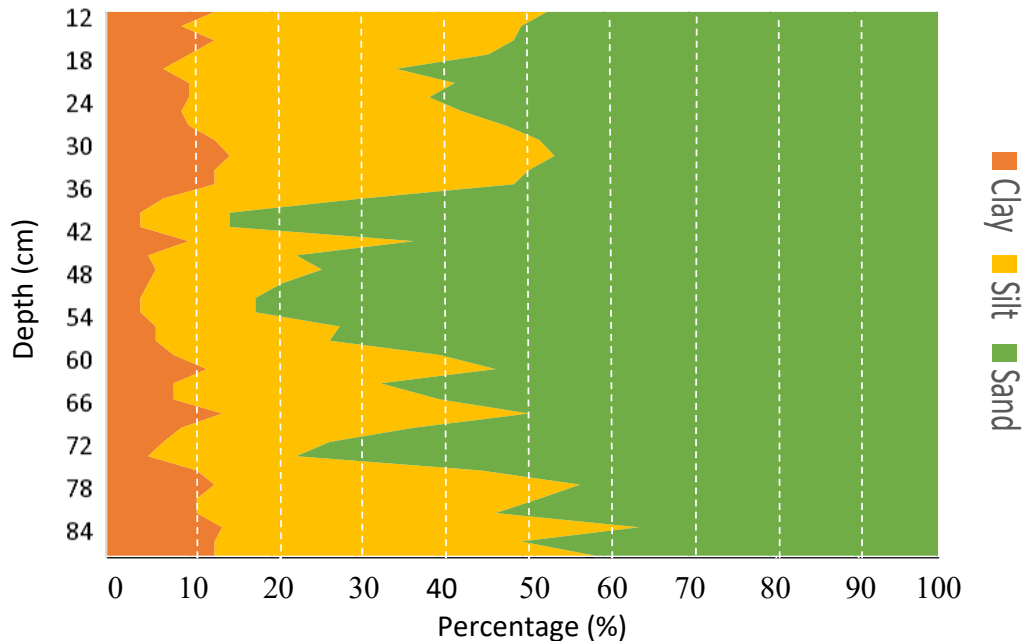
Figure 42. Core 4 stratigraphic profile of clay (left), silt (center), and sand (right) distribution.

5.4.5 Core 5 Composition

The dominant grain-size class in Core 5 was silt, with an average of 17% clay, 74% silt, and 9% sand (Figure 43). Clay composition ranged from 11 – 23%. The lowest percentage of clay was at 10 – 12 cm, and the highest percentage at 78 – 80 cm. Silt composition ranged from 56 – 86%. The lowest percentage of silt was at 72 – 74 cm, and the highest percentage at 10 – 12 cm. Sand composition ranged from 0.5 – 29%. The lowest percentage of sand was at 20 – 22 cm, and the highest percentage at 72 – 74 cm. The lowest average percent of sand composition from the overall five cores was in Core 5. The highest average percent of clay composition and silt composition from the overall five cores was in Core 5. Clay, silt, and sand distribution percentages were normalized to 100% (Appendix E).
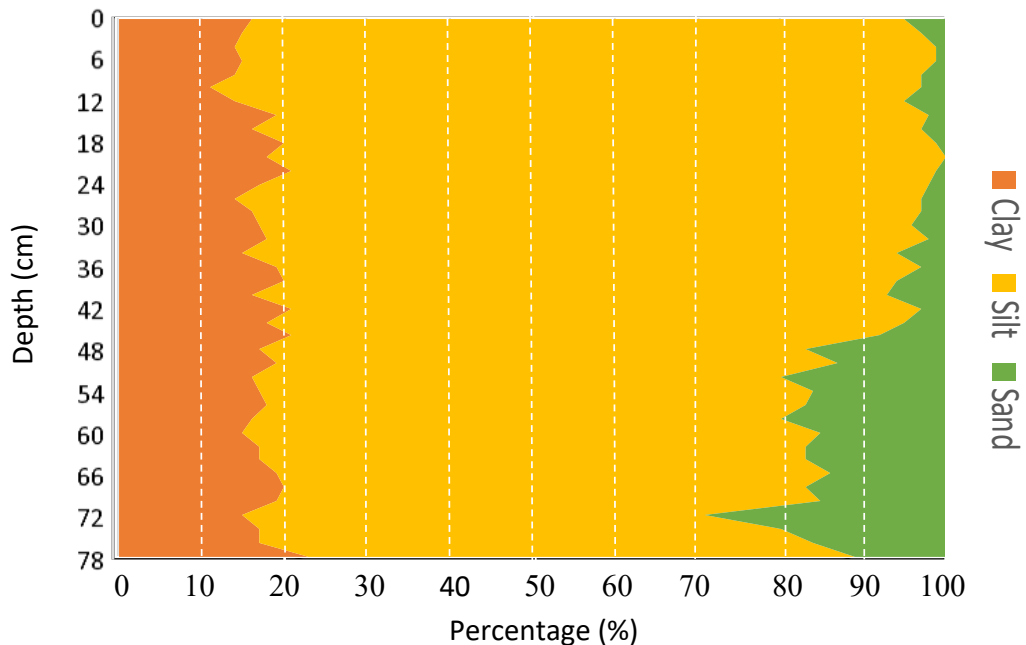
Figure 43. Core 5 stratigraphic profile of clay (left), silt (center), and sand (right) distribution.

5.5 End Member Mixing Analysis Results

5.5.1 End Member 1 Description

End Member 1 is bimodal (Figure 26; p.50) and represented 16.65% of the total variance. End Member 1 had a poorly sorted mode in the silt range (4 – 8 phi / 0.0625 – 0.0039 mm) and a subordinate mode in the fine to very fine sand range (2 – 4 phi / 0.25 – 0.0625 mm) (Figure 26). The end member was found in all samples of Core 2, Core 3, and Core 5 and predominately in most samples from Core 1 (Figure 44). End Member 1 was least represented in Core 4 as it only constitutes 2.83% of the core. Core 5 represented the highest percentage of End Member 1 at 32.00%. End Member 1 represented 80.28% of the end member distribution in sample 10 from Core 1 (Figure 44).

5.5.2 End Member 2 Description

End Member 2 was bimodal (Figure 26) and represented 22.08% of the total variance. End Member 2 was like End Member 1 but was significantly coarse-grained along with a narrower mode. End Member 2 had a narrow mode at the medium silt range (5 – 6 phi / 0.031 – 0.0156 mm) and a subordinate mode in the medium to fine sand range (1 – 3 phi / 0.50 – 0.125 mm) (Figure 26). End Member 2 was found in all samples of Core 2, Core 3, and Core 5 and predominately in most samples from Core 1 (Figure 44). End Member 2 was least represented in Core 4 as it only constitutes 1.76% of the core (Figure 44). Core 5 represented the highest percentage of End Member 2 at 46.67%. End Member 2 represented 82.82% of the end member distribution in sample 6 from Core 5 (Figure 44).
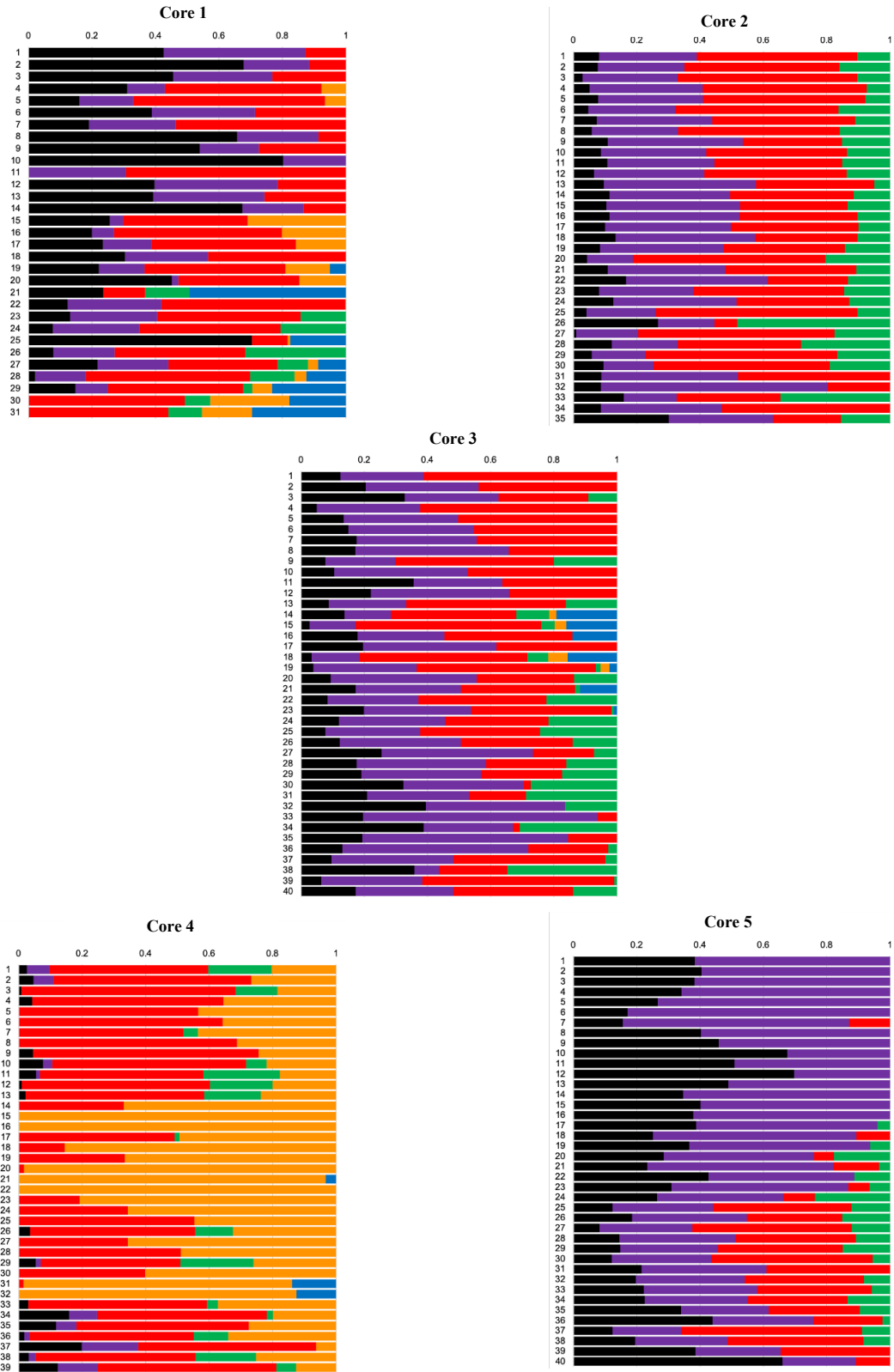
Figure 44. Endmember distribution for each sample from each core.
End Member 1 = black, End Member 2 = purple, End Member 3 = red, End Member 4 = green, End Member 5 = orange, and End Member 6 = blue.

5.5.3 End Member 3 Description

End Member 3 was bimodal (Figure 26) and represented 23.45% of the total variance. End Member 3 had a transition mode at the very fine sand to coarse silt range (3 – 5 phi / 0.125 – 0.031 mm) and broad silt to coarse-grained clay transition (5 – 10 phi / 0.031 – 0.001 mm), followed by a fine tail of clay size grains (> 10 phi / > 0.001 mm) (Figure 26). End Member 3 was associated with all five cores and was found in all samples of Core 2 (Figure 44). End Member 3 was least represented in Core 5 as it only constitutes 16.33% of the core. Core 2 represented the highest percentage of End Member 3 at 43%. End Member 3 represented 71% of the end member distribution in sample 9 from Core 4 (Figure 44).

5.5.4 End Member 4 Description

End Member 4 was tri-modal (Figure 26) and represented 4.61% of the total variance. End Member 4 had a broad mode in the clay range (> 8 phi / > 0.0039 mm), a narrow subordinate mode in the fine sand (2 – 3 phi / 0.25 – 0.125 mm), and a broad subordinate mode in the coarse to medium silt range (4 – 6 phi / 0.0625 – 0.0156 mm) (Figure 26). End Member 4 was associated with all cores and was found in the lower portion of Core 1 and Core 5 (Figure 44). End Member 4 was least represented in Core 1 as it only constitutes 4.05% of the core. Core 2 represented the highest percentage of End Member 4 at 13.96%. End Member 4 represented 48.14% of the end member distribution in sample 26 from Core 2 (Figure 44).

5.5.5 End Member 5 Description

End Member 5 was bimodal (Figure 26) and represented 31.40% of the total variance. End Member 5 had a narrow mode at the fine sand range (2 – 3 phi / 0.25 –

0.125 mm) and a broad subordinate mode in the medium to very fine silt transition (5 – 8 phi / 0.031 – 0.0039 mm) with a fine tail in the clay range (> 8 phi / > 0.0039 mm) (Figure 26). End Member 5 had the highest mode of the overall cores, with 51% of the end member distribution having a fine sand grain-size. End Member 5 was associated with all samples in Core 4 and was totally absent in Core 2 and Core 5 (Figure 44). Several samples were completely represented by 100% of End Member 5 (samples 15, 16, and 22) in Core 4 (Figure 45). Core 4 represented the highest percentage of End Member 5 at 48.32%. End Member 5 was least represented in Core 1 and Core 3, where it only constitutes 5.30% and 0.38%, respectively.
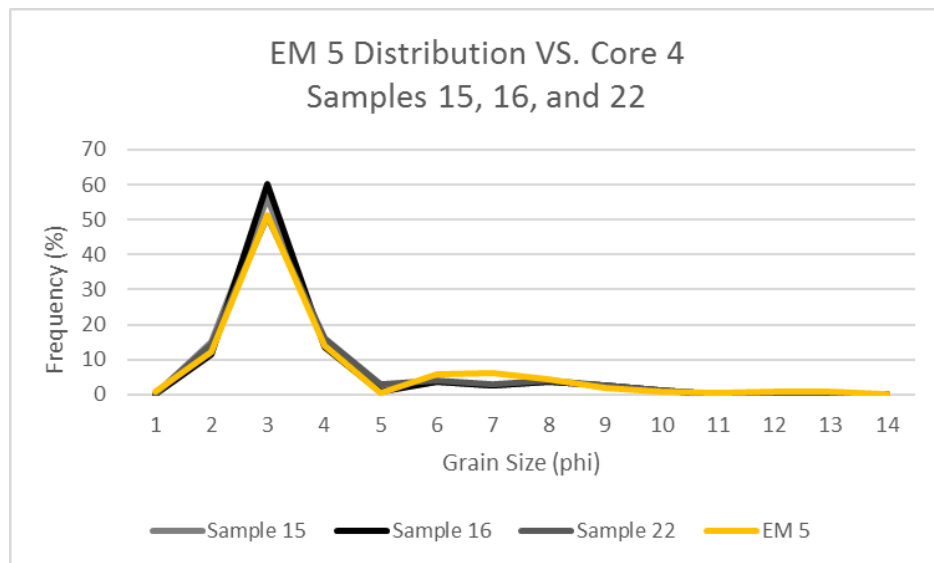
Figure 45. Samples 15, 16, and 22 grain-size distribution from Core 4 representing 100% of End Member 5 grain-size distribution.

5.5.6 End Member 6 Description

End Member 6 was tri-modal (Figure 26) and represented 1.79% of the total variance. End Member 6 had a broad mode in the sand range (0 – 4 phi / 1.0 – 0.0625 mm), a broad subordinate mode in the coarse to medium silt transition (4 – 6 phi / 0.0625 – 0.0156 mm), followed by another broad subordinate mode in the fine silt to clay

transition (6 – 10 phi / 0.0156 – 0.001 mm) with a fine tail in the finer-grained clay range

(> 10 phi / > 0.001 mm) (Figure 26). The grain-size distribution of End Member 6 was

very poorly sorted. End Member 6 had the highest mode with the coarsest grain-size. End

Member 6 was associated with Core 1, Core 3, and Core 4 and was totally absent in Core

2 and Core 5 (Figure 44). End Member 6 was least represented in Core 4 as it only

constitutes 0.76% of the core. End Member 6 represented 49.33% of the end member

distribution in sample 21 from Core 1 (Figure 44).

5.6 Radiocarbon Results

Radiocarbon dating of bulk sediment analysis for eight samples (two samples

from Core 1, two samples from Core 2, two samples from Core 3, one sample from Core

4, and one sample from Core 5 were conducted (Table 8). The stratigraphic position of

the radiocarbon samples collected was recorded in each core (Table 8). The radiocarbon

dating technique was calibrated to measure ^{14}C before present (BP) and referred to as age

in years. The age of the oldest sample was $24,850 \pm 80$ years from Core 1 at 43 – 45 cm.

The age of the youngest sample was $1,305 \pm 15$ years from Core 4 at 58 – 60 cm. Within

Core 1, the oldest sample was located at 43 – 45 cm, and the youngest sample was

located at 67 – 69 cm. Within Core 2, the oldest sample was located at 28 – 30 cm, and

the youngest sample was located at 61 – 63 cm. Within Core 3, the oldest sample was

located at 46 – 48 cm, and the youngest sample was located at 23 – 25 cm.

Table 8. ^{14}C radiocarbon dates of eight samples reported.

Core Name	Sample Depth (cm)	Conventional Radiocarbon Age (^{14}C a $_{BP}$)
Core 1	43 – 45	24,850 ± 80
Core 1	67 – 69	22,100 ± 60
Core 2	28 – 30	23,370 ± 60
Core 2	61 – 63	22,870 ± 60
Core 3	23 – 25	17,200 ± 35
Core 3	46 – 48	23,570 ± 60
Core 4	58 – 60	1,305 ± 15
Core 5	26 – 28	21,716 ± 114

CHAPTER VI

DISCUSSION

This chapter discusses the interpretations of the results to answer the objectives, goals, and hypotheses. The first section interprets sediment profiles showing climatic conditions outside the cave environment by using RGB wavelength color, loss on ignition (LOI), and magnetic susceptibility. The second section interprets grain composition differences between sediment profiles in main passages and side passages using the grain-size distribution dataset. The third section provides interpretations of the goals to determine the different lithological sediment facies and flow history in defined cave zones by grain-size distribution and EMMA. The last section interprets the age of the organics with the sediment to determine if reworking of sediment layers occurs.

6.1 Comparison of Core Sediments Between Passage Types

Sediment core samples were collected from various passage types within Russell Cave to determine if there are differences in sediment bank composition in these passages. Core 1, Core 2, Core 4, and Core 5 were collected from the active portion of the main passage of Russell Cave along discontinuous sediment banks (Figure 21). Core 3 was collected from a side passage (Figure 21), which appeared to be an inactive portion of the cave. This inactive side passage appeared only to receive high water conditions during back flooding.

Sediment profiles were analyzed to determine color distribution, loss on ignition (LOI), and magnetic susceptibility to determine broad climatic changes recorded within cores. It was hypothesized that sediment profiles would show a stable past climate on the surface. To verify this hypothesis, cores should show no drastic changes in color (ex. red

changing to light gray), magnetic susceptibility, and/or organic content. When analyzing the color of sediments within cores, it was found that drastic color changes occur in all cores (Figure 28). Core 1 and Core 4 showed the greatest number of drastic changes in color, while Core 5 showed the least amount of drastic changes. When comparing magnetic susceptibility and organic content to color changes, there is a correlation between these parameters and drastic color changes. For example, changes from dark gray/brown to light gray/yellow at the bottom of Core 2 corresponds to a drop in magnetic susceptibility. Similar correlations exist in all cores when color changes occur.

Organic material percentages result in darker colors within cores (higher organic content) and correspond to decreases in magnetic susceptibility. Overall, there is a relationship between the organic content and magnetic susceptibility in all core samples (Figure 46). Based on drastic changes to sediment color, organic content, and magnetic susceptibility within individual cores, the hypothesis that these deposits represent stable climatic conditions outside the cave is false. Instead, various climatic changes are likely recorded in these sediments; however, the magnitude and nature of these changes are unable to be determined and/or quantified in this thesis.
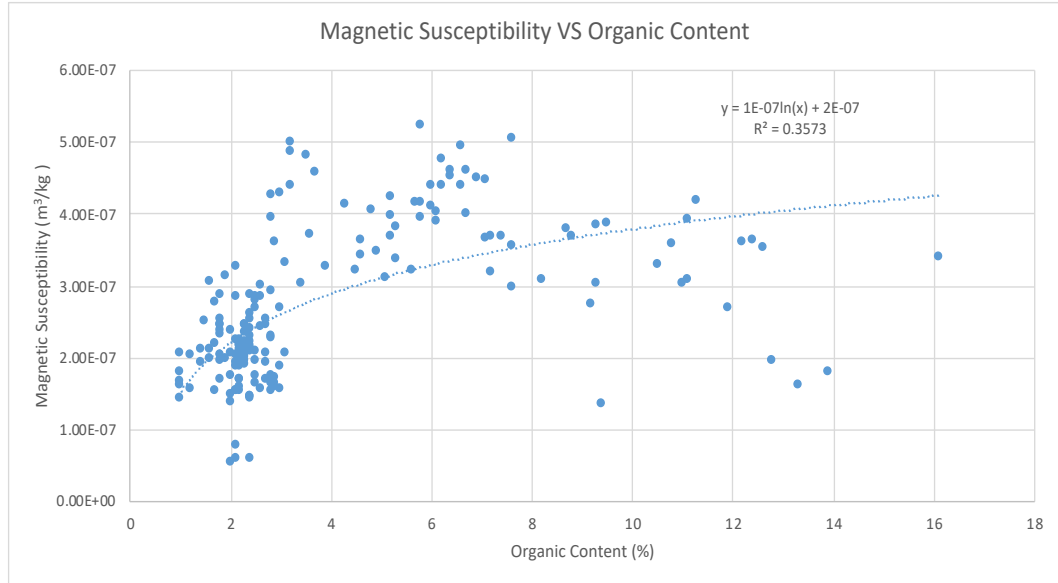
Figure 46. Relationship between magnetic susceptibility and organic content between all 185 samples from Russell Cave.

It was hypothesized that the composition of sediment cores in main passages would primarily be composed of sand, and the composition of side passages would primarily be composed of clay. Core 1 and Core 4 from the main passage all appeared to contain higher percentages of sand (averages between 32% and 61%) than the side passage (21%). Core 2 contains the same percentage of sand (21%) as the side passage (21%). Core 5 has a lower percentage of sand than the side passage (21%). Based on average grain-size percentages from each total core, the hypothesis of grain-size distribution and passage type (main vs. side) is false.

When analyzing the grain-size distribution of each core, Core 1, Core 2, Core 3, and 5 have a similar distribution (Figures 34, 35, 36, and 38), and Core 4 has a skewed (towards the sand grain-size; Figure 37) and consistent distribution that differs from the other four cores. This suggests that overall similar flow conditions resulted in the deposition of the sediment banks at Core 1, Core 2, Core 3, and Core 5. The grain-size distribution of Core 4 appears to be the result of higher energy deposition in the main passage. These

distributions indicate that overall grain-size distribution is not dependent upon the passage type. Furthermore, these distributions suggest that multiple flow regimes exist within a single passage type, resulting in differing grain-size distributions of sediment banks.

6.2 Determination of Sedimentary Facies and EMMA

Based on the grain-size composition of core sediments, two clastic cave sedimentary facies were identified within these samples from Russell Cave. These two facies were: 1) Channel facies, and 2) Slackwater facies (Bosh and White, 2004). All cores appeared to contain both facies; however, it was nearly impossible to differentiate the facies defined by Bosh and White (2004) with these cores. It is also possible that several cores may contain Backswamp facies because back flooding commonly occurs in Russell Cave, which would produce the conditions leading to the deposition of Backswamp facies.

End Member Mixing Analysis (EMMA) was conducted on grain-size distributions in order to determine the mechanism of deposition represented within each core. Six end members were identified by EMMA. These end members represent the fundamental grain-size distributions that, when combined with all other end members, explain the variance observed within the overall grain-size distribution.

End members can be attributed to various depositional conditions (Dietze et al., 2012). End Member 1 is interpreted as a two-component fluvial depositional system of medium to fine silts and clays and fine to very fine sands (Figure 47). Transportation of the finer-grained fraction (silts and clays) is by suspension, and the coarser-grained fraction (sands) is transported by saltation. End Member 2 is interpreted as a two-component fluvial depositional system of medium silts and medium to fine sands (Figure

47). Transport of silt-grained fraction is by suspension, and transport of sand-grained fraction is by saltation. End Member 3 is interpreted as a fluvial depositional system, where both fluvial saltation (sands) and suspended fractions (silts) are contributing (Figure 47) (Dietze et al., 2012; Collins et al., 2017). Transportation of the coarser-grained fine to very fine sands fraction is by saltation, and the finer-grained silts and clays fraction (sands) is transported by suspension. End Member 4 is interpreted as a fine-grained sand fraction deposited by saltation and/or suspension settling by fluvial transport in the channel (Figure 47). The silt-grained fraction represents a shorter time of suspension deposition, and the poorly sorted clay grain fraction represents suspended transport of mixed debris or soil reworking with a mixed composition (Collins et al., 2017). Three possibilities for a tri-modal mixture can be interpreted (Collins et al., 2017): 1) different transport mechanisms in a sediment trap, 2) very poorly sorted sediment load from a flash flood/back flood, or 3) reworking and transport of surficial soil by gravity or fluvial processes. End Member 5 is interpreted as a fluvial depositional system, where both fluvial saltation (sands) and suspended fractions (silts) are contributing (Figure 47) (Dietze et al., 2012; Collins et al., 2017). These result from changes in the shear velocity and vertical components of the current (Collins et al., 2017). End Member 5 indicates a nearly constant flow velocity during deposition (Figure 47). End Member 6 is interpreted as a coarse traction channel deposit, with fine sand fraction occurring by fluvial saltation and suspension settling, and suspension transport/settling of mixed silts and clays derived from reworking of surficial soil deposits (Figure 47).

The dominant deposition of all the EMs was fluvial transport. End Member 1 and End Member 2 were found in all five cores and had a similar size distribution (Figure 47).

These represent a combination of medium to fine sands deposited during normal flow conditions with suspended silts and clays being deposited by suspension settling in slack water conditions by a migrating channel. These EMs are interpreted to represent normal flow conditions within the cave. End Member 3 was found in all cores, and End Member 5 was only found in Core 1, Core 3, and Core 4 (Figure 47). These both had a similar size distribution (Figure 26). End Member 3 is interpreted to represent higher energy flow conditions, likely due to the initial stages of flooding. This gives End Member 3 a higher percentage of the sand grain-size percentage. End Member 4 is interpreted to represent the transition from high energy flow conditions to back flood conditions (extremely slow, suspension settling conditions), giving End Member 4 a trimodal mixture (Figure 47). End Member 5 is interpreted to represent high energy flow conditions, likely due to the retreat stages of flooding when high energy flow conditions return after back flooding. End Member 6 is interpreted to represent flow conditions during the higher than normal conditions that exist after passage flooding during the return to normal flow conditions.
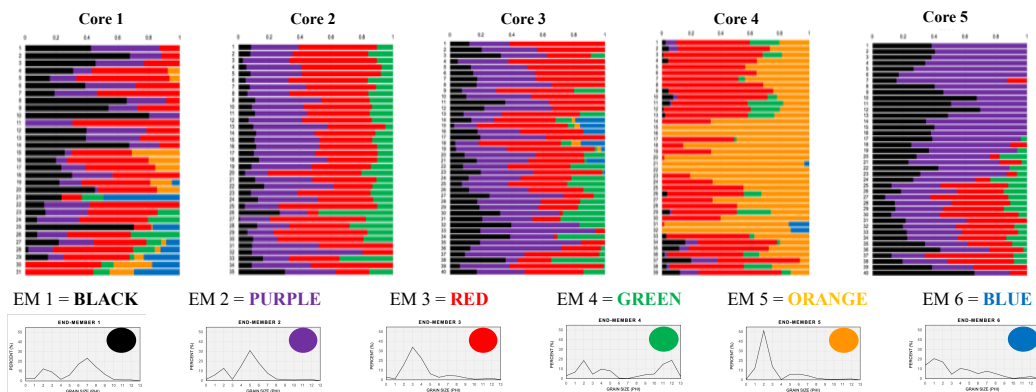
Figure 47. Interpretations of the different end member depositional conditions (refer to Appendix F for larger image of figure).

6.3 Age Determination of Sediments and Sediment Reworking

It was hypothesized that the age of the eight sediment samples collected from the

five cores would be younger than 2000 years. Core 1, Core 2, Core 3, and Core 5 sample

dates returned radiocarbon ages that were older than expected ($17{,}200 \pm 35 - 24{,}850 \pm$

80), Core 4 sample date returned a radiocarbon age that was within the 2000 years old

hypothesis ($1{,}305 \pm 15$). Based on the findings of radiocarbon dating, it appears that the

hypothesis of the age of the sediments is younger than 2000 years is false.

It was also hypothesized that the vertical profiles of sediment banks would show

layers with no reworking after deposition. The radiocarbon dates reported from both Core

1 and Core 2 are inverted (oldest date from the top), and Core 3 had radiocarbon dates

that were normal (oldest date from bottom). Due to only one radiocarbon sample date

being reported from Core 4 and Core 5, it could not be determined if the vertical profiles

were normal or inverted; however, the single age of the organic fraction still determined

if the sediment is younger than 2,000 years. It is important to note that the radiocarbon

age dates only give an age of material dated (bulk organic fraction) and not actual ages of

clastic materials or sedimentation dates. However, these radiocarbon age dates can be

estimates of the maximum age of sedimentation, as deposition could not occur before

organic material existed.

These radiocarbon dates reported suggest that sediment reworking is occurring

within the cave passages. Reworking places older material from upstream deposits above

younger materials, as seen in Core 1 and Core 2. Therefore, the hypothesis that vertical

profiles of sediment banks would show no reworking after depositions is false. Instead, it

appears that some of these sediment banks have been reworked, or some of the materials

found within sediment banks were deposited downstream of a reworked sediment bank. This is an important finding because cave deposits are often referred to as stable, unaffected records of the past. This suggests that cave sediment banks within fluviokarst systems are not closed systems with respect to reworking and mixing.

Additionally, it appears that the bulk of the cave sediment is derived from sedimentation associated with the Last Glacial Maximum (~ 20 kya) and has been trapped and reworked within the cave since. This was implied by radiocarbon dating, inverted dates, sediment color, and decreases in magnetic susceptibility. For example, Core 2 shows reworking (inverted dates) of sediments of lighter color, which lighter colors are typically seen in sediments from cold and/or dry environments (Figure 47) (Ellwood et al., 1996). Other researches with similar findings are Sasowsky et al. (1995), Granger et al. (2001), Sroubek et al. (2001), Anthony and Granger (2004), Anthony and Granger (2006), and Herman et al. (2012).
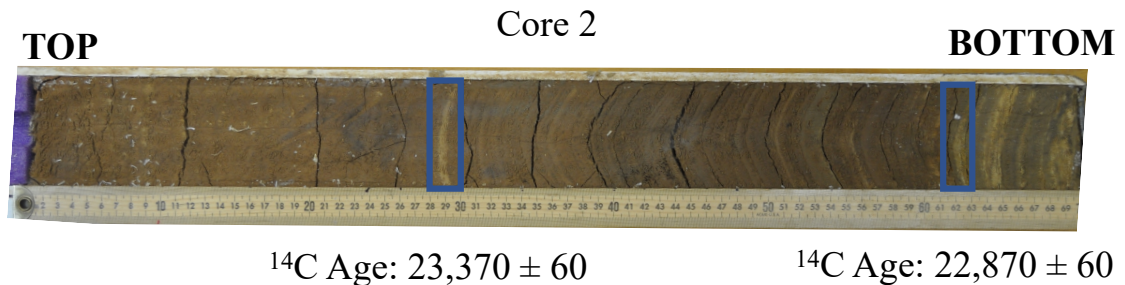
Figure 48. Core 2 showing reworking and radiocarbon dating ages over 20,000 years.

CHAPTER VII

SUMMARY AND CONCLUSIONS

This chapter is a recap of the findings of this thesis. Limitations of this study are discussed in this section. Possible future research is discussed to improve the limited understanding of sediments in fluvial karst systems.

Knowledge of clastic cave sediment preservation in discontinuous sediment banks adds significantly to karst sedimentology (surface and subsurface) in Jackson County, Alabama. The use of cave sediment cores as the primary data source allowed interpretations of the nature of the sediments by giving insight on textural characteristics, depositional history, and environmental landscape disturbances. The different techniques and data collection methods tested on the cave sediment cores were Red-Green-Blue (RGB) color, loss on ignition (LOI), magnetic susceptibility grain-size analysis, end member mixing analysis (EMMA), and ^{14}C radiocarbon dating.

Analyses of cave sediment profiles by the different techniques addressed the following goals: 1) to identify the different lithological sediment facies in defined cave zones and 2) understand how the flow history in these zones were preserved in the sediments. The following hypotheses were tested: 1) sediment profiles show a stable past climate outside the cave environment, 2) composition of sediment profile in main passages was primarily composed of sand, and composition in side passages was primarily composed of clay, 3) the age of the sediments is younger than 2000 years, and 4) vertical profiles of sediment banks show bedding layers with no reworking after deposition.

Based on drastic changes to sediment color, organic content, and magnetic susceptibility within individual cores, it appears that these sediment deposits do not represent stable climatic conditions outside the cave. It was found that drastic color changes occur in all five cores, and there is a correlation between magnetic susceptibility and organic content with these color changes. Higher organic material percentages result in darker colors within cores (higher organic content) and correspond to decreases in magnetic susceptibility. Various climatic changes are recorded in these sediments; however, the magnitude and nature of these changes is unable to be determined and/or quantified.

Based on average grain-size percentages from each total core, it was determined that the overall grain-size distribution does not depend upon if the passage type is main or side. It was hypothesized that the composition of sediment cores in main passages would primarily be composed of sand, and the composition of side passages would primarily be composed of clay. However, overall variable flow conditions resulted in the deposition of the sediment banks within Core 1, Core 2, Core 3, and Core 5, while Core 4 experienced more stable flow conditions. These distributions suggest that multiple flow regimes exist throughout time within a single passage type, resulting in differing grain-size distributions of sediment banks.

Based on the grain-size composition, two lithological sediment facies were identified within the five sediment profiles: 1) Channel facies and 2) Slackwater facies. An additional third facies, known as Backswamp facies caused by back flooding, may occur in some of the sediment profiles; however, it is nearly impossible to differentiate these facies within these cores.

Based on the six EMMA grain-size distributions models, interpretations of flow conditions in these cave passages zones can be determined using the five sediment core profiles. The dominant deposition of all the end members was fluvial transport. Two end members (End Member 1 and End Member 2) were interpreted to represent normal flow by a migrating channel. End Member 3 was interpreted to represent higher energy flow conditions, likely due to the initial stages of flooding. End Member 4 was interpreted to represent the transition from high energy flow conditions to back flood conditions (extremely slow, suspension settling conditions). End Member 5 was interpreted to represent constant high energy flow conditions during deposition, likely due to the retreat stages of flooding when high energy flow conditions return after back flooding. Finally, End Member 6 was interpreted to represent flow conditions during the higher than normal conditions that exist after passage flooding during the return to normal flow conditions. Using end member analysis as the change in depositional mechanism may help refine future studies of sediment flux within cave systems.

Based on findings from radiocarbon dating, the age of the eight sediment samples collected from the five cores were not all younger than 2000 years. Seven of the eight sediments samples returned radiocarbon ages that were older than expected from Core 1, Core 2, Core 3, and Core 5 ($17,200 \pm 35 - 24,850 \pm 80$). The oldest sediment sample age returned was $24,850 \pm 80$ from Core 1 depth $43 - 45$. Sediments deposition in sediment banks from Russell Cave could have an age younger than 2,000 years, as seen in Core 4 sample with a radiocarbon age of $1,305 \pm 15$ years.

The sediment cores do not represent undisturbed sediment layers based on the radiocarbon age dating. Inverted radiocarbon dates with younger age sediments below

90

older age sediments were reported from both Core 1 and Core 2, and Core 3 had radiocarbon dates that were normal (oldest date from bottom). Radiocarbon dates shows that sediment reworking occurs within the cave passages by reworking of older sediments from upstream being deposited above younger sediments downstream of a reworked sediment bank, as seen in Core 1 and Core 2. This also shows that cave sediment banks within fluviokarst systems are not closed systems with respect to reworking and mixing, despite cave deposits often being referred to as stable, unaffected records of the past. Additionally, it appears that the bulk of the cave sediment is derived from sedimentation associated with the Last Glacial Maximum (~ 20 kya) and has been trapped and reworked within the cave since.

The limitations of this research involved difficulties with coring equipment (length of PVC core barrel) due to physical limitations caused by the size of the cave passage), PVC core barrel diameter that prevented coring of coarser, gravel-sized deposits, and limited funding for radiocarbon dating. Some improvements to future studies would be to add more radiocarbon dates to allow a correlation of the sediment profiles between all five cores. Additionally, sediment coring of complete sediment profile instead of three-foot core sections should be conducted. Finally, coring across the entire discontinuous transect of a sediment bank to evaluate lateral changes should be conducted. Additional analyses that should be conducted in future research includes radioisotope dating techniques using non-naturally occurring ^{137}Cesium, and naturally occurring ^{210}Lead, and ^{7}Beryllium for determining recent sediment deposition. Future research including smear slides for determining the composition of sediment and possibility source location of clastic materials, radioisotope dating techniques to

determine sediment deposition, leading to interpretations of sediment accumulation rates. Finally, pollen analysis may help determine the paleoclimate conditions that existed on the surface near the time of deposition.

This research on clastic cave sediment improves the limited understanding of sediments in fluvial karst systems, especially in this region of the Southeastern United States, and it is a starting point for further research investigations. The most significant findings of this research were the age of organic material within sediment cores appear to correlate to near the last glacial maximum, the identification of reworking of material from upstream sediment banks, and the mechanisms identified by end member analysis of deposition. These findings improve the understanding of the movement of sediment within Russell Cave and need to be expanded upon to improve the understanding of sediment deposits within other fluviokarst systems.

LITERATURE CITED

Anthony, D.M. and Granger, D.E., 2004. A Late Tertiary Origin for Multilevel Caves Along the Western

    Escarpment of the Cumberland Plateau, Tennessee and Kentucky, Established by Cosmogenic

    super (26) Al and super (10) Be. *Journal of Cave and Karst Studies*, *66*(2), pp.46-55.

Anthony, D.M., and Granger, D.E., 2006. Five million years of Appalachian landscape evolution preserved

    in cave sediments. *in* Harmon, R.S., Wicks, C. (eds.): Perspectives on Karst Geomorphology,

    Hydrology, and Geochemistry. *Geological Society of America Special Paper 404*, pp.39-50.

Audra, P., Mocochain, L., Camus, H., Gilli, É., Clauzon, G. and Bigot, J.Y., 2004. The effect of the

    Messinian Deep Stage on karst development around the Mediterranean Sea. Examples from

    Southern France. *Geodinamica Acta*, *17*(6), pp.389-400.

Audra, P. and Palmer, A.N., 2011. The pattern of caves: controls of epigenic

    speleogenesis. *Géomorphologie: relief, processus, environnement*, *17*(4), pp.359-378.

Bakalowicz, M., 2005. Karst groundwater: a challenge for new resources. *Hydrogeology Journal*, *13*(1),

    pp.148-160.

Bengtsson, L., Enell, M. and Berglund, B.E., 1986. Handbook of Holocene palaeoecology and

    palaeohydrology. *Chemical analysis*, pp.423-451.

Bray, L.G., 1972. Preliminary oxidation studies on some cave waters from South Wales. Cave Research

    Group of Great Britian, Transactions, 14. pp.59-66.

Briggs, L.I., Gill, D., Briggs, D.Z. and Elmore, R.D., 1980. Transition from open marine to evaporite

    deposition in the Silurian Michigan Basin. In *Developments in Sedimentology,* 28. (pp. 253-270).

    Amsterdam, Elsevier.

Brown, J.K. and Smith, J.K., 2000. Wildland fire in ecosystems: effects of fire on flora. *Gen. Tech. Rep.*

    RMRS-GTR-42-vol. 2. Ogden, UT: US Department of Agriculture, Forest Service, Rocky

    Mountain Research Station. 257 pp.

Bosch, R.F. and White, W.B., 2004. Lithofacies and transport of clastic sediments in karstic aquifers.

    In *Studies of Cave Sediments* (pp. 1-22). Springer, Boston, MA.

Burdick, D.W. and Strimple, H.L.R., 1982. Genevievian and Chesterian crinoids of Alabama. *Alabama*

    Geological Survey Bulletin, 121. pp.1-277.

Butts, C., 1926. The Paleozoic rocks, Geology of Alabama. *Alabama Geological Survey Special Report*, *14*. pp.41-230.

Campbell, M.R., 1893. Geology of the Big Stone Gap Coal Field of Virginia and Kentucky. *US Geological Survey Bulletin*, pp.28-38.

Chang, H. H. 1988. Fluvial processes in river engineering. In Krieger Publishing, Malabar, Florida, 432 pp.

Chester, E.W., 1995. An overview of forest diversity in the Interior Low Plateaus Physiographic Province. TD Landis and B. Cregg, tech. Cords: National Proceedings, Forest and Conservation Nursery Associations. *USDA Forest Service, Pacific Northwest Research Station, Gen. Tech. Rep. PNW-GTR-365,* pp.109-115.

Collins, J.D., O'Grady, P., Langford, R.P. and Gill, T.E., 2017. End-member mixing analysis (EMMA) applied to sediment grain size distributions to characterize formational processes of the main excavation block, Unit 2, of the Rimrock Draw Rockshelter, Harney Basin, Eastern Oregon (USA). *Archaeometry*, *59*(2), pp.331-345.

Collins, J.D., Langford, R.P., Gill, T.E. and Bowen, M.W., 2018. Using End-Member Mixing Analysis (EMMA) of grain sizes to model transportational and depositional processes and determine stratigraphic relationships at Rimrock Lake and Hay Lake playas, Harney Basin, eastern Oregon, USA. (unpublished)

Crawford, N.C., 1984. Karst landform development along the Cumberland Plateau Escarpment of Tennessee. In *Groundwater as a geomorphic agent,* Allen and Unwin, Boston, pp.294-338.

Dasher, G. R., 1994. On Station. Huntsville, Alabama 35810-4431, USA. National Speleology Society, Inc.

Davis, D.G., 1980. Cave development in the Guadalupe Mountains: a critical review of recent hypotheses. *National Speleology Society Bulletin, 42(3)*, pp.42-48.

Delcourt, P.A. and Delcourt, H.R., 1980. Pollen preservation and Quaternary environmental history in the southeastern United States. *Palynology*, *4*(1), pp.215-231.

Dietze, M. and Dietze, E., 2013. EMMAgeo: end member modelling algorithm and supporting functions for grain-size analysis. *R package version 0.9*, *1*.

Dietze, E. and Dietze, M., 2019. Grain-size distribution unmixing using the R package EMMAgeo. *E&G-Quaternary Science Journal*, *68*, pp.29-46.

Dietze, E., Hartmann, K., Diekmann, B., IJmker, J., Lehmkuhl, F., Opitz, S., Stauch, G., Wünnemann, B. and Borchers, A., 2012. An end member algorithm for deciphering modern detrital processes from lake sediments of Lake Donggi Cona, NE Tibetan Plateau, China. *Sedimentary Geology*, *243*, pp.169-180.

Dougherty, P.H. (ed.)., 1985. *Caves and karst of Kentucky* (No. 12). Kentucky Geological Survey, University of Kentucky, Lexington, KY.

Dreybrodt, W., 1988. Processes in karst systems. In *Physical Environment*, (Vol. 4.), Springer, Heidelberg, 288 pp.

Drysdale, R., Pierotti, L., Piccini, L. and Baldacci, F., 2001. Suspended sediments in karst spring waters near Massa (Tuscany), Italy. *Environmental Geology*, *40*(8), pp.1037-1050.

Egemeier, S.J., 1973. "Cavern Development by Thermal Waters with a Possible Bearing on Ore Deposition," PhD Thesis, Stanford University, Stanford, CA., 88 pp.

Ellwood, B.B., Petruso, K.M., Harrold, F.B. and Korkuti, M., 1996. Paleoclimate characterization and intra-site correlation using magnetic susceptibility measurements: an example from Konispol Cave, Albania. *Journal of Field Archaeology*, *23*(3), pp.263-271.

Evans, J.E. and Soreghan, M., 2015. Long-distance sediment transport and episodic resedimentation of Pennsylvanian dust (eolian silt) in cave passages of the Mississippian Leadville Limestone, southwestern Colorado, USA. *Caves and Karst Across Time*, *516(1)*, pp.1-22.

Ferguson, C.C. and Stearns, R.G., 1967. Stratigraphy and petrology of the Upper Mississippian of southernmost Tennessee. *in* Smith, W. E., (ed.): A field guide to Mississippian sediments in northern Alabama and south-central Tennessee. *5th* Annual Field Trip Alabama Guidebook, *Geological Society of America*, pp. 53-60.

Ferm, J. C. and Ehrlich, R., 1967. Petrology and stratigraphy of the Alabama coalfields, *in* Ferm, J. C., Ehrlich, R., and Neatherly, T. L., (eds.): A field guide to Carboniferous detrital rocks in northern Alabama. *Geological Society of America Coal Division and Alabama Geological Society*, Tuscaloosa, AL., pp. 11-15.

Folk, R.L. and Ward, W.C., 1957. Brazos river bar: a study in the significance of grain size parameters. *Journal of Sedimentary Research*, *27*(1), pp.3-26

Ford, D.C. and Williams, P.W., 1989. Karst Hydrogeology and Geomorphology. *Academic Division of Unmwin Hyman Ltd*, London, 601 pp.

Ford, D.C. and Williams, P.W., 2007. Karst Hydrogeology and Geomorphology. John Wiley & Sons, 576 pp.

Francis, J.K. and Loftus, N.S., 1977. Chemical and physical properties of the Cumberland Plateau and Highland Rim forest soils. USDA, *Forest Service Research Paper SO-138*, pp.1-44.

Galloway, D.L., Hudnut, K.W., Ingebritsen, S.E., Phillips, S.P., Peltzer, G., Rogez, F. and Rosen, P.A., 1998. Detection of aquifer system compaction and land subsidence using interferometric synthetic aperture radar, Antelope Valley, Mojave Desert, California. *Water Resources Research*, *34*(10), pp.2573-2585.

Gillieson, D., 1986. Cave sedimentation in the New Guinea highlands. *Earth Surface Processes and Landforms*, *11*(5), pp.533-543.

Godwin, J., 2008. The Biological Inventory of the Cave and Karst Systems of the Nature Conservancy's Sharp-Bingham Mountain Preserve. *Alabama National Heritage Program*, pp.1-40.

Goldscheider, N. and Drew, D., 2007. *Methods in Karst Hydrogeology*. Taylor and Francis Group, Leiden, Netherlands, 264 pp.

Granger, D.E., Fabel, D. and Palmer, A.N., 2001. Pliocene− Pleistocene incision of the Green River, Kentucky, determined from radioactive decay of cosmogenic 26Al and 10Be in Mammoth Cave sediments. *Geological Society of America Bulletin*, *113*(7), pp.825-836.

Griffin, J.W., 1974. Investigations in Russell Cave, Russell Cave National Monument, Alabama. in *Publications in Archaeology* 13. U.S. Department of the Interior, National Park Service, Washington, DC.

Gulley, J., Martin, J.B., Screaton, E.J. and Moore, P.J., 2011. River reversals into karst springs: a model for cave enlargement in eogenetic karst aquifers. *Geological Society of America Bulletin*, *123*(3-4), pp.457-467.

Gunn, J., 1983. Point-recharge of limestone aquifers—a model from New Zealand karst. *Journal of Hydrology*, *61*(1-3), pp.19-29.

Hack, J.T., 1966. Interpretation of Cumberland Escarpment and Highland Rim, South-central Tennessee and northeast Alabama. *United States Geological Survey Professional Paper, 524-C,* pp.1-16.

Hack, J.T., 1974. Investigations in Russell Cave, Russell Cave National Monument, Alabama. *Publications in Archaeology*, *13*(1), pp.16-28.

Haywick, D.W., Kopaska-Merkel, D.C. and Keyes, R., 2016. Petrographic and faunal characterization of Monteagle and Hartselle-equivalent strata in northeastern Alabama. *Gulf Coast Association of Geological Societies Transactions, 66*(1), pp.211-229.

Heck, J., 2013. LacCore Grain Size Pretreatment SOP. Limnological Research Center, University of Minnesota, pp.1-6.

Heiri, O., Lotter, A.F. and Lemcke, G., 2001. Loss on ignition as a method for estimating organic and carbonate content in sediments: reproducibility and comparability of results. *Journal of paleolimnology*, *25*(1), pp.101-110.

Herman, E.K., Toran, L. and White, W.B., 2012. Clastic sediment transport and storage in fluviokarst aquifers: an essential component of karst hydrogeology. *Carbonates and Evaporites*, *27*(3-4), pp.211-241.

Hjulstrom, F., 1935. Studies of the morphological activity of rivers as illustrated by the River Fyris, Bulletin. *Geological Institute Upsalsa*, *25*(1), pp.221-527.

Horsey, C.A., 1981. Depositional environments of the Pennsylvanian Pottsville Formation in the Black Warrior basin of Alabama. *Journal of Sedimentary Research*, *51*(3), pp.799-806.

Hunter, J.A. Moser, P.H., 1990. Ground Water Availability in Jefferson County, Alabama, Alabama Geological Survey Special Map 224. Scale [ca. 1:125,000].

Jackson, J.A. (ed.)., 1997. *Glossary of geology*, (4th ed). American Geological Institute, Alexandria, VA., 769 pp.

Jaillet, S., Pons-Branchu, E., Brulhet, J. and Hamelin, B., 2004. Karstification as geomorphological evidence of river incision: the karst of Cousance and the Marne valley (eastern Paris Basin). *Terra Nova*, *16*(4), pp.167-172.

Jameson, R.A., 1991. Concept and classification of cave breakdown: An analysis of patterns of collapse in Friars Hole Cave System, West Virginia. *in* Kasting, E.H., and Kastning, K.M., (eds.): Appalachian Karst. *National Speleological Society*, Huntsville, Ala., pp.35-44.

Kambesis, P., 2014. Karst Geology of the Classic TAG Region (Tennessee, Alabama, Georgia). *in* Schenk-Brown, J., (eds.): *2014 NSS Convention Guidebook*, Huntsville, AL, pp.2-23

Klimchouk, A.B., 1995. Karst morphogenesis in the epikarstic zone. *Cave and Karst science*, *21*(2), pp.45-50.

Klimchouk, A.B., 1996. The dissolution and conversion of gypsum and anhydrite. *International Journal of Speleology*, *25*(3), pp.21-36.

Klimchouk, A.B., 2007. Hypogene speleogenesis: hydrogeological and morphogenetic perspective. Special Paper, 1. *National Cave and Karst Research Institute*, Carlsbad, NM, 106 pp.

Klimchouk, A.B., 2009. Morphogenesis of hypogenic caves. *Geomorphology*, *106*(1-2), pp.100-117.

Küchler, A.W., 1965. Potential natural vegetation of the conterminous United States. *Soil Science*, *99*(5), pp.356.

Leonard, L.A., 1997. Controls of sediment transport and deposition in an incised mainland marsh basin, southeastern North Carolina. *Wetlands*, *17*(2), pp.263-274.

Loch, R.J. and Donnollan, T.E., 1983. Field rainfall simulator studies on two clay soils of the Darling Downs, Queensland. II. Aggregate Breakdown, sediment properties and soil erodibility. *Soil Research*, *21*(1), pp.47-58.

Logan, J., 2019. Tennessee–A Tale of Three Climates. *Tennessee's Climate, THE COCORAHS 'STATE CLIMATE' SERIES,* University of Tennessee.

Maier, R.M. and Pepper, I.L., 2009. Earth environments. in *Environmental microbiology* (2 ed.)*,* Academic Press, pp.57-82.

Martin, W. H., Boyce, S. G. and Echternacht, A.C., (eds.)., 1993. Biodiversity of the southeastern United States: upland terrestrial communities. John Wiley and Sons, Inc. New York, NY., 373 pp.

McNab, W.H. and Avers, P.E., 1994. Ecological subregions of the United States: section descriptions. Administrative Publication WO-WSA-5. *US Department of Agriculture, Forest Service, Washington, DC*, 267. pp.

Milici, R.C., 1974. Stratigraphy and depositional environments of Upper Mississippian and Lower

      Pennsylvanian rocks in the southern Cumberland Plateau of Tennessee, *in* Briggs, G., (ed.):

      Carboniferous of the Southeastern United States. *Geological Society of America Special Paper*

      148, pp.115-133.

Miller, C.F., 1957. Radiocarbon Dates from an Early Archaic Deposit in Russell Cave, Alabama. *American*

      Antiquity, *23*(1), pp.84-84.

Miller, B.A. and Schaetzl, R.J., 2015. Digital classification of hillslope position. *Soil Science Society of*

      America Journal, *79*(1), pp.132-145.

Michie, N. A., 1997. "An investigation of the climate, carbon dioxide and dust in Jenolan Caves," N.S.W.

      PhD Thesis, Macquarie University, Sydney, AU., 298 pp.

Monroe, W.H., 1970. *A glossary of karst terminology.* Washington: U.S. Gov. Print. Off.

Moore, H.L., 1994. A geologic trip across Tennessee by interstate 40. *University of Tennessee Press,*

      Knoxville, 339 pp.

Nardin, E., Goddéris, Y., Donnadieu, Y., Le Hir, G., Blakey, R.C., Pucéat, E. and Aretz, M., 2011.

      Modeling the early Paleozoic long-term climatic trend. *GSA Bulletin*, *123*(5-6), pp.1181-1192.

Norton, J.B., Sandor, J.A. and White, C.S., 2003. Hillslope soils and organic matter dynamics within a

      Native American agroecosystem on the Colorado Plateau. *Soil Science Society of America*

      Journal, *67*(1), pp.225-234.

Palmer, A.N., 1991. Origin and morphology of limestone caves. *Geological Society of America*

      Bulletin, *103*(1), pp.1-21.

Palmer, A.N., 2001. Dynamics of cave development by allogenic water. *Acta carsologica*, *30*(2), pp.13-32.

Palmer, A.N., 2007. Cave geology. Dayton, OH: Cave Books.

Palmer, A.N., 2011. Distinction between epigenic and hypogenic maze caves. *Geomorphology*, *134*(1-2),

      pp.9-22.

Pashin, J.C., 1994. Cycles and stacking patterns in Carboniferous rocks of the Black Warrior foreland

      basin. *Transactions of the Gulf Coast Association of Geological Societies, 44(1)*, pp.556-565.

Pashin, J.C., 2005. Pottsville stratigraphy and the Union Chapel lagerstätte. Pennsylvanian Footprints in the

      Black Warrior Basin of Alabama: *Alabama Paleontological Society Monograph*, (1), pp.39-58.

Pickle, J.D., 1985. "Dynamics of clastic sedimentation and watershed evolution within a low-relief karst drainage basin, Mammoth Cave Region, Kentucky," MS Thesis, University of New Mexico, Albuquerque, NM., 147 pp.

Rasband, W.S., 2019. ImageJ, U. S. National Institutes of Health, Bethesda, MD, USA. https://imagej.nih.gov/ij/

Raymond, D.E., Osborne, W.E., Copeland, C.W. and Neathery, T.L., 1988. Alabama stratigraphy. *Geological Survey of Alabama Circular 140, Tuscaloosa, AL*.

Rodgers, J., 1953. Geologic map of east Tennessee with explanatory text. *Tennessee Geological Survey Bulletin, 58*(1), 168 pp.

Ruhe, R.V. and Walker, P.H., 1968. Hillslope models and soil formation. *Congress of Soil Science, 9(1)*, pp.15-30.

Sapp, C.D. and Emplaincourt, J., 1975. Physiographic regions of Alabama. *Geological Survey Alabama Special Map 168*.

Sasowsky, I.D. and White, W.B., 1994. The role of stress release fracturing in the development of cavernous porosity in carbonate aquifers. *Water Resources Research*, *30*(12), pp.3523-3530.

Sasowsky, I.D., White, W.B. and Schmidt, V.A., 1995. Determination of stream-incision rate in the Appalachian plateaus by using cave-sediment magnetostratigraphy. *Geology*, *23*(5), pp.415-418.

Shahack-Gross, R., Berna, F., Karkanas, P. and Weiner, S., 2004. Bat guano and preservation of archaeological remains in cave sites. *Journal of Archaeological Science*, *31*(9), pp.1259-1272.

Simpson, L.C. and Florea, L.J., 2009. The Cumberland Plateau of Eastern Kentucky. *in* Palmer A.N. and Palmer, M.V., (eds.): Caves and Karst of America. *National Speleological Society*, Huntsville, AL., pp.70-78.

Smith, E.A., 1894. Geological map of Alabama, with explanatory chart. *Geological Survey of Alabama, Montgomery, AL*.

Smith, D.I. and Atkinson, T.C., 1976. The erosion of limestones. *The science of speleology. Academic Press, London*, pp.151-177.

Soil Survey Staff., 2019. Natural Resources Conservation Service, United States Department of Agriculture. *Web Soil Survey*. Available online. Accessed [November/15/2019].

Sroubek, P., Diehl, J.F., Kadlec, J. and Valoch, K., 2001. A Late Pleistocene palaeoclimate record based on mineral magnetic properties of the entrance facies sediments of Kulna Cave, Czech Republic. *Geophysical Journal International*, *147*(2), pp.247-262.

Stearns, R. G., 1963. Monteagle Limestone, Hartselle Formation, and Bangor Limestone; a new Mississippian nomenclature for use in middle Tennessee, with a history of its development. *Tennessee Department of Conservation Information Circular*, *11*(1), 18 pp.

Stearns, R.G. and Reesman, A.L., 1986. Cambrian to Holocene structural and burial history of Nashville dome. *AAPG Bulletin*, *70*(2), pp.143-154.

Szabo, M.W., Osborne, W.E., Copeland Jr, C.W. and Neathery, T.L., 1988. Geologic map of Alabama: *Geological Survey of Alabama Special Map, 220*.

Thomas, W. A., 1967. Mississippian facies in Alabama. in Ferm, J. C., Ehrlich, R., and Neathery, T. L., (eds.): A field guide to Carboniferous detrital rocks in northern Alabama. Annual Field Trip Guidebook, Coal Division, *Geological Society of America*, pp.21-23.

Thomas, W. A., 1972. Regional Paleozoic stratigraphy in Mississippi between Ouachita and Appalachian Mountains. *American Association of Petroleum Geologists Bulletin*, *56*(1), pp.81-106.

Thomas, W. A., 1979. Mississippian stratigraphy of Alabama, *in* The Mississippian and Pennsylvanian (Carboniferous) Systems in the United States - Alabama and Mississippi. *U. S. Geological Survey Professional Paper, 1110-I*, pp.I1-I22.

Thomas, W. A., Mack, G. H., and Waters, J. A., 1980. Depositional setting of the Mississippian Hartselle Sandstone and lower Bangor Limestone in northwest Alabama (Field trip number 2). *in* Tull, J. F., (ed.): Field trips for the Southeastern Section of the Geological Society of America, Birmingham, Alabama. *Alabama Geological Society*, Tuscaloosa, AL, pp.29-44.

Thornberry-Ehrlich, T. L., 2009. Geologic resources inventory scoping summary Russell Cave National Monument, Alabama. Geologic Resources Division, *National Park Service*, Lakewood, CO. http://www.nature.nps.gov/geology/inventory/ gre_publications.cfm

Thornberry-Ehrlich, T.L., 2014. *Russell Cave National Monument: Geologic Resources Inventory Report*. US Department of the Interior, National Park Service, Natural Resource Program Center.

Available at: http://npshistory.com/publications/ruca/nrr-2014-856.pdf (accessed 13 November 2019)

Thrailkill, J., Sullivan, S.B. and Gouzie, D.R., 1991. Flow parameters in a shallow conduit-flow carbonate aquifer, Inner Bluegrass Karst Region, Kentucky, USA. *Journal of Hydrology*, *129*(1-4), pp.87-108.

Tihansky, A.B., 1999. Sinkholes, West-Central Florida, Land Subsidence in the United States. *US Geological Survey Circular*, *1182*, Reston, VA., pp.121-140.

Torode, B., 1990. Russell Cave, Doran Cove quad. Sera Cave Carnival 1990, pp.24-26.

Vail, P. R., 1959. "Stratigraphy and lithofacies of Upper Mississippian rocks in the Cumberland Plateau," PhD Thesis, Northwestern University, Evanston, IL., 143 pp.

Vega, A.J. and Binkley, M.S., 1993. Tropical cyclone formation in the North Atlantic basin, 1960–1989. *Climate Research*, *3*(1), pp.221-232.

Wanless, H.R., 1946. *Pennsylvanian geology of a part of the southern Appalachian coal field* (Vol. 13). Geological Society of America, Memphis, TN., 162 pp.

Weltje, G.J., 1997. End member modeling of compositional data: Numerical-statistical algorithms for solving the explicit mixing problem. *Mathematical Geology*, *29*(4), pp.503-549.

Weltje, G.J. and Prins, M.A., 2003. Muddled or mixed? Inferring palaeoclimate from size distributions of deep-sea clastics. *Sedimentary Geology*, *162*(1-2), pp.39-62.

Weltje, G.J. and Prins, M.A., 2007. Genetically meaningful decomposition of grain-size distributions. *Sedimentary Geology*, *202*(3), pp.409-424.

White, W.B., 1988. Geomorphology and Hydrology of Karst Terrains. Oxford University Press, NY, 464 pp.

White, W.B., 1999. Conceptual models for karstic aquifers. *Karst modeling*, *5*(1), pp.11-16.

White, W.B., 2002. Karst hydrology: recent developments and open questions. *Engineering geology*, *65*(2-3), pp.85-105.

White, W.B., 2007. A brief history of karst hydrogeology: contributions of the NSS. J*ournal of Cave and Karst Studies*, *69*(1), pp.13-26.

Widga, C. and Colburn, M., 2015. Paleontology and paleoecology of guano deposits in Mammoth Cave, Kentucky, USA. *Quaternary Research*, *83*(3), pp.427-436.

Williams, D.D., 1993. Nutrient and flow vector dynamics at the hyporheic/groundwater interface and their effects on the interstitial fauna. *Hydrobiologia*, *251*(1), pp.185-198.

Wilson Jr, C.W. and Stearns, R.G., 1958. Structure of the Cumberland Plateau, Tennessee. *Geological Society of America Bulletin*, *69*(10), pp.1283-1296.

APPENDIX A

PHOTOGRAPHS OF CORES

<u>Core 1</u>

Core 2

Core 3

106
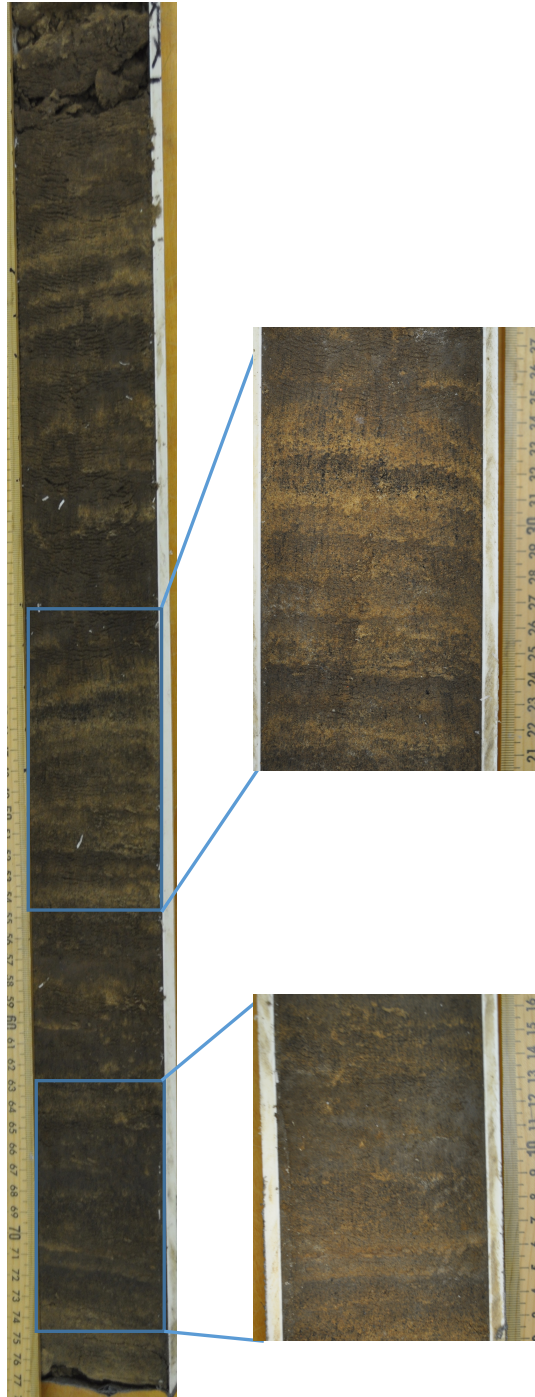
Core 4
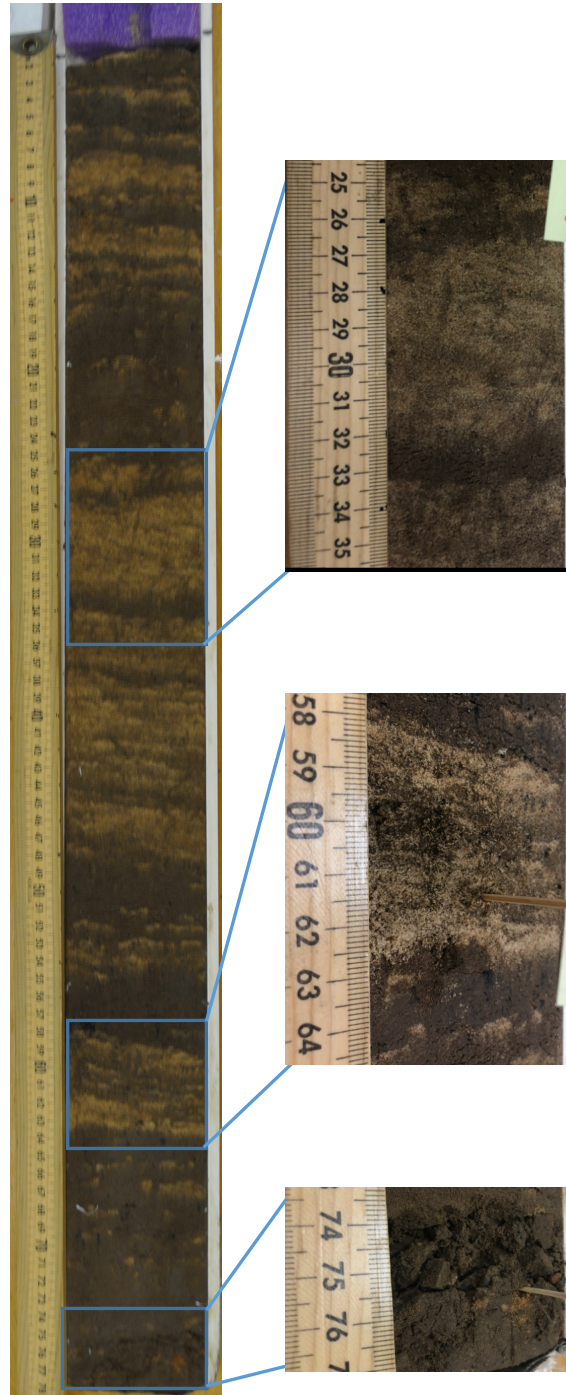
Core 5
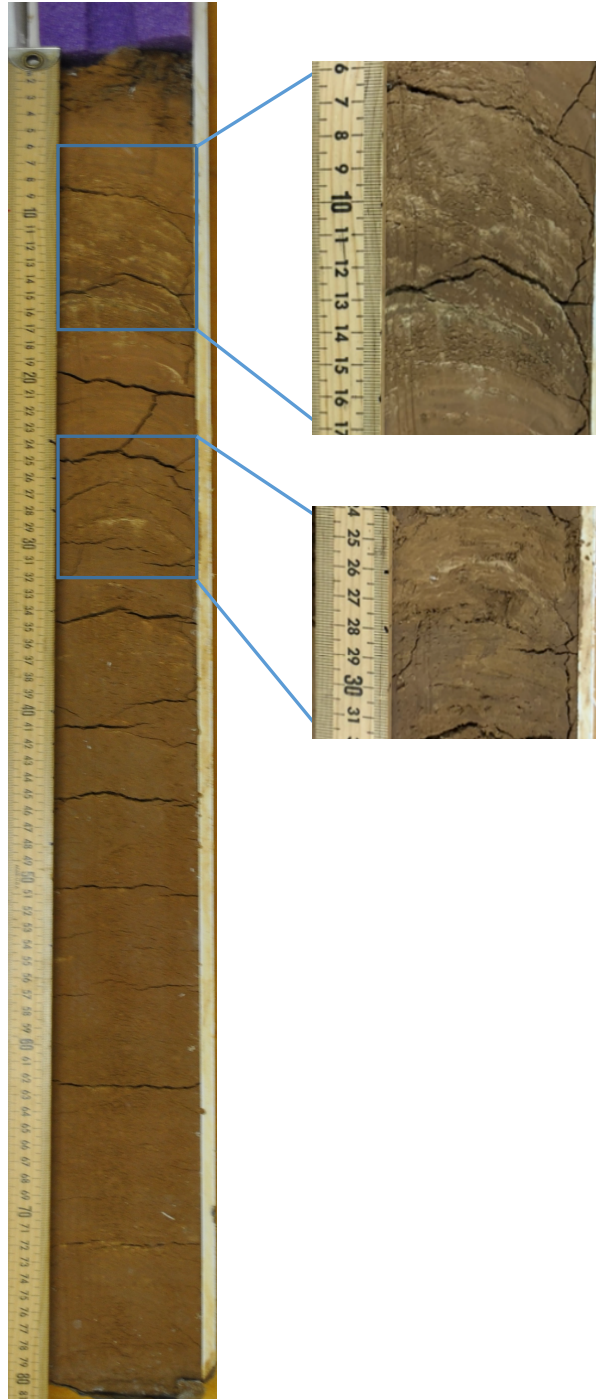
APPENDIX B

PERCENTILE PHI VALUES INTERPOLATED FROM CUMULATIVE WEIGHT PERCENTAGE

Phi Values of Core 1

Sample Number	Sample Depth (cm)	5%	16%	25%	50%	75%	84%	95%
1	14 – 16	1.70	2.80	3.71	4.99	6.36	6.88	7.97
2	16 – 18	1.58	2.71	3.71	5.43	6.65	7.14	8.26
3	18 – 20	1.85	2.82	3.58	5.13	6.42	6.95	8.07
4	20 – 22	1.25	1.86	2.35	4.13	6.10	6.79	7.97
5	22 – 24	1.22	1.87	2.34	3.83	5.74	6.54	7.83
6	24 – 26	1.33	2.18	2.82	4.66	6.25	6.87	8.04
7	26 – 28	1.65	2.43	2.89	4.40	5.99	6.69	7.94
8	28 – 30	1.67	3.06	3.96	5.47	6.79	7.37	8.48
9	30 – 32	1.36	2.35	3.09	5.12	6.71	7.39	8.75
10	32 – 34	1.74	4.04	4.59	5.94	7.05	7.67	8.84
11	34 – 36	1.26	2.11	2.55	3.77	5.18	6.07	7.59
12	36 – 38	1.52	2.67	3.43	4.90	6.38	6.94	8.16
13	38 – 40	1.29	2.41	3.18	4.79	6.36	6.95	8.21
14	40 – 42	1.28	2.34	3.25	5.30	6.70	7.28	8.42
15	42 – 44	0.78	1.39	1.75	3.26	5.85	6.65	7.89
16	44 – 46	1.04	1.55	1.96	3.45	5.76	6.60	7.87
17	46 – 48	1.01	1.59	2.07	3.87	5.88	6.62	7.84
18	48 – 50	2.02	2.72	3.27	4.72	6.37	6.97	8.22
19	50 – 52	0.67	1.52	2.02	3.77	5.89	6.66	7.94
20	52 – 54	1.10	1.68	2.18	4.27	6.42	7.04	8.33
21	54 – 56	0.46	0.98	1.66	4.08	6.61	7.60	9.65
22	56 – 58	1.32	2.13	2.61	4.13	5.84	6.69	8.43
23	58 – 60	1.25	2.21	2.76	4.35	6.13	6.94	9.16
24	60 – 62	1.24	2.30	2.91	4.34	6.14	6.96	10.12
25	62 – 64	1.55	1.64	2.34	5.40	6.83	7.35	8.11
26	64 – 66	1.07	2.10	2.66	4.29	6.30	7.26	10.75
27	66 – 68	0.69	1.80	2.46	4.37	6.23	6.98	8.85
28	68 – 70	0.63	1.70	2.26	3.74	5.71	6.68	8.99
29	70 – 72	0.34	1.52	2.10	3.81	6.01	6.83	8.57

Phi Values of Core 2

Sample Number	Sample Depth (cm)	5%	16%	25%	50%	75%	84%	95%
1	0 – 2	1.72	2.52	3.03	4.39	6.03	6.87	8.99
2	2 – 4	1.67	2.50	3.01	4.39	6.12	6.97	9.66
3	4 – 6	1.78	2.51	2.97	4.25	5.88	6.78	9.02
4	6 – 8	1.86	2.60	3.11	4.37	5.93	6.79	8.87
5	8 – 10	1.82	2.59	3.11	4.40	6.02	6.86	8.91
6	10 – 12	1.77	2.52	3.01	4.34	6.03	6.93	9.79
7	12 – 14	2.02	2.73	3.25	4.50	6.08	6.91	9.10
8	14 – 16	1.82	2.56	3.05	4.37	6.09	6.96	9.76
9	16 – 18	2.16	3.06	3.57	4.72	6.25	7.05	9.64
10	18 – 20	1.87	2.66	3.20	4.51	6.13	6.95	9.40
11	20 – 22	2.06	2.80	3.33	4.61	6.27	7.06	9.64
12	22 – 24	2.05	2.74	3.25	4.50	6.09	6.90	9.46
13	24 – 26	2.16	3.02	3.50	4.64	6.06	6.85	8.84
14	26 – 28	2.07	2.87	3.39	4.64	6.22	6.98	9.22
15	28 – 30	2.11	2.98	3.49	4.68	6.19	6.96	9.39
16	30 – 32	2.06	2.86	3.41	4.65	6.15	6.92	8.99
17	32 – 34	2.07	3.08	3.38	4.60	6.16	6.95	9.02
18	34 – 36	2.17	3.05	3.56	4.73	6.24	6.98	9.04
19	36 – 38	2.10	2.90	3.41	4.60	6.17	7.00	9.54
20	38 – 40	1.50	2.27	2.67	3.98	6.01	6.98	10.14
21	40 – 42	2.04	2.79	3.33	4.59	6.18	6.96	9.05
22	42 – 44	2.21	3.19	3.72	4.83	6.38	7.12	9.36
23	44 – 46	2.03	2.71	3.19	4.48	6.18	7.00	9.58
24	46 – 48	2.07	2.88	3.43	4.68	6.24	7.01	9.28
25	48 – 50	1.77	2.43	2.84	4.12	5.92	6.82	9.03
26	50 – 52	2.59	3.61	4.19	5.66	7.51	8.58	11.27
27	52 – 54	1.57	2.34	2.71	4.03	5.88	6.84	10.03
28	54 – 56	1.95	2.67	3.21	4.61	6.56	7.55	10.63
29	56 – 58	1.51	2.28	2.68	4.05	5.98	6.91	9.74
30	58 – 60	1.65	2.39	2.82	4.25	6.24	7.12	10.07
31	60 – 62	2.03	2.69	3.21	4.52	5.87	6.56	8.08
32	62 – 64	2.18	3.17	3.75	4.72	5.81	6.40	7.72
33	64 – 66	2.03	2.76	3.30	4.74	6.86	7.93	10.79
34	66 – 68	1.89	2.61	3.12	4.40	5.90	6.69	8.40
35	68 – 70	1.56	2.73	3.49	4.98	6.56	7.27	9.39

Phi Values of Core 3

Sample Number	Sample Depth (cm)	5%	16%	25%	50%	75%	84%	95%
1	0 – 2	1.47	2.31	2.77	4.20	5.98	6.75	8.36
2	2 – 4	1.74	2.65	3.23	4.61	6.25	6.91	8.47
3	4 – 6	1.71	2.76	3.46	4.99	6.58	7.26	8.94
4	6 – 8	1.63	2.46	2.95	4.19	5.79	6.56	7.91
5	8 – 10	1.83	2.63	3.17	4.47	6.05	6.74	8.14
6	10 – 12	1.68	2.65	3.22	4.51	6.02	6.67	7.84
7	12 – 14	1.53	2.61	3.20	4.56	6.16	6.84	8.35
8	14 – 16	1.80	2.90	3.45	4.65	6.11	6.76	7.96
9	16 – 18	1.27	2.23	2.74	4.21	6.13	7.00	10.05
10	18 – 20	1.55	2.56	3.14	4.41	6.89	6.59	7.80
11	20 – 22	1.33	2.51	3.20	4.80	6.51	7.11	8.47
12	22 – 24	1.63	2.73	3.36	4.68	6.14	6.74	7.86
13	24 – 26	1.29	2.30	2.85	4.28	6.21	7.00	9.57
14	26 – 28	0.53	1.68	2.33	4.11	6.21	6.95	8.83
15	28 – 30	0.55	1.67	2.22	3.60	5.58	6.56	8.48
16	30 – 32	0.70	1.93	2.60	4.33	6.09	6.75	7.97
17	32 – 34	1.43	2.67	3.30	4.61	6.22	6.88	8.20
18	34 – 36	0.59	1.62	2.19	3.68	5.72	6.64	8.55
19	36 – 38	0.90	1.82	2.40	3.90	5.60	6.56	8.37
20	38 – 40	1.66	2.85	3.43	4.63	6.15	6.94	9.11
21	40 – 42	0.68	1.96	2.67	4.39	6.07	6.81	8.51
22	42 – 44	1.11	2.14	2.76	4.35	6.14	6.97	10.17
23	44 – 46	1.03	2.15	2.80	4.43	6.15	6.85	8.46
24	46 – 48	1.18	2.35	3.05	4.56	6.25	7.02	10.09
25	48 – 50	1.33	2.42	3.05	4.48	6.25	7.10	10.39
26	50 – 52	1.81	2.77	3.35	4.65	6.24	6.99	9.36
27	52 – 54	2.22	3.30	3.87	4.95	6.49	7.18	8.91
28	54 – 56	2.12	3.10	3.67	4.87	6.42	7.16	9.68
29	56 – 58	2.05	3.04	3.62	4.89	6.45	7.19	9.80
30	58 – 60	2.24	3.59	4.19	5.36	6.79	7.61	10.43
31	60 – 62	2.15	3.21	3.81	5.05	6.72	7.59	10.61
32	62 – 64	3.09	4.08	4.44	5.53	6.80	7.52	9.78
33	64 – 66	2.88	3.65	4.11	4.92	6.19	6.83	8.44
34	66 – 68	2.60	3.77	4.32	5.64	6.99	7.83	10.68
35	68 – 70	2.60	3.47	3.98	4.85	6.17	6.83	8.29
36	70 – 72	2.40	3.31	3.81	4.80	6.16	6.87	8.76
37	72 – 74	2.09	2.85	3.33	4.54	6.16	6.88	8.77
38	74 – 76	2.20	3.15	3.77	5.69	7.29	8.02	10.93
39	76 – 78	1.71	2.50	2.99	4.27	5.98	6.75	8.55
40	78 – 80	1.79	2.72	3.31	4.71	6.40	7.12	9.43

Phi Values of Core 4

Sample Number	Sample Depth (cm)	5%	16%	25%	50%	75%	84%	95%
1	12 – 14	1.01	1.51	1.92	3.28	5.64	6.68	9.48
2	14 – 16	1.05	1.51	1.88	2.99	5.20	6.22	7.74
3	16 – 18	1.19	1.66	2.04	2.94	5.41	6.58	8.94
4	18 – 20	1.09	1.47	1.78	2.82	5.21	6.32	8.10
5	20 – 22	1.03	1.34	1.59	2.40	3.85	5.42	7.39
6	22 – 24	1.09	1.44	1.73	2.66	4.83	6.12	8.02
7	24 – 26	1.03	1.36	1.62	2.53	4.76	6.08	8.26
8	26 – 28	1.09	1.48	1.79	2.73	4.79	6.03	8.05
9	28 – 30	1.13	1.57	1.93	2.92	5.14	6.25	7.83
10	30 – 32	1.11	1.59	1.99	3.09	5.62	6.63	8.63
11	32 – 34	1.11	1.61	2.02	3.17	5.85	6.88	10.11
12	34 – 36	1.12	1.59	1.98	3.03	5.55	6.67	9.65
13	36 – 38	1.10	1.54	1.89	2.97	5.53	6.66	9.20
14	38 – 40	0.62	1.19	1.41	2.03	4.03	5.53	7.61
15	40 – 42	0.33	1.02	1.18	1.62	2.27	2.90	6.60
16	42 – 44	0.43	1.07	1.22	1.64	2.23	2.89	6.68
17	44 – 46	1.02	1.32	1.57	2.41	4.64	6.09	8.14
18	46 – 48	0.48	1.12	1.31	1.83	2.90	4.64	7.06
19	48 – 50	0.65	1.19	1.40	1.97	3.19	4.86	7.24
20	50 – 52	0.34	1.03	1.21	1.73	2.77	4.41	7.12
21	52 – 54	0.31	0.98	1.17	1.67	2.57	3.89	6.81
22	54 – 56	0.35	1.03	1.21	1.70	2.59	3.79	6.80
23	56 – 58	0.50	1.13	1.34	1.90	3.62	5.22	7.25
24	58 – 60	0.72	1.21	1.41	1.98	3.29	4.85	7.12
25	60 – 62	1.02	1.35	1.62	2.54	4.68	5.92	7.63
26	62 – 64	1.04	1.43	1.76	2.87	5.40	6.53	8.68
27	64 – 66	0.64	1.21	1.43	2.11	4.23	5.66	7.58
28	66 – 68	0.93	1.32	1.59	2.53	4.76	6.00	7.72
29	68 – 70	1.06	1.48	1.84	3.12	5.77	6.79	9.96
30	72 – 72	0.69	1.24	1.48	2.32	4.67	6.00	7.77
31	72 – 74	0.34	1.03	1.23	1.79	3.46	5.24	7.53
32	74 – 76	0.31	0.99	1.19	1.72	2.88	4.69	7.01
33	76 – 78	1.03	1.41	1.73	2.78	5.27	6.41	8.32
34	78 – 80	1.12	1.64	2.07	3.62	5.92	6.74	8.41
35	80 – 82	1.05	1.50	1.87	3.16	5.57	6.51	7.99
36	82 – 84	1.02	1.41	1.74	2.87	5.34	6.48	8.58
37	84 – 86	1.23	1.94	2.42	4.04	6.06	6.83	8.44
38	86 – 88	1.06	1.50	1.86	3.06	5.60	6.68	9.19
39	88 – 90	1.10	1.70	2.19	3.68	5.87	6.75	8.62

Phi Values of Core 5

Sample Number	Sample Depth (cm)	5%	16%	25%	50%	75%	84%	95%
1	0 – 2	3.01	3.88	4.28	5.27	6.52	7.04	8.49
2	2 – 4	3.27	4.14	4.46	5.40	6.50	6.96	8.25
3	4 – 6	3.47	4.22	4.53	5.42	6.46	6.91	8.04
4	6 – 8	3.42	4.16	4.45	5.30	6.42	6.92	8.09
5	8 – 10	3.18	4.02	4.30	5.10	6.32	6.89	8.29
6	10 – 12	3.11	3.79	4.17	4.93	6.04	6.67	7.93
7	12 – 14	3.02	3.59	4.03	4.83	6.18	6.87	8.43
8	14 – 16	3.30	4.13	4.43	5.37	6.64	7.27	8.74
9	16 – 18	3.19	4.08	4.44	5.46	6.57	6.98	8.07
10	18 – 20	3.83	4.50	4.95	5.89	6.80	7.27	8.31
11	20 – 22	3.71	4.35	4.69	5.64	6.68	7.15	8.38
12	22 – 24	4.00	4.60	5.05	5.96	6.86	7.41	8.61
13	24 – 26	3.52	4.30	4.64	5.59	6.64	7.11	8.41
14	26 – 28	3.16	4.03	4.34	5.27	6.43	6.91	8.15
15	28 – 30	3.14	3.99	4.33	5.32	6.54	7.02	8.29
16	30 – 32	3.05	3.94	4.31	5.30	6.55	7.10	8.65
17	32 – 34	3.36	4.17	4.49	5.44	6.66	7.29	8.89
18	34 – 36	2.96	3.61	4.08	4.97	6.36	6.96	8.53
19	36 – 38	3.18	4.01	4.34	5.36	6.66	7.32	8.94
20	38 – 40	2.91	3.67	4.17	5.24	6.68	7.42	9.26
21	40 – 42	2.86	3.51	4.03	4.98	6.42	7.02	8.76
22	42 – 44	3.20	4.12	4.49	5.57	6.79	7.46	9.27
23	44 – 46	2.98	3.70	4.17	5.18	6.58	7.24	8.91
24	46 – 48	2.82	3.55	4.09	5.22	6.76	7.59	10.25
25	48 – 50	2.39	2.91	3.38	4.63	6.36	7.13	9.36
26	50 – 52	2.58	3.17	3.66	4.86	6.55	7.32	9.67
27	52 – 54	2.30	2.76	3.24	4.47	6.24	7.04	9.40
28	54 – 56	2.40	2.98	3.46	4.70	6.36	7.09	9.18
29	56 – 58	2.40	2.96	3.44	4.72	6.47	7.25	9.74
30	58 – 60	2.25	2.74	3.24	4.51	6.24	6.97	8.83
31	60 – 62	2.45	3.04	3.52	4.76	6.33	6.95	8.43
32	62 – 64	2.36	2.95	3.46	4.75	6.44	7.17	8.97
33	64 – 66	2.23	2.89	3.46	4.80	6.40	7.07	8.87
34	66 – 68	2.52	3.13	3.63	4.92	6.61	7.36	9.56
35	68 – 70	2.09	2.91	3.58	5.04	6.67	7.38	9.00
36	70 – 72	2.21	3.09	3.82	5.28	6.68	7.29	8.76
37	72 – 74	1.62	2.36	2.78	4.25	6.12	6.93	8.93
38	74 – 76	2.17	2.76	3.31	4.68	6.42	7.15	8.96
39	76 – 78	2.24	2.98	3.59	4.98	6.50	7.10	8.32
40	78 – 80	2.52	3.40	4.09	5.57	6.89	7.52	8.63

APPENDIX C

WATER CONTENT, ORGANIC MATTER, AND MAGNETIC SUSCEPTIBILITY RAW DATA

LOI and MS Raw Data for Core 1

Depth (cm)	Initial Weight (IW)	Oven Dry Weight (DW$_{105}$)	LOI$_{105}$ (Percent)	Furnace Dry Weight (DW$_{550}$)	LOI$_{550}$ (Percent)	MS (m^3/kg)
14 – 16	2.41	2.07	14.11	1.96	3.92	3.79E-07
16 – 18	3.55	3.02	14.93	2.88	4.32	3.63E-07
18 – 20	2.89	2.41	16.61	2.27	5.02	4.15E-07
20 – 22	2.81	2.54	9.61	2.44	3.94	3.25E-07
22 – 24	3.37	3.03	10.09	2.92	3.63	3.69E-07
24 – 26	3.01	2.51	16.61	2.38	5.18	3.68E-07
26 – 28	3.71	3.07	17.25	2.91	5.21	3.96E-07
28 – 30	3.92	3.54	9.69	3.37	4.53	4.03E-07
30 – 32	4.05	3.49	13.83	3.33	4.31	3.41E-07
32 – 34	3.50	2.82	19.43	2.64	6.05	4.50E-07
34 – 36	4.31	3.60	16.47	3.38	5.85	4.01E-07
36 – 38	3.95	3.24	17.97	3.01	6.52	4.45E-07
38 – 40	4.55	3.84	15.60	3.61	5.99	4.10E-07
40 – 42	4.44	3.80	14.41	3.57	6.05	3.87E-07
42 – 44	3.74	3.42	8.56	3.14	8.19	3.08E-07
44 – 46	4.43	4.09	7.67	2.37	41.91	2.96E-07
46 – 48	4.51	3.97	11.97	3.33	16.12	3.38E-07
48 – 50	5.05	4.33	14.26	4.10	4.87	3.35E-07
50 – 52	4.80	4.01	16.46	3.72	7.23	3.66E-07
52 – 54	4.31	3.91	9.28	3.79	2.82	3.31E-07
54 – 56	5.74	4.56	20.56	4.30	5.70	4.15E-07
56 – 58	3.99	3.46	13.28	3.31	4.34	4.11E-07
58 – 60	5.26	4.20	20.15	3.92	6.67	4.60E-07
60 – 62	4.27	3.67	14.05	3.45	5.99	4.37E-07
62 – 64	5.18	4.22	18.53	3.92	6.89	3.65E-07
64 – 66	5.39	4.22	21.71	3.85	8.77	3.68E-07
66 – 68	3.90	3.32	14.87	3.01	9.34	3.82E-07
68 – 70	4.42	3.58	19.00	3.27	8.66	3.77E-07
70 – 72	4.85	3.88	20.00	3.45	10.85	3.91E-07
72 – 74	4.34	3.74	13.82	3.27	12.57	3.52E-07
74 – 76	4.89	4.01	18.00	3.52	12.00	3.59E-07

LOI and MS Raw Data for Core 2

Depth (cm)	Initial Weight (IW)	Oven Dry Weight (DW$_{105}$)	LOI$_{105}$ (Percent)	Furnace Dry Weight (DW$_{550}$)	LOI$_{550}$ (Percent)	MS (m^3/kg)
0 – 2	3.61	3.07	14.96	3.01	1.63	2.11E-07
2 – 4	3.02	2.54	15.89	2.49	1.97	2.35E-07
4 – 6	3.83	3.24	15.40	3.17	2.16	1.99E-07
6 – 8	4.83	4.04	16.36	3.94	2.23	2.00E-07
8 – 10	4.70	3.97	15.53	3.89	2.26	1.93E-07
10 – 12	3.25	2.73	16.00	2.66	1.85	1.95E-07
12 – 14	3.80	3.16	16.84	3.07	2.23	1.97E-07
14 – 16	4.90	4.09	16.53	4.00	2.20	2.00E-07
16 – 18	4.15	3.44	17.11	3.37	2.32	2.00E-07
18 – 20	4.59	3.83	16.56	3.74	2.35	2.04E-07
20 – 22	4.96	4.14	16.53	3.98	2.69	2.04E-07
22 – 24	5.44	4.49	17.46	4.40	2.22	2.11E-07
24 – 26	4.43	3.70	16.48	3.61	1.90	1.98E-07
26 – 28	4.82	3.99	17.22	3.88	2.27	2.08E-07
28 – 30	4.75	3.89	18.11	3.75	2.34	1.90E-07
30 – 32	5.02	4.16	17.13	4.06	2.40	2.06E-07
32 – 34	4.90	4.06	17.14	3.94	2.48	2.07E-07
34 – 36	5.05	4.20	16.83	4.11	2.38	2.10E-07
36 – 38	5.51	4.53	17.79	4.41	2.43	2.10E-07
38 – 40	6.16	5.08	17.53	4.94	2.37	2.14E-07
40 – 42	5.08	4.17	17.91	4.08	2.39	2.29E-07
42 – 44	4.47	3.70	17.23	3.60	2.17	2.16E-07
44 – 46	4.52	3.73	17.48	3.66	2.14	2.22E-07
46 – 48	5.91	4.81	18.61	4.66	2.31	2.20E-07
48 – 50	6.18	5.07	17.96	4.95	2.17	2.16E-07
50 – 52	5.38	4.52	15.99	4.40	2.22	2.24E-07
52 – 54	5.04	4.20	16.67	4.10	2.15	1.86E-07
54 – 56	6.28	5.31	15.45	5.17	2.27	2.15E-07
56 – 58	4.95	4.14	16.36	4.02	2.66	2.52E-07
58 – 60	6.00	4.88	18.67	4.99	1.77	2.37E-07
60 – 62	N/A	4.82	N/A	4.72	2.07	1.91E-07
62 – 64	5.13	4.29	16.37	4.17	2.11	7.64E-08
64 – 66	5.42	4.55	16.05	4.42	2.43	5.91E-08
66 – 68	5.76	4.91	14.76	4.79	2.04	5.36E-08
68 – 70	6.20	5.35	13.71	5.24	2.06	5.75E-08

LOI and MS Raw Data for Core 3

Depth (cm)	Initial Weight (IW)	Oven Dry Weight (DW_{105})	LOI_{105} (Percent)	Furnace Dry Weight (DW_{550})	LOI_{550} (Percent)	MS (m^3/kg)
0 – 2	5.42	3.85	28.97	3.55	7.55	2.96E-07
2 – 4	5.06	4.77	5.73	3.54	5.60	3.19E-07
4 – 6	3.88	2.97	23.45	2.81	5.07	3.09E-07
6 – 8	5.15	3.93	23.69	3.66	4.94	3.45E-07
8 – 10	4.49	3.47	22.72	3.26	5.23	4.21E-07
10 – 12	5.00	3.78	24.40	3.45	6.25	4.39E-07
12 – 14	5.37	4.39	18.25	4.09	5.76	3.92E-07
14 – 16	4.58	3.48	24.02	3.21	6.69	3.98E-07
16 – 18	5.37	4.21	21.60	3.88	7.40	3.68E-07
18 – 20	6.13	4.75	22.51	4.36	7.63	3.55E-07
20 – 22	5.94	4.72	20.54	4.36	7.23	3.18E-07
22 – 24	6.46	4.88	24.46	4.42	9.24	2.72E-07
24 – 26	5.16	4.03	21.90	3.60	9.32	3.01E-07
26 – 28	5.90	4.64	21.36	4.11	11.04	3.02E-07
28 – 30	6.29	4.82	23.37	4.24	11.11	3.08E-07
30 – 32	6.34	4.75	25.08	4.25	9.38	1.34E-07
32 – 34	6.14	4.56	25.73	3.95	12.80	1.94E-07
34 – 36	6.77	5.50	18.76	4.89	10.77	3.56E-07
36 – 38	4.19	3.31	21.00	2.88	11.93	2.68E-07
38 – 40	5.17	3.60	30.37	3.07	13.28	1.59E-07
40 – 42	4.46	3.17	28.92	2.67	13.87	1.78E-07
42 – 44	4.50	3.29	26.89	2.75	12.42	3.63E-07
44 – 46	5.30	3.95	25.47	3.48	10.54	3.27E-07
46 – 48	4.53	3.40	24.94	3.05	9.50	3.86E-07
48 – 50	4.49	3.48	22.49	3.06	11.30	4.16E-07
50 – 52	4.21	3.22	23.52	2.95	6.65	4.37E-07
52 – 54	5.08	3.98	21.65	3.62	6.94	4.48E-07
54 – 56	5.52	4.29	22.28	3.97	6.37	4.59E-07
56 – 58	5.92	4.59	22.47	4.21	6.24	4.74E-07
58 – 60	5.97	4.60	22.95	4.15	7.57	5.02E-07
60 – 62	4.53	3.51	22.52	3.23	6.65	4.94E-07
62 – 64	5.63	4.28	23.98	4.03	5.84	5.21E-07
64 – 66	6.35	4.83	23.94	4.65	3.53	4.80E-07
66 – 68	5.82	4.50	22.68	4.30	3.15	4.98E-07
68 – 70	3.13	3.10	0.96	4.77	3.25	4.86E-07
70 – 72	5.66	4.36	22.97	4.17	3.02	4.28E-07
72 – 74	5.42	4.31	20.48	4.16	2.80	3.94E-07
74 – 76	4.60	3.65	20.65	3.50	2.78	4.26E-07
76 – 78	6.21	4.76	23.35	4.49	3.23	4.37E-07
78 – 80	4.79	3.62	24.43	3.40	3.68	4.57E-07

LOI and MS Raw Data for Core 4

Depth (cm)	Initial Weight (IW)	Oven Dry Weight (DW105)	LOI105 (Percent)	Furnace Dry Weight (DW550)	LOI550 (Percent)	MS (m³/kg)
12 – 14	4.24	3.59	15.33	3.59	4.46	3.19E-07
14 – 16	3.01	2.63	12.62	2.63	3.42	3.01E-07
16 – 18	3.20	2.72	15.00	2.72	2.94	3.60E-07
18 – 20	2.78	2.38	14.39	2.38	2.10	3.25E-07
20 – 22	3.69	3.23	12.47	3.23	2.48	2.77E-07
22 – 24	3.61	3.19	11.63	3.17	1.58	3.05E-07
24 – 26	4.01	3.54	11.72	3.52	1.70	2.76E-07
26 – 28	3.64	3.11	14.56	3.10	1.94	3.13E-07
28 – 30	2.75	2.28	17.09	2.27	2.64	3.00E-07
30 – 32	3.87	3.20	17.31	3.20	2.81	2.90E-07
32 – 34	3.60	3.01	16.39	3.02	2.65	2.84E-07
34 – 36	3.92	3.31	15.56	3.31	1.81	2.85E-07
36 – 38	3.70	3.18	14.05	3.18	2.52	2.67E-07
38 – 40	4.01	3.62	9.73	3.62	1.38	2.11E-07
40 – 42	3.28	3.12	4.88	3.13	0.96	1.41E-07
42 – 44	3.06	2.91	4.90	2.90	1.03	1.66E-07
44 – 46	3.85	3.49	9.35	3.47	1.73	2.17E-07
46 – 48	2.83	2.61	7.77	2.60	1.15	2.02E-07
48 – 50	3.31	3.07	7.25	3.05	0.98	2.05E-07
50 – 52	4.50	4.22	6.22	4.21	0.95	1.78E-07
52 – 54	3.57	3.40	4.76	3.40	1.18	1.54E-07
54 – 56	3.21	3.03	5.61	3.03	0.99	1.60E-07
56 – 58	4.03	3.72	7.69	3.71	1.62	1.98E-07
58 – 60	3.57	3.37	5.60	3.36	1.79	1.69E-07
60 – 62	3.55	3.16	10.99	3.16	2.85	2.26E-07
62 – 64	3.85	3.35	12.99	3.35	2.69	2.45E-07
64 – 66	4.19	3.69	11.93	3.69	2.44	2.13E-07
66 – 68	3.47	2.99	13.83	2.98	2.35	2.44E-07
68 – 70	5.09	4.34	14.73	4.32	2.55	2.84E-07
72 – 72	3.96	3.37	14.90	3.37	2.37	2.51E-07
72 – 74	3.32	2.97	10.54	2.98	2.35	2.44E-07
74 – 76	3.86	3.52	8.81	3.52	1.42	1.91E-07
76 – 78	3.74	3.29	12.03	3.30	1.82	2.43E-07
78 – 80	4.45	3.93	11.69	3.91	1.79	2.30E-07
80 – 82	4.59	3.94	14.16	3.94	1.78	2.43E-07
82 – 84	4.55	3.93	13.63	3.92	1.79	2.52E-07
84 – 86	3.87	3.35	13.44	3.35	2.39	2.59E-07
86 – 88	3.42	2.95	13.74	2.94	2.38	2.86E-07
88 – 90	3.88	3.39	12.63	3.39	2.06	2.83E-07

LOI and MS Raw Data for Core 5

Depth (cm)	Initial Weight (IW)	Oven Dry Weight (DW$_{105}$)	LOI$_{105}$ (Percent)	Furnace Dry Weight (DW$_{550}$)	LOI$_{550}$ (Percent)	MS (m^3/kg)
0 – 2	3.70	3.01	18.65	2.92	2.99	2.68E-07
2 – 4	4.06	3.28	19.21	3.21	2.43	2.20E-07
4 – 6	3.66	2.94	19.67	2.87	2.38	2.39E-07
6 – 8	3.89	3.11	20.05	3.03	2.26	2.33E-07
8 – 10	4.07	3.28	19.41	3.22	2.13	2.03E-07
10 – 12	2.52	2.04	19.05	2.00	1.96	2.04E-07
12 – 14	3.35	2.74	18.21	2.67	1.48	2.48E-07
14 – 16	4.39	3.47	20.96	3.39	2.59	2.42E-07
16 – 18	3.41	2.77	18.77	2.71	1.81	2.03E-07
18 – 20	3.58	2.82	21.23	2.73	2.50	1.95E-07
20 – 22	2.87	2.26	21.25	2.17	3.13	2.04E-07
22 – 24	2.93	2.33	20.48	2.27	2.16	1.89E-07
24 – 26	3.48	2.75	20.98	2.67	2.20	1.86E-07
26 – 28	3.02	2.43	19.54	2.35	2.49	1.72E-07
28 – 30	3.76	3.00	20.21	2.93	2.01	1.74E-07
30 – 32	3.15	2.54	19.37	2.46	2.77	2.27E-07
32 – 34	3.00	2.43	19.00	2.38	2.46	1.64E-07
34 – 36	4.16	3.39	18.51	3.30	2.65	1.69E-07
36 – 38	3.08	2.49	19.16	2.42	2.81	1.64E-07
38 – 40	3.37	2.70	19.88	2.62	2.96	1.85E-07
40 – 42	4.26	3.42	19.72	3.31	2.93	1.71E-07
42 – 44	4.10	3.27	20.24	3.17	2.76	1.73E-07
44 – 46	3.81	3.05	19.95	2.94	2.65	1.54E-07
46 – 48	3.39	2.74	19.17	2.65	2.93	1.63E-07
48 – 50	3.60	2.96	17.78	2.89	3.02	1.54E-07
50 – 52	3.59	2.98	16.99	2.90	2.36	1.42E-07
52 – 54	4.66	3.85	17.38	3.74	2.86	1.58E-07
54 – 56	5.43	4.47	17.68	4.34	2.69	1.92E-07
56 – 58	4.40	3.60	18.18	3.48	2.79	1.53E-07
58 – 60	4.08	3.40	16.67	3.30	2.37	1.45E-07
60 – 62	4.37	3.63	16.93	3.54	2.21	1.57E-07
62 – 64	3.89	3.28	15.68	3.21	2.43	1.44E-07
64 – 66	4.70	3.96	15.74	3.88	2.02	1.48E-07
66 – 68	4.36	3.69	15.37	3.59	2.18	1.51E-07
68 – 70	4.61	3.88	15.84	3.76	2.08	1.51E-07
70 – 72	4.86	4.07	16.26	4.00	2.20	1.68E-07
72 – 74	3.58	3.07	14.25	3.00	1.96	1.36E-07
74 – 76	4.06	3.45	15.02	3.37	1.75	1.52E-07
76 – 78	4.45	3.77	15.28	3.66	2.14	1.53E-07
78 – 80	4.81	4.02	16.42	3.92	2.24	1.69E-07

APPENDIX D

SEDIMENT TEXTURE CLASSIFICATION PLOTTED ON SHEPARD DIAGRAMS

<u>Shepard Diagram of Core 1</u>

Shepard Diagram

1 – Clay

2 – Sandy clay

3 – Silty clay

4 – Sandy silty clay

5 – Clayey sand

6 – Silty clayey sand

7 – Sandy clayey silt

8 – Clayey silt

9 – Sand

10 – Silty sand

11 – Sandy silt

12 – Silt
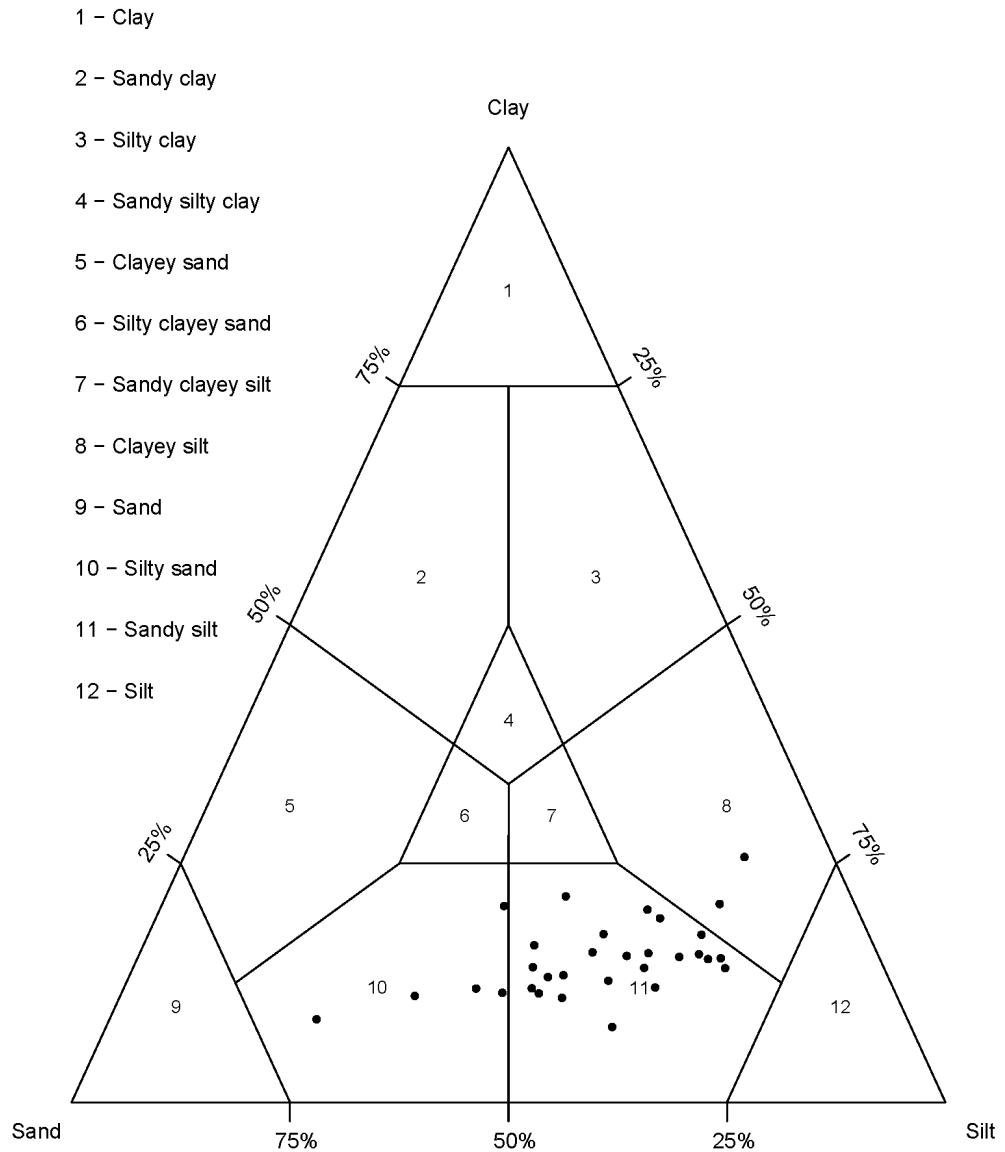
Shepard Diagram of Core 2
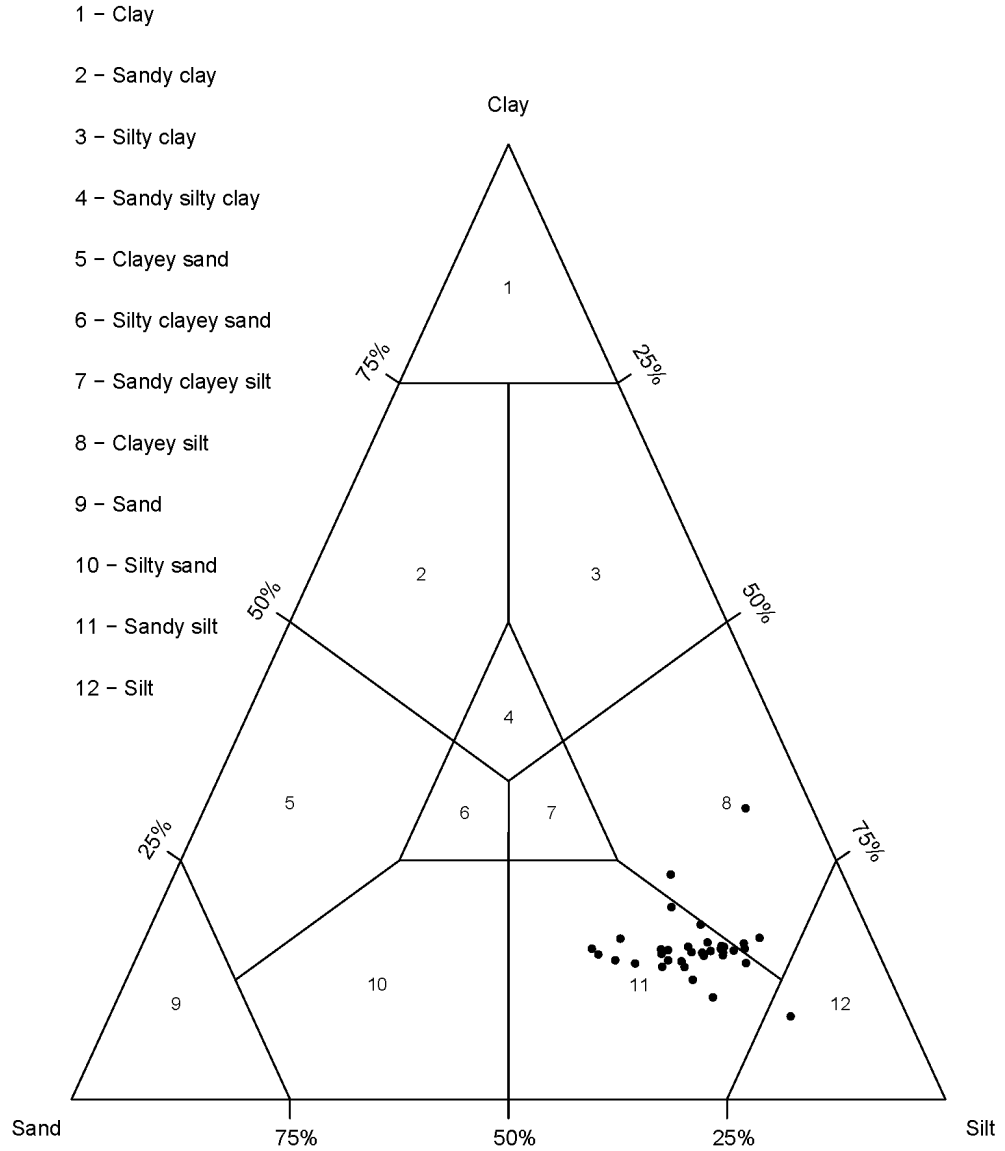
Shepard Diagram of Core 3

Shepard Diagram

1 – Clay

2 – Sandy clay

3 – Silty clay

4 – Sandy silty clay

5 – Clayey sand

6 – Silty clayey sand

7 – Sandy clayey silt

8 – Clayey silt

9 – Sand

10 – Silty sand

11 – Sandy silt
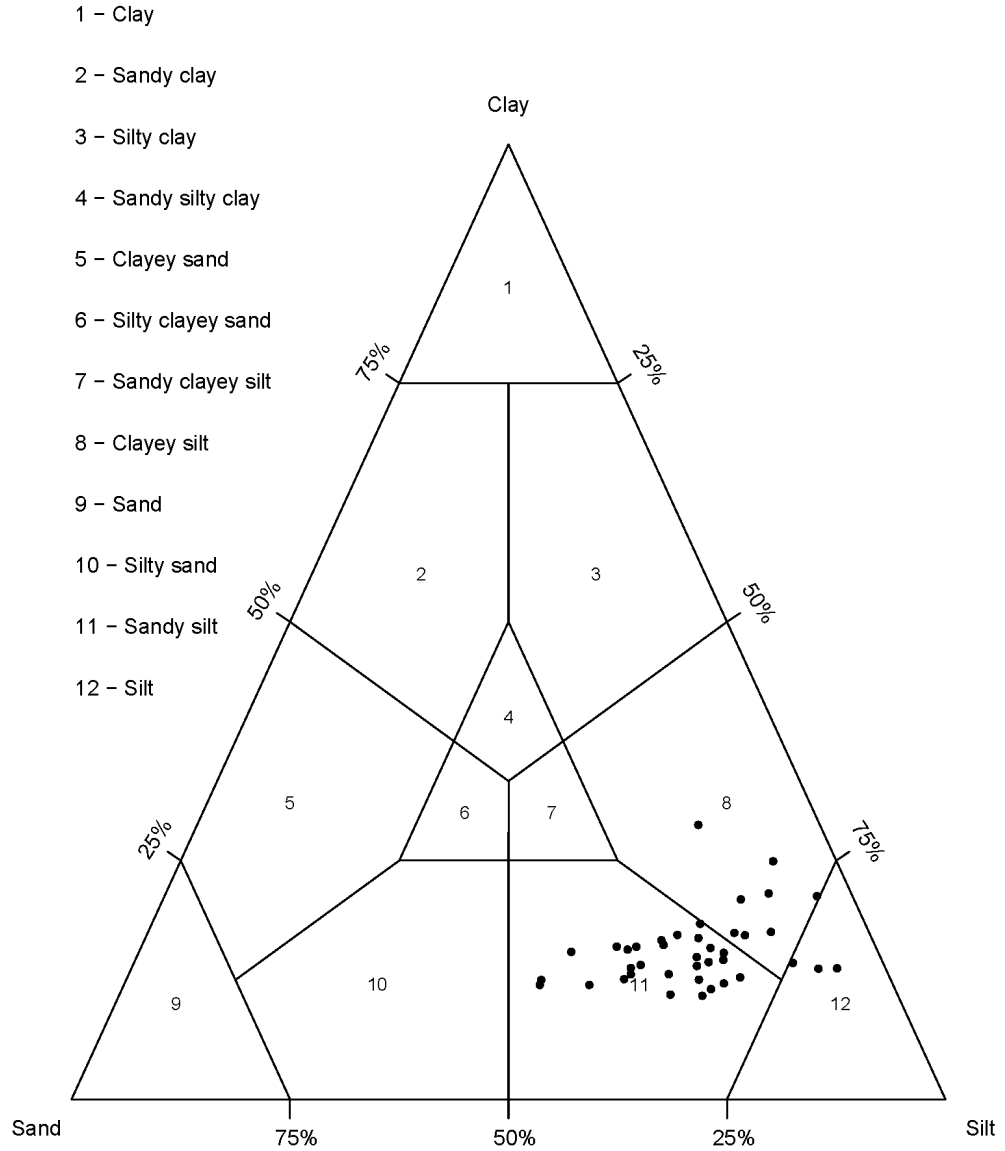
12 – Silt

Shepard Diagram of Core 4

Shepard Diagram

1 – Clay

2 – Sandy clay

3 – Silty clay

4 – Sandy silty clay

5 – Clayey sand

6 – Silty clayey sand

7 – Sandy clayey silt

8 – Clayey silt

9 – Sand

10 – Silty sand

11 – Sandy silt
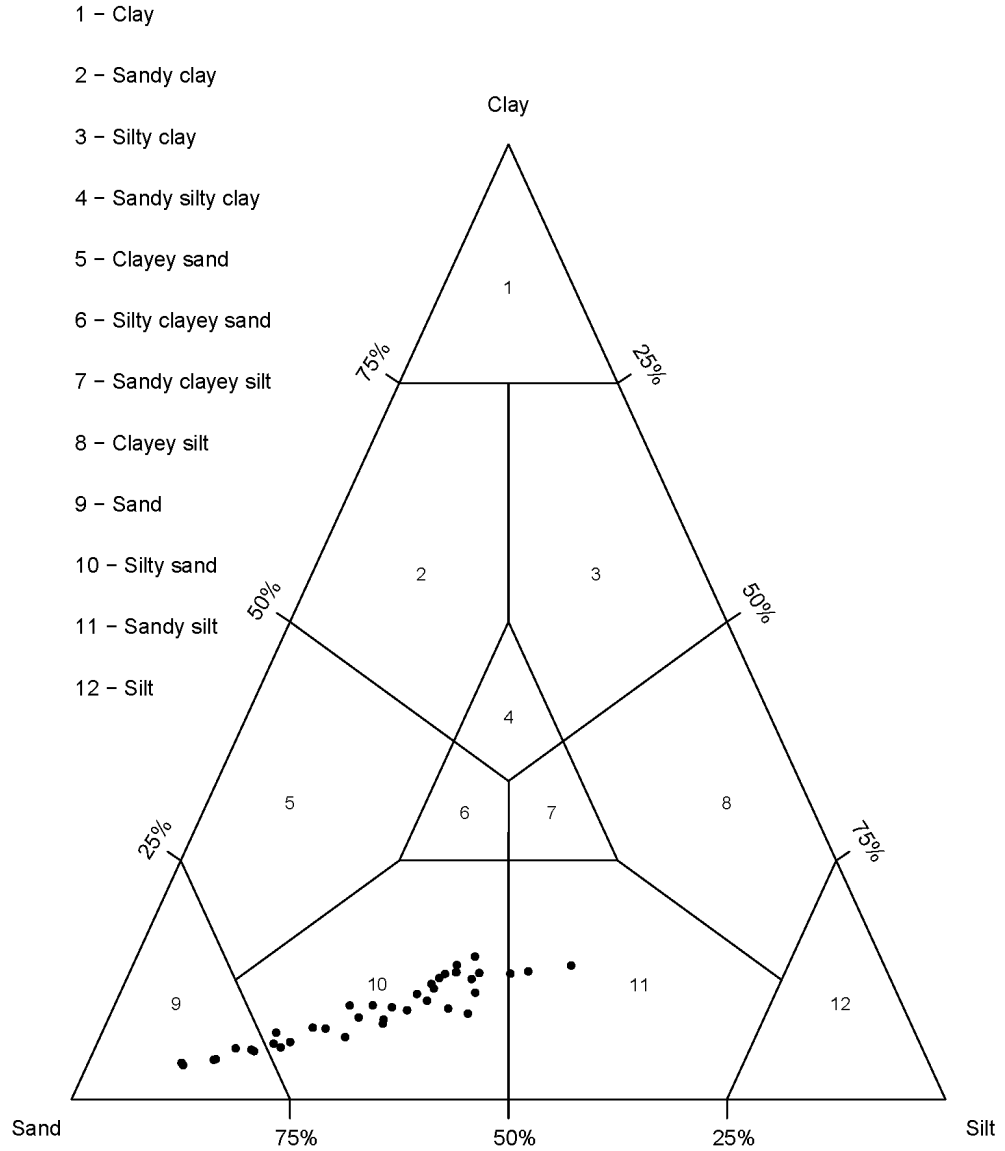
12 – Silt

Shepard Diagram of Core 5

Shepard Diagram

1 – Clay

2 – Sandy clay

3 – Silty clay

4 – Sandy silty clay

5 – Clayey sand

6 – Silty clayey sand

7 – Sandy clayey silt

8 – Clayey silt

9 – Sand

10 – Silty sand

11 – Sandy silt

12 – Silt

Clay

75%

25%

50%

50%

25%

75%

Sand

75%

50%

25%
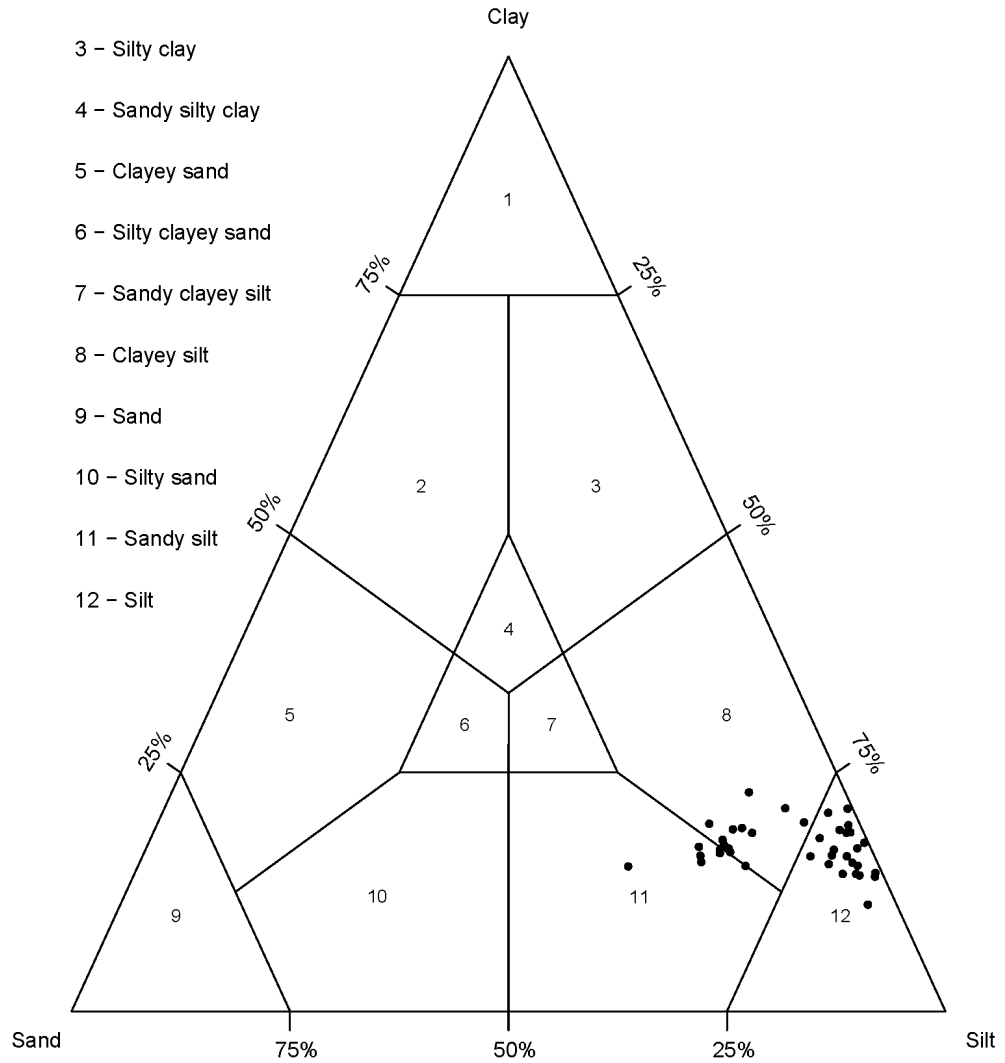
Silt

APPENDIX E

NORMALIZED CLAY, SILT, AND SAND DISTRIBUTION PERCENTAGES

Distribution Percentages of Core 1

Depth (cm)	Clay	Silt	Sand
14	14	68	18
16	18	63	19
18	15	67	18
20	13	50	37
22	11	51	38
24	14	59	27
26	12	61	27
28	21	64	15
30	20	56	24
32	26	64	10
34	8	58	34
36	15	65	20
38	15	62	23
40	19	58	23
42	12	40	48
44	11	44	45
46	11	48	41
48	16	64	20
50	12	47	41
52	16	45	39
54	20	39	41
56	13	55	32
58	15	56	29
60	16	58	26
62	21	46	33
64	18	52	30
66	16	52	32
68	13	48	39
70	14	46	40
72	9	23	68
74	11	34	55
Average	**15**	**53**	**32**

Distribution Percentages of Core 2

Depth (cm)	Clay	Silt	Sand
0	15	61	24
2	16	59	25
4	14	61	25
6	14	63	23
8	14	63	23
10	15	60	25
12	15	65	20
14	16	60	24
16	16	69	15
18	16	63	21
20	16	65	19
22	15	65	20
24	14	70	16
26	16	66	18
28	16	68	16
30	15	67	18
32	15	67	18
34	16	69	15
36	16	67	17
38	16	52	32
40	16	65	19
42	17	70	13
44	16	63	21
46	16	66	18
48	14	57	29
50	30	62	8
52	15	55	30
54	20	59	21
56	15	53	32
58	17	54	29
60	11	68	21
62	9	78	13
64	23	57	20
66	12	65	23
68	18	63	19
Average	**16**	**63**	**21**

Distribution Percentages of Core 3

Depth (cm)	Clay	Silt	Sand
0	13	57	30
2	15	64	21
4	18	63	19
6	11	63	26
8	13	66	21
10	12	67	21
12	14	65	21
14	13	70	17
16	16	54	30
18	11	67	22
20	17	61	22
22	12	69	19
24	16	57	27
26	16	49	35
28	12	47	41
30	13	57	30
32	14	66	20
34	13	47	40
36	12	53	35
38	15	67	18
40	14	57	29
42	16	56	28
44	14	58	28
46	16	60	24
48	17	59	24
50	16	65	19
52	18	71	11
54	17	69	14
56	17	67	16
58	22	69	9
60	21	66	13
62	21	75	4
64	14	81	5
66	25	68	7
68	14	78	8
70	14	76	10
72	15	67	18
74	29	57	14
76	13	62	25
78	17	63	20
Average	**16**	**63**	**21**

Distribution Percentages of Core 4

Depth (cm)	Clay	Silt	Sand
12	13	40	47
14	9	41	50
16	13	36	51
18	10	36	54
20	7	28	65
22	10	32	58
24	10	29	61
26	9	34	57
28	10	38	52
30	13	39	48
32	15	39	46
34	13	38	49
36	13	36	51
38	7	24	69
40	4	11	85
42	4	11	85
44	10	27	63
46	5	18	77
48	6	20	74
50	5	16	79
52	4	14	82
54	4	14	82
56	6	22	72
58	6	21	73
60	8	32	60
62	12	35	53
64	8	25	67
66	8	32	60
68	14	37	49
70	9	28	63
72	7	20	73
74	5	18	77
76	11	34	55
78	13	44	43
80	11	41	48
82	11	36	53
84	14	50	36
86	13	37	50
88	13	46	41
Average	**9**	**30**	**61**

Distribution Percentages of Core 5

Depth (cm)	Clay	Silt	Sand
0	16	79	5
2	15	82	3
4	14	85	1
6	15	84	1
8	14	83	3
10	11	86	3
12	14	81	5
14	19	79	2
16	16	81	3
18	20	79	1
20	18	82	0
22	21	78	1
24	17	81	2
26	14	83	3
28	16	81	3
30	17	79	4
32	18	80	2
34	15	79	6
36	19	78	3
38	20	74	6
40	16	77	7
42	21	76	3
44	18	77	5
46	21	71	8
48	17	66	17
50	19	68	13
52	16	64	20
54	17	67	16
56	18	65	17
58	16	64	20
60	15	70	15
62	17	66	17
64	17	66	17
66	19	67	14
68	20	63	17
70	19	66	15
72	15	56	29
74	17	63	20
76	17	67	16
78	23	66	11
Average	**17**	**74**	**9**

INTERPRETATIONS OF END MEMBER DEPOSITIONAL CONDITIONS
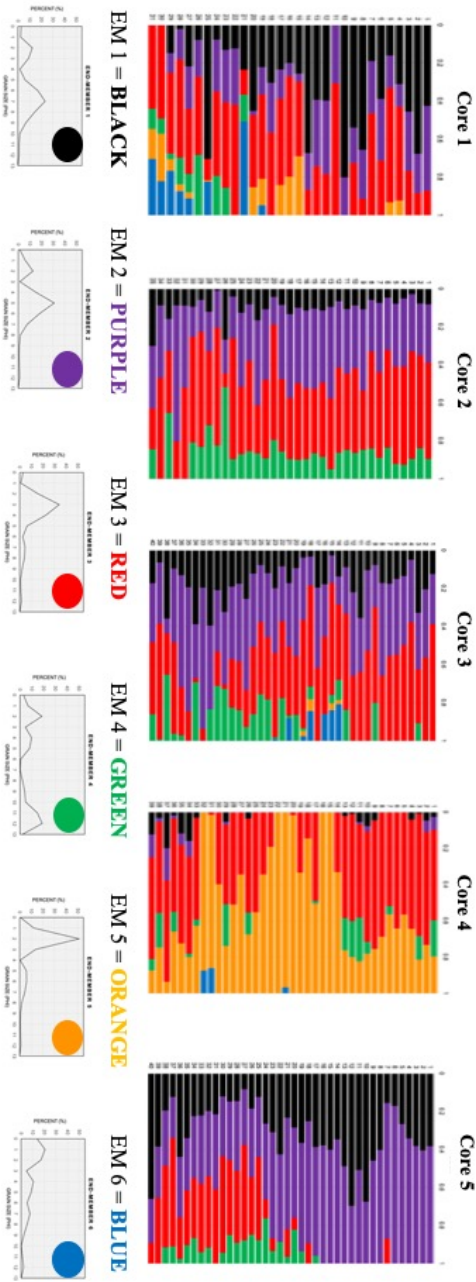
Fort Hays State University
FHSU Scholars Repository
Non-Exclusive License Author Agreement

I hereby grant Fort Hays State University an irrevocable, non-exclusive, perpetual license to include my thesis ("the Thesis") in *FHSU Scholars Repository*, FHSU's institutional repository ("the Repository").

I hold the copyright to this document and agree to permit this document to be posted in the Repository, and made available to the public in any format in perpetuity.

I warrant that the posting of the Thesis does not infringe any copyright, nor violate any proprietary rights, nor contains any libelous matter, nor invade the privacy of any person or third party, nor otherwise violate FHSU Scholars Repository policies.

I agree that Fort Hays State University may translate the Thesis to any medium or format for the purpose of preservation and access. In addition, I agree that Fort Hays State University may keep more than one copy of the Thesis for purposes of security, back-up, and preservation.

I agree that authorized readers of the Thesis have the right to use the Thesis for non-commercial, academic purposes, as defined by the "fair use" doctrine of U.S. copyright law, so long as all attributions and copyright statements are retained.

To the fullest extent permitted by law, both during and after the term of this Agreement, I agree to indemnify, defend, and hold harmless Fort Hays State University and its directors, officers, faculty, employees, affiliates, and agents, past or present, against all losses, claims, demands, actions, causes of action, suits, liabilities, damages, expenses, fees and costs (including but not limited to reasonable attorney's fees) arising out of or relating to any actual or alleged misrepresentation or breach of any warranty contained in this Agreement, or any infringement of the Thesis on any third party's patent, trademark, copyright or trade secret.

I understand that once deposited in the Repository, the Thesis may not be removed.

Thesis: _Analysis of Clastic Cave Sediment in a Fluviokarst system, Russell Cave, Northeast Alabama_

Author: _Jonathan Camelo_

Signature: _Jonathan Camelo_

Date: _April 30, 2020_